

# UC Irvine

## UC Irvine Electronic Theses and Dissertations

### Title

A Combinatorial Approach to Promote Regeneration after Spinal Cord injury via Biomaterials, Neural stem cells, and Immunomodulation

### Permalink

<https://escholarship.org/uc/item/5b65z6q1>

### Author

Nekanti, Usha

### Publication Date

2022

### Copyright Information

This work is made available under the terms of a Creative Commons Attribution-NonCommercial-NoDerivatives License, available at <https://creativecommons.org/licenses/by-nc-nd/4.0/>

Peer reviewed|Thesis/dissertation

UNIVERSITY OF CALIFORNIA,  
IRVINE

**A Combinatorial Approach to Promote Regeneration after Spinal Cord injury via  
Biomaterials, Neural stem cells, and Immunomodulation**

**DISSERTATION**

submitted in partial satisfaction of the requirements for the degree of

DOCTOR OF PHILOSOPHY

in Biomedical Sciences

by

**Usha Nekanti**

**Dissertation Committee:**

Professor Aileen J. Anderson, Chair

Professor Brian J Cummings

Professor Aileen J Anderson

Professor Lisa Flanagan

Professor Wendy Liu

Professor Momoko Watanabe

2022

Figure diagrams created with [BioRender.com](https://BioRender.com)

© 2022 Usha Nekanti

## **DEDICATION**

To my loving husband, Pradyumna Kumar Nuvvula for being my unwavering support through all my failures and successes. I could not have done any of this without his endless dedication, encouragement, and patience.

## TABLE OF CONTENTS

|  |      |
|--|------|
| LIST OF FIGURES  | vi   |
| LIST OF TABLES   | viii |
| ACKNOWLEDGEMENTS   | ix   |
| CURRICULUM VITAE   | xi   |
| ABSTRACT OF THE THESIS   | xiv  |
| CHAPTER 1  | 1    |
| Introduction   |      |
| CHAPTER 2:   | 09   |
| Acute Biomaterial Bridge Implantation and Chronic Neural Stem Cell<br>Transplantation to Facilitate Axonal Regeneration, Myelination, and Connectivity<br>After Spinal Cord Injury                 |      |
| CHAPTER 3:   | 74   |
| Combination of Biomaterial Bridge Implantation and Interleukin-10 Expression to Modulate<br>the Inflammatory Response and Promote Neural Regeneration and Connectivity after Spinal<br>Cord Injury |      |
| CHAPTER 4  | 101  |
| Summary and Conclusion   |      |
| REFERENCES   | 106  |

## LIST OF FIGURES

|  | Page |
|--|------|
| Figure 2.1<br>Experimental design Schematic/Schematic diagram  | 52   |
| Figure 2.2<br>Innate Immune Cell Time Course in C57BL/6 Mice Injured Spinal Cord   | 54   |
| Figure 2.3<br>In Vitro Assessment of hNSC Fate in the Presence of PLG Substrate and Immune Cues  | 55   |
| Figure 2.4<br>Stereological analysis of hNSC fate and distribution along the spinal cord   | 57   |
| Figure 2.5<br>PLG bridge creates a permissive injury environment for hNSC engraftment and influences hNSC fate.  | 59   |
| Figure 2.6<br>Combination of PLG bridge implantation and hNSC transplantation enhances axonal regeneration and oligodendrocytic myelination  | 61   |
| Figure 2.7<br>Transsynaptic pseudorabies virus (PRV) tracing indicates that the regenerated CST axons through the PLG bridge are synaptic connected  | 63   |
| Figure 2.8<br>Locomotor behavior assessment of paw placement errors on the horizontal ladder beam and Catwalk gait analysis  | 65   |
| Supplemental Figure 2.1<br>Innate immune cell time course in Rag1 immunodeficient mice injured spinal cord   | 67   |
| Supplemental Figure 2.2<br>Peritoneal PMN or macrophages (MØ) cell profiling to generate condition media for hNSC In vitro fate analysis   | 68   |
| Supplemental Figure 2.3<br>CRYM-ZsGreen1 mice showing GFP expression in CST and tdTomato membrane reporter expression in mT-mNSC, optimization of anti-CD4 immunosuppression paradigm, and motor recovery assessment | 69   |
| Supplemental Figure 2.4  | 71   |

Validation of PRV labeling in young and aged naive mice.

|  |    |
|--|----|
| Figure 3.1   | 95 |
| Anti-inflammatory cytokine IL-10 and PLG alters macrophage activation state                      |    |
| Figure3.2  | 96 |
| Locomotor behavioral assessment of paw placement errors on the horizontal ladder beam            |    |
| Figure 3.3   | 97 |
| PLG bridge implantation and localized expression of IL-10 promote axonal growth and myelination  |    |
| Figure 3.4   | 98 |
| PRV functional synaptic connectivity assessment within the injury site                           |    |
| Figure 3.5   | 99 |
| PRV functional synaptic connectivity assessment in the motor cortex and PVN regions of the brain |    |

## LIST OF TABLES

|           |  |            |
|-----------|--|------------|
| Table 2.1 | List of primary antibodies, sources, and dilutions | Page<br>73 |
| Table 3.1 | List of Primers                                    | 100        |

## ACKNOWLEDGEMENTS

I would like to thank Dr. Aileen J Anderson and Dr. Brian J Cummings for their mentorship, guidance, encouragement, and friendship over the last several years. I would especially like to express my deepest gratitude to my advisor, Dr. Aileen Anderson, for believing in me with this project and giving me the freedom to work on flexible timings. Thank you for your unwavering support and guidance, I am truly honored and proud to be her graduate student. I would like to thank my committee members Dr. Brian J Cummings, Dr. Lisa Flanagan, Dr. Wendy Liu, and Dr. Momoko Watanabe for their input, guidance, and time throughout my Ph.D. I would also like to thank my past committee member Dr. Ana Solodkin for her counsel and tutelage on neural pathways.

I deeply appreciate our collaborators: Dr. Lonnie Shea for providing biomaterial scaffolds and lentiviral vectors for this study and Dr. Xiangmin Xu for helping us with the retrograde pseudorabies virus (PRV) tracing experiment to examine the synaptic connectivity of the regenerated fibers. I am grateful to Dr. Lorna Carlin and the UCI School of Medicine for supporting my research through the Excellence in Research Award.

I would like to extend a special thanks to Pooja Sakthivel, Dr. Atena Zahedi, and Rebecca Nishi who were instrumental in this project. Without your assistance, all this work would not have been possible. Thank you to all the members of the Anderson and Cummings laboratories who were always there for me. Special thanks to Dana Creasman for assistance with CatWalk data analysis and to Joshua David, Cherie, Chris Nelson, and Javier Lepe for assistance with the surgeries and anything else I needed help with. I always knew I could rely on them. I would like to thank my CIRM internship students (Norbert Hernandez, Joshua Martinez,

Lindsey Lawmaster) and undergraduate students (Xingyuan Chen, Glenn Lee Guardamondo, Anthony Hieu Ngotran, and Charlie Shi) for helping me throughout this dissertation.

Finally, I'd like to express my gratitude to my parents, in-laws, my two children, and my husband for their unwavering love and support.

## CURRICULUM VITAE

### **Usha Nekanti, M.Sc.**

Graduate student Ph.D. in Biomedical Sciences, Anatomy and Neurobiology Department,  
University of California Irvine, California, USA

#### **Education:**

PhD Candidate 2014-June 2022  
Department of Anatomy and Neurobiology  
University of California-Irvine, CA-USA  
Mentor: Aileen J. Anderson

Master of Science: Biotechnology 2005-2007  
University of Mysore, Mysore, India

Bachelor of Science: Chemistry, Botany and Biotechnology 2002-2005  
Karnataka University, Karnataka, India

#### **Research Experience:**

**2014 - 2022: Graduate Researcher, University of California-Irvine, CA, USA.**

- Combinatorial approaches of biodegradable poly(lactide-co-glycolide) (PLG) bridge implantation, anti-inflammatory cytokine expression, and Neural Stem Cells (NSCs) transplantation to enhance axonal regeneration, myelination and promote the locomotor recovery in spinal cord injured mice.
- Profiling the inflammatory microenvironment of Spinal Cord Injury with PLG-biomaterial bridge: PLG-bridge supports axonal regeneration by modulating the inflammatory response at the injury site.

**2010 - 2013: Junior Specialist/Research Volunteer, Aileen Anderson's lab,  
University of California Irvine, CA, USA.**

- Derivation of neural stem cells from human pluripotent stem cells under xeno-free conditions. (PMID: 24715528)
- Effect of inflammatory microenvironment of spinal cord injury on human Neuronal Stem Cells (NSC) fate.
- Differential effect of Macrophage subsets pro-inflammatory (M1) and anti-inflammatory phenotype (M2) on neural stem cell fate

**2008 - 2010: Research Associate, Stempeutics Research Ltd, Bangalore, India.**

- Isolation, Characterization, and Long-term Expansion of Mesenchymal stem cells derived from Wharton's jelly of umbilical cord (WJ- MSCs) (PMID: 19619003).
- Characterization of Wharton's jelly-derived Mesenchymal stem cells under hypoxic conditions (2% oxygen) (PMID: 20877435).
- Clinical Scale Production of Mesenchymal stem cells from bone marrow, umbilical cord blood, umbilical cord tissue, adipose tissue, and dental pulp tissue (PMID: 20880767).

**2007 - 2008: Senior Research Fellow, Institute of Animal health & veterinary Biologicals, Bangalore, India.**

- Quantification of protective antibody level in Pre and Post Foot and Mouth Disease (FMD) Vaccinated animals using ELISA.
- Identification of FMD virus types O, A, C & ASIA-1 from samples of infected animals.
- Rabies Vaccine production under cGMP facilities.

**Publications:**

1. **Nekanti U**, Sakthivel P\*, Zahedi A\*, Creasman AD, Nishi R, H, Guo Z, Lin X, Dumont C, Cummings BJ, Shea LD, Xu X, Anderson AJ “Biomaterial scaffold and neural stem cell to support neural regeneration, myelination, and restore connectivity following spinal cord injury” (In preparation).
2. **Nekanti U**, Zahedi A\*, Sakthivel P\*, Park J, Nishi R, H, Guo Z, Lin X, Dumont C, Cummings BJ, Shea LD, Xu X, Anderson AJ “PLG bridge implantation and interleukin-10 expression to modulate the inflammatory response and foster neural Regeneration, connectivity following spinal cord injury” (In preparation).
3. **Nekanti U**, Zahedi A\*, Sakthivel P\*, Park J, Nishi R, Cummings BJ, Shea LD, Xu X, Anderson AJ “Combinatorial approach of human neural stem cell transplantation and IL-10 delivery to minimize tissue degeneration and promote repair following spinal cord injury (In preparation)
4. Nguyen HX, **Nekanti U**, Haus DL, Funes G, Moreno D, Kamei N, Cummings BJ & Anderson AJ (2013). “Induction of early neural precursors and derivation of tripotent neural stem cells from human pluripotent stem cells under xeno-free conditions” - *Journal of Comparative Neurology* 2014 Aug, 522(12):2767-83.
5. **Nekanti U**, Vinay B Rao, Avinash G Bahirvani, Majahar Jan, Satish Totey, Malancha Ta. “Long-term Expansion and Pluripotent Marker Array Analysis of Wharton’s Jelly-Derived Mesenchymal Stem Cells” -*Stem Cells and Development*. 2010 Jan; 19(1):117-30.
6. **Nekanti U**, Sumitava Dastidar, Parvathy Venugopal, Satish Totey, Malancha Ta. “Increased proliferation and analysis of differential gene expression in human Wharton’s Jelly-derived mesenchymal stromal cells under hypoxia”- *International journal for Biological sciences* 2010 Aug; 6(5):499-511.
7. **Nekanti U**, Lipsa Mohanty, Parvathy Venugopal, Sudha Balasubramanian, Satish Totey, Malancha Ta. “Optimization and Scale up of Wharton’s Jelly-derived Mesenchymal Stem Cells for Clinical Applications”- *Stem Cell Research* 2010 Aug, 5: 244-254

**Presentations:**

- **Usha Nekanti**, Norbert Hernandez, Rebecca Nishi, Xingyuan Chen, Glenn Guardamondo, Stephanie K Seidlits, Brian Cummings, Lonnie Shea & Aileen J.

Anderson “Acute Biomaterial Bridge Implantation combined with delayed Neural Stem Cell Transplantation to Facilitate Axonal Regeneration and Myelination in Spinal Cord Injury” **The New York Stem Cell Foundation Conference 2020.**

- **Usha Nekanti**, Norbert Hernandez, Rebecca Nishi, Xingyuan Chen, Glenn Guardamondo, Brian Cummings, Lonnie Shea & Aileen J. Anderson “Biomaterials Pave the Path for Stem Cell-Mediated Regeneration in Spinal Cord Injury” **12th Annual Emerging Scientists Symposium. REMIND & UCI MIND 2020.**
- **Usha Nekanti**, Glenn Guardamondo, Anthony Ngotran, Lindsey Lawmaster and Aileen J. Anderson “Combinatorial Approach for Spinal Cord Injury: Effect of Biomaterial and Innate Immune Response on Human Neural Stem Cells Fate”. **Cell Symposium: Neuroimmune Axis Long Beach, CA, USA 2019.**
- **Usha Nekanti**, Glenn Guardamondo, Anthony Ngotran, Lindsey Lawmaster and Aileen J. Anderson “Combinatorial approach of Biomaterial Bridge, Neural Stem cells Transplantation and Modulation of Inflammation to Regenerate Injured Spinal Cord.” **The International Society for Stem Cell Research, Los Angeles USA 2019.**
- **Usha Nekanti** and Aileen J. Anderson “Combinatorial therapies for spinal cord injury to promote locomotor recovery”. Grad day, Anatomy and Neurobiology department. University of California; Irvine, CA, USA-2019.
- **Usha Nekanti**, Glenn Guardamondo, Anthony Ngotran, Lindsey Lawmaster and Aileen J. Anderson “Spinal Cord Injury: Effect of Biomaterial and Immune Response on Human Neural Stem Cells Fate”. Grad day, Anatomy and Neurobiology department. University of California; Irvine, CA, USA-2018. **(First place winner for best poster).**
- **Usha Nekanti** and Aileen Anderson. “Bridge the Gap! Bridging spinal cord lesion to support axonal regeneration and restore lost communication”. Grad day, Anatomy and Neurobiology department. University of California; Irvine, CA, USA-2016.
- **Usha Nekanti**, Sumitava Dastidar, Satish Totey & Malancha Ta “The effect of hypoxia on gene expression & growth kinetics of Wharton’s Jelly derived Mesenchymal Stem Cells”. Sue and Bill Gross Stem Cell Research Center, University of California, Irvine; Irvine, CA, USA 2011

**Awards and Recognitions:**

- 2019 The International Society for Stem Cell Research Travel Grant awarded by School of Medicine, University of California, Irvine.
- 2019 The Dr. Lorna Carlin Excellence in Research Award, School of Medicine, University of California, Irvine.
- 2018 Best Poster Award at the Annual Anatomy and Neurobiology grad day, UC Irvine

## **ABSTRACT OF THE DISSERTATION**

A Combinatorial Approach to Promote Regeneration after Spinal Cord injury via  
Biomaterials, Neural stem cells, and Immunomodulation

by

Usha Nekanti

Doctor of Philosophy in Biomedical Sciences

University of California Irvine, 2022

Professor Dr. Aileen J. Anderson, Chair

Spinal cord injury (SCI) disrupts the blood-spinal cord barrier, allowing immune cells to infiltrate spinal cord tissue and further exacerbating the injury. This causes CNS cell death, axonal dieback, demyelination, and build-up of inhibitory factors that limit axonal and myelin regeneration. Several decades of extensive SCI research have made it clear that this complex problem requires combinatorial solutions. This dissertation investigates three therapeutic approaches for SCI: **(A) implantation of multi-channel poly (lactide-co-glycolide) (PLG) biomaterial** that can bridge the defect and guide axonal growth through inhibitory barriers; **(B) human Neural Stem Cell (hNSC)** transplantation to replenish lost CNS cells and to myelinate regenerating axons; and **(C) expression of anti-inflammatory cytokines like interleukin-10 (IL-10)** to modulate the SCI inflammatory milieu and offer neuroprotection. The first chapter introduces the conceptual background for these studies. The second chapter investigates the combination of acute PLG bridge implantation and chronic hNSC transplantation for SCI. Highlights of this chapter include enhancement of hNSC engraftment, hNSC migration along regenerated axons growing into the bridge, hNSC differentiation into oligodendrocytes and myelinating host axons, hNSC-derived neurons

integrating into mouse neural circuitry, and improvement in motor recovery. Additionally, I show novel evidence supporting the formation of a synaptic circuit connecting corticospinal neurons in the motor cortex and the forelimb neuromuscular junction via the PLG bridge. This study highlights the significance of a guided bridge conduit in the injury site to reestablish lost connections and hNSC transplantation to myelinate the spared and regenerated circuitry and unleash the full potential of hNSC-based regenerative therapies. The third chapter investigates the effect of localized lentiviral expression of IL-10 with or without PLG bridge implantation on outcomes after spinal cord injury. Highlights of this chapter include: IL-10 modulates the inflammatory microenvironment and significantly enhances regeneration and myelination in the PLG bridge, and this combined approach resulted in a synergistic improvement in motor recovery. Additionally, using transsynaptic PRV tracing, I demonstrate the bridge supports the rewiring of spinal neuronal circuitry from the motor cortex and PVN of the hypothalamus and further enhancement in PVN circuitry with IL-10 delivery.

# CHAPTER 1

## Introduction

### **1.1 Introduction to Spinal Cord Injury (SCI)**

SCI is a debilitating condition that causes loss of sensory, motor, and reflex function below the level of injury. According to the National Spinal Cord Injury Statistical Center, the estimated number of people with SCI in the United States is 294,000, with a range of 250,000 to 368,000. Causes of SCI include motor vehicle crashes (38.6%), falls (32.2%), violence (14%), sports (7.8%), medical/surgical (4.2%) and other accounts (3.2%). SCI permanently alters a patient's quality of life due to deficits in locomotion, reaching, grasping, trunk stability, micturition, bowel, bladder function, and sexual function, as well as inducing neuropathic pain and autonomic dysreflexia. Currently, therapeutic approaches mainly address secondary complications and rehabilitation to improve functional outcomes [1].

### **1.2 SCI Pathophysiology**

The pathophysiology of SCI is defined by the primary and secondary injury mechanisms. Primary injury results from the initial mechanical trauma, whereas secondary injury results from subsequent damage caused by the interplay of environmental factors at the injury site. The acute phase after the initial trauma involves damage to nerve cells, myelin, blood vessels, and supporting bone structure, followed by hemorrhage, thrombosis, vasospasm, edema, and necrosis [2, 3]. Events within the acute phase such as neuroinflammation, oxidative stress, anterograde and retrograde axonal degeneration, and demyelination continue into the subacute phase and chronic phase, contributing to the formation of a fluid-filled lentiform-shaped cyst surrounded by astroglial scar [4, 5]. Critically, reactive astrocytes in scar tissue release extracellular matrix molecules and

growth-inhibiting molecules such as chondroitin sulfate proteoglycans (CSPGs), forming a physical and chemical barrier to the axonal regeneration [6, 7].

### **1.3 Therapeutic approaches for spinal cord injury**

Therapeutic strategies for SCI fall under two general categories: neuroprotective and neurogenerative [2, 8-10]. Neuroprotective strategies focus on specific pathological factors that contribute to secondary tissue degeneration and the formation of regenerative-inhibiting barriers. Approaches include limiting the effects of secondary damage-cell death, demyelination, and axonal degeneration as well as modulating the inflammatory response [11-15]. Neuroregenerative strategies include creating a permissive environment for neuronal regeneration, minimizing scar formation, enriching the progenitor cells or neural cells by cell transplantation, blocking axon growth inhibitory factors, glial scar digestion, and administration of neurotrophic factors [16-23]. My dissertation work highlights the use of three interventions to support neuroprotection and regeneration of injured spinal cord: (i) Biomaterial scaffold implantation, (ii) Stem cell transplantation, and (iii) Immunomodulation. Each of these is introduced in the section below.

### **1.4 Biomaterial scaffold implantation**

Biomaterials have shown great promise for fostering axonal regeneration following SCI [18, 24-30]. Biomaterials scaffolds can be naturally or synthetically derived structures, many of which have potential applications in regenerative medicine. Naturally derived material includes collagen, fibrin, chitosan, matrigel, and hyaluronic acid [31-33]. Synthetic polymers include poly (lactide-co-glycolide) (PLG), polycaprolactone (PCL), polylactide (PLA), and polyethylene glycol (PEG) [16, 18, 34-37]. In the context of SCI, biomaterial

scaffold implantation can provide mechanical stability to the injury site, a drug, biological molecule, or cell delivery strategy, and an aid to axonal regeneration [38, 39].

In these studies, I utilized PLG because this material is biocompatible, biodegradable, and the only biomaterial approved by the FDA for clinical implantation. Our laboratory has collaborated with the Shea laboratory for well over a decade to develop novel, porous, multi-channel, biodegradable PLG bridges. These bridges consist of micro-textured porous walls that are optimized for cellular infiltration and easy exchange of nutrients, as well as linear longitudinal channels to guide the axonal regeneration [18]. Implantation of PLG bridges also stabilizes the injury site by preventing the formation of a cystic cavity and attenuating glial scar formation [18]. Regenerated axons within the PLG-bridge channels stained positive for neurofilament (NF-200) and were observed in bridge channels two weeks post-injury. Axonal density increased over time and reached a maximum by six months post-injury [26]. Using a transgenic mouse model implanted with a PLG bridge, we showed that large numbers of corticospinal tract (CST) axons regenerated, traveled through the implanted PLG bridge, exited the caudal end of the bridge, and extended up to 2.5 mm into the spared parenchyma [16]. CST axons were co-stained for the GAP-43 growth cone marker, an indicator of regeneration. This axonal regrowth was correlated with locomotor recovery as demonstrated on the ladder beam paw placement task [16]. Overall, these experiments show that the PLG bridge supports robust axonal regeneration, including the highly refractory CST.

Critically, further studies on axonal regeneration in the PLG bridge revealed that only 13% of regenerated axons in the channels were myelinated [40]. Among these, a small proportion of the axons were myelinated by oligodendrocytes; the majority of myelination

was contributed by Schwann cells [18]. Schwann cells are peripheral axon myelinating cells that rapidly invade the spinal cord after injury and can spontaneously remyelinate spared axons in the CNS. However, myelin sheaths formed by Schwann cells are not thick enough and thus are suboptimal to restore axonal conduction in the CNS [41, 42]. Oligodendrocyte myelination is an essential factor for the efficient transmission and integration of electric signals to restore motor and sensory function following SCI. In a healthy rodent spinal cord, it has been estimated that 40-60% of myelinated axons are myelinated by oligodendrocytes [43, 44]. These data indicate that there is a further requirement to maximize the oligodendrocytic myelination of regenerated axons. An underlying hypothesis of my dissertation work is that NSC transplantation and differentiation into oligodendrocytes could provide a path by which to enhance the myelination of regenerating axons in the PLG bridge.

### **1.5 Stem Cell transplantation**

Stem cell transplantation is a promising therapeutic strategy for spinal cord injury (SCI) and has been extensively investigated in numerous pre-clinical studies. Stem cell therapies have been shown to promote motor recovery through multiple mechanisms, including ameliorating secondary injury, replacing damaged and dead cells, remyelinating spared axons, secreting neurotrophic factors that further support neuronal plasticity and tissue repair, and stimulating endogenous stem cells [45-49].

Various cell populations have been tested in animal models of SCI. These include Neural Stem Cells (NSC), which have the ability to differentiate into and replace all three types of CNS cells: neurons, astrocytes, and oligodendrocytes, as well as secrete neurotrophic

factors [17, 50]; Mesenchymal Stem Cells (MSCs) which have the ability to release anti-inflammatory cytokines and secrete neurotrophic factors [51, 52]; and Schwann Cells (SCs), which have been shown to remyelinate host CNS axons and secrete neurotrophic factors [53, 54].

In this study, I tested human fetal CNS tissue derived NSC (hNSC). Pre-clinical studies from my lab have shown that subacute or chronic hNSC transplanted into SCI models exhibited a predominantly oligodendrocyte fate and remyelinated host axons, resulting in improvements in the locomotor function [17, 50], that were reversed by selective ablation of human cells. These data suggest stable integration of transplanted NSCs which is required for functional recovery [17].

While NSC transplantation studies are promising in terms of functional improvement, the timing and the post-SCI immune niche have a dramatic effect on NSC fate, migration, and functional integration, and consequently the overall efficacy of these cells after SCI [17]. Previous studies from my lab on rodent SCI demonstrated that the majority of cells transplanted during the sub-acute (9 days post-injury, DPI) and chronic (30 DPI) time points migrated away from the injury epicenter, differentiated as oligodendrocytes and neurons, and supported functional recovery [55] [56] [57]. Conversely, hNSC transplanted at acute (0 DPI) time points migrated towards the injury epicenter, predominantly differentiated as astrocytes, and did not support the locomotor recovery [56]. In a parallel study, my lab found that the acute injury environment is characterized by the presence of infiltrated polymorphonuclear neutrophils (PMNs), which direct hNSC fate towards the astroglial lineage and regulate the migration patterns of hNSC [58] [57] [56]. In contrast, the subacute and chronic injury microenvironment is dominated by the presence of macrophage

(M $\phi$ )/microglial cues, which drive neuronal and oligodendrocyte lineage selection [58]. Accordingly, in this dissertation (Chapter 2), I strategized to combine acute PLG bridge implantation with chronic hNSC transplantation since macrophage cues in the chronic environment are beneficial in promoting neuronal and oligodendrocytic fates while reducing the scar-forming astrocytic fate.

## **1.6 Immunomodulation**

Traumatic injury to the spinal cord results in breakdown of blood spinal barrier (BSB), leading to the infiltration of immune cells into spinal cord tissue [58]. In recent decades, the inflammatory response to SCI has been intensively studied due to its divergent roles in contributing to neuropathology and stimulating reparative mechanisms [59, 60]. The early inflammatory response involves activation of the resident immune cells (microglia) and infiltrating leukocytes (neutrophils and macrophages). Macrophages/microglia exist in a wide range of activated states and can be broadly characterized as pro-inflammatory or pro-regenerative depending on the stimuli they encounter in the injured spinal cord. Immediately following SCI, macrophages/microglia adopt a pro-inflammatory phenotype in response to pro-inflammatory cytokines, such as interferon-gamma and TNF-alpha. This classical M1 pro-inflammatory phenotype response is needed in for an appropriate response to infection or injury. Nonetheless, an exaggerated pro-inflammatory response by M1 macrophages/microglia following SCI results in substantial irreversible tissue damage to the spinal cord [2]. Indeed, pro-inflammatory macrophages/microglia produce an array of neurotoxins: pro-inflammatory cytokines and chemokines, free radicals, and nitric oxide, all of which contribute to further secondary damage within the injured cord [2]. The alternative

M2 pro-regenerative phenotype, on the other hand, participates in the repair mechanism by phagocytizing cellular debris, removing inhibitory myelin components, and promoting neuroregeneration through the release of neurotrophic factors and anti-inflammatory cytokines [59-61]. Modulation of the inflammatory response after acute SCI can prevent the accumulation of growth inhibitory factors, myelin debris, neuronal cell death, and scar tissue - all of which inhibit neuronal regeneration. Numerous immunomodulatory treatments for SCI have thus been investigated in animal models and clinical trials. For example, (i) expression of anti-inflammatory cytokines (IL-10 and IL-4) induces an anti-inflammatory phenotype in local macrophages, limits axon dieback, and promotes axon regeneration after SCI [14, 62]; (ii) Systemic and localized delivery of methylprednisolone (glucocorticoids) reduces leukocyte infiltration, decreases inflammatory cytokines, and protects oligodendrocytes from apoptosis after SCI [63] [64]; and (iii) monoclonal antibodies against CD11d reduce monocyte and neutrophil infiltration into the injured spinal cord [65].

In this study, I used lentiviral delivery to locally express anti-inflammatory cytokine IL-10 in the injured spinal cord. IL-10 is an anti-inflammatory cytokine that induces an M2 phenotype in macrophages via activation of the Jak1/STAT3 pathway and suppression of nuclear factor-kB (NF-kB), a transcription factor critical for pro-inflammatory cytokine production [66]. Numerous studies report IL-10 delivery at the injury site modulates inflammation and minimizes the secondary damages [62, 67-72]. Previous studies from our lab have shown IL-10 encoding lentivirus delivery drives sustained IL-10 expression for up to 28 days in the injured spinal cord. This treatment has been shown to influence the phenotype of infiltrating immune cells, suppress pro-inflammatory cytokine production, and promote motor recovery after SCI [14, 73]. In this dissertation (Chapter 3), I investigate the

combination of PLG bridge implantation and IL-10 delivery in an immunodeficient (Rag1) mouse cervical SCI model to modulate neuroinflammation and promote motor recovery by reestablishing the synaptic neural circuitry through the PLG bridge.

## **CHAPTER 2:**

### **Acute Biomaterial Bridge Implantation and Chronic Neural Stem Cell Transplantation to Facilitate Axonal Regeneration, Myelination, and Connectivity After Spinal Cord Injury**

#### **ABSTRACT**

Although injured axons can regrow and form connections below the level of injury, regeneration in the injured spinal cord is limited by physical and chemical barriers. Acute implantation of a multichannel poly(lactide-co-glycolide) (PLG) bridge can mechanically stabilize the injury site and provides a permissive environment for rapid cellularization and

robust axonal regrowth through this inhibitory milieu. However, our previous and in this study illustrate limited myelination of the regenerated axons. We have shown that human neural stem cells (hNSC) transplantation allows for axon remyelination, but hNSC fate is highly influenced by the SCI inflammatory microenvironment. Accordingly, we investigated the effect of the PLG bridge on innate immune cell infiltration time course *in vivo* and the combined effect of PLG and immune niche on hNSC fate *in vitro*. Last, we investigate the therapeutic outcome of the combination of PLG bridge implantation and hNSC transplantation *in vivo*. This study provides insight into the dynamics of the SCI innate inflammatory milieu in presence of an implanted PLG bridge, identifying modulation of the cellular inflammatory response. We demonstrated that PLG scaffold can influence hNSC fate choice and the response of these cells to inflammatory cues derived from innate immune cells, specifically by PMN & M $\phi$ . hNSC transplantation into the spared parenchyma in the chronic post-SCI period supported robust engraftment, migration, and differentiation, and revealed novel evidence for the extensive capacity of these cells to migrate into PLG bridge channels along regenerating axons, demonstrating integration into the host spinal cord as both myelinating oligodendrocytes and synaptically connected neurons. Beyond axon regeneration into and through the PLG bridge, we show novel evidence that axons in the PLG bridge form a synaptically connected circuit that includes ipsilateral forelimb muscle and is associated with motor recovery. hNSC transplantation significantly enhanced the total number of regenerating and myelinated axons identified within the PLG bridge. Furthermore, CRYM-GFP mice with reporter mT-mNSC transplantation showed evidence of donor cell-mediated CST myelination within the PLG bridge. Finally, the combination of acute bridge implantation and hNSC transplantation improved ipsilateral forelimb recovery

vs. hNSC transplant alone at 16 WPT. Together these data represent a highly novel approach to enhance neurorepair through a temporally layered approach using acute bridge implantation and chronic cell transplantation to spare tissue, promote regeneration, and maximize the function of new axonal connections.

## **INTRODUCTION**

Spinal Cord Injury (SCI) is a debilitating condition that results in paralysis due to neuron and oligodendrocyte cell death, axonal degeneration, loss of myelin, and a limited ability of the central nervous system (CNS) to regenerate. Currently, there are no promising therapies available to fully restore lost function following SCI. In contusion/compression SCI, translational research has focused on neuroprotective strategies to limit the initial expansion of injury. However, penetrating SCI, which accounts for a significantly smaller proportion of injuries (14% of cases in the general population and 28% of cases in the military population) [74], offers little opportunity to ameliorate the initial damage via acute neuroprotection. Penetrating injuries thus necessitate a different approach to restoring function; for example, reconnection of spinal pathways via a biomaterial bridge to support true axonal regeneration, as opposed to plasticity-based approaches.

Pathophysiological events that onset after the initial mechanical trauma cause further tissue degeneration and reactive astroglial scar tissue formation [7]. Contrary to the early beliefs that CNS axons cannot grow after injury, axons in the spinal cord do retain some growth potential; however, this potential is limited by the presence of inhibitory scar tissue, growth inhibitory molecules like chondroitin sulfate proteoglycans (CSPGs), and myelin-associated glycoprotein molecules [7] [75] [9] [76] [77] [2] [4]. Critically, over three decades

of research on SCI regeneration have made it clear that this multifactorial problem will require a combinatorial solution to support neuroprotection, axonal regeneration, and repopulation of CNS cells at the injury site [48] [26] [18]. We have previously reported that implantation of poly(lactide-co-glycolide) (PLG) bridge fills the defect and drives the axonal growth through an inhibitory milieu [16]. PLG bridge implantation mitigates axonal dieback, reduces secondary tissue degeneration, and minimizes scar formation [26]. PLG bridge architecture consists of micro-textured wall that allows for rapid ingrowth of cells that fill the space normally occupied by a cystic cavity, and linear longitudinal channels that guide the axonal regeneration into, through the PLG bridge and re-entering spared host tissue [48] [26] [18] [16].

Although numerous studies have investigated the regenerative potential of both natural and synthetic polymer-based biomaterials for SCI [78] [24] [79], few studies have shown regrowth of axons through the entire biomaterial [16] [80] [27]. Koffler et al. showed that host 5HT-labeled serotonergic axons regenerate into an empty 3D-printed scaffold and reach the caudal end of the channel; however, this study identified no improvement in functional recovery [27]. In contrast, we demonstrated improved functional recovery using the PLG bridge, which enables descending motor fibers, including the corticospinal tract (CST), to grow through the bridge and cross into the spared parenchyma below the implantation site [16]. However, only a small percentage of the regenerated axons in the PLG bridge were myelinated, an essential factor for efficient transmission of signals from the motor cortex to the spinal cord [40].

Endogenous stem cells are distributed throughout both the grey and white matter of the CNS and become activated in response to SCI [42] [81]. However, the capacity of these cells for remyelination after may be limited by both time and distance away from the injury epicenter [82] [83] suggesting that intrinsic capacity to contribute to repair within the bridge is insufficient. Transplantation of human neural stem cells (hNSC) is one clinically relevant alternative by which the myelination level of regenerating axons could be enhanced. Pre-clinical studies from our group have shown that subacute hNSC transplantation into SCI mice resulted in extensive hNSC-derived myelination and improved locomotor recovery [50], which was reversed by, selective ablation of the transplanted hNSC [17]. Accordingly, we sought to test the hypothesis that transplanted hNSCs have an ability to migrate into the channels of the PLG bridge and contribute to the myelination of newly formed axons to further enhance locomotor functional recovery.

While NSC transplantation studies are promising in terms of functional improvement, the timing and the post-SCI immune niche have a dramatic effect on NSC fate, migration, and functional integration, and consequently the overall efficacy of these cells after SCI [17]. Our previous studies have shown that the immune environment of the injured spinal cord is critical in determining hNSC fate, migration, and potential for repair [55] [56] [57]. Critically, we have previously performed immune profiling showing the presence of infiltrating F4/80+ macrophages and Gr-1+ neutrophils in the PLG bridge and alteration of associated secreted immune factors [84] [48] [14]. These data suggest that, if transplanted hNSC are capable of migrating into the PLG bridge, these cells will encounter an altered immune microenvironment.

In this report, we first establish the effect of the PLG bridge on the time course of the innate immune response after SCI (**Fig. 2.1A**). Next, we test the impact of infiltrating immune cells on hNSC fate *in vitro* using a conditioned media paradigm (**Fig. 2.1B**). Last, we investigate the therapeutic outcome of the combination of PLG bridge implantation and hNSC transplantation *in vivo* (**Fig 2.1C**), with an assessment of hNSC fate, axonal regeneration and myelination status, and locomotor recovery. The combination of PLG bridge implantation and hNSC transplantation *in vivo* resulted in enhancement of hNSC engraftment, axonal regeneration and myelination, and improved locomotor recovery. Additionally, we report novel evidence identifying formation of a synaptic circuit connecting corticospinal neurons and the forelimb neuromuscular junction. We further show donor human NSC navigated along regenerated axons to migrate into the bridge, differentiated into oligodendrocytes, and myelinated host axons. Finally, we show donor human-derived neurons in spared parenchyma integrate into mouse host circuitry, exhibiting synaptic connectivity. These data together suggest combining PLG bridge implantation with hNSC transplantation can modify and bypass inhibitory barriers to regeneration in the injury niche, paving the way for promising translational approaches to treat SCI.

## **MATERIALS & METHODS**

### **Ethics statements**

Animal care, behavior acquisition, and data analysis were performed by investigators blinded to experimental groups. All animal housing conditions, procedures, and animal care were approved by the Institutional Animal Care and Use Committee (IACUC): protocols AUP-

17-071, AUP 17-115. The University of California, Irvine Human Stem Cell Research Oversight Committee approved the usage of human neural stem cell line UCI 161 for in vivo transplants (UCI hSCRO protocol 2006-5294) and in vitro work protocol (UCI hSCRO 2007-5493).

### **Animal models**

In this study, three strains of mice were used, C57BL/6 (JAXmice # 000664, The Jackson Laboratory, Bar Harbor, ME), immunodeficient background Rag1 mice (JAXmice # 002216, The Jackson Laboratory, Bar Harbor, ME), and CRYM-ZsGreen1 transgenic mice (MMRRC\_036627-UCD). Profiling of the innate inflammatory microenvironment following SCI was performed in all adult female C57BL/6 mice (**Fig. 2.1**) and Rag1 mice (**Supplemental Fig. 2.1**). hNSC transplantation studies were conducted in female immunodeficient Rag1 mice at 11 to 20 weeks old (**Figs. 2.3-2.4**). Both male and female Crym-ZsGreen1 transgenic mice (9 to 15 weeks old) were used to transplant mT-mNSC. Mice were housed in cages with 2-5 cagemates. Mice with anatomical defects, surgical errors including bruising during clamping, incomplete or over hemisection injuries, transplantation injection errors, or poor health conditions such as infections, decreased activity, and significant weight loss, were excluded from the study. All the exclusions were made by the investigator blinded to experimental groups.

### **Fabrication of multiple channel bridges for in vivo implantation studies**

The poly(lactide-co-glycolide) (PLG) bridges were generated using a gas foaming/particulate leaching method as previously described [40], [18]. The final bridge

dimensions were 1.15 mm in length, 1.25 mm in width, and 2 mm in height, containing 9 channels.

### **Spinal cord injury**

A mouse C5 hemisection injury and postoperative care was performed as previously described [16]. Briefly, the mice were anesthetized using 2% isoflurane for 5 minutes before surgery. C5 laminectomies were performed to reach the C5 vertebrae of the spinal cord. All mice received unilateral 1-1.1 mm hemisection at the left side to remove the spinal cord segment (**Fig. 2.1A**), followed by immediate implantation of the PLG bridge or gelfoam (Pfizer, New York, NY) into the gap. Animals were randomly assigned to gelfoam and PLG bridge groups. The exposed muscle was sutured using 5-0 chromic gut, and the skin was closed using wound clips. All mice were placed in cages with clean Alpha-Dri bedding on top of heating pads at 37°C overnight. The following Subcutaneous injections were administered post-op: Baytril (2.5mg/kg) once a day for two weeks, lactated ringers (50mL/kg) once a day for five days, and buprenorphine (0.05mg/kg) every 12 hours for three days. Expression of bladders was done manually twice a day for the study duration. Since Rag1 mice are immunodeficient and CRYM-ZsGreen1 transgenic mice were on an immunosuppression paradigm, and to avoid bladder infections, rotating antibiotics were given for the duration of the study. This includes oral antibiotics dissolved in drinking water ciprofloxacin (10mg/100mL), Sulfamethoxazole/Trimethoprim (2mL/100mL), and ampicillin (20mg/mL) and rotated every two weeks.

### **Immune cell isolation post-injury and flow cytometric analysis**

To perform an innate immune cell time course following SCI in C57BL/6 mice (**Fig. 2.2**) and immunodeficient background Rag1 mice (**Supplemental Fig. 2.1**), we dissected spinal cord vertebrae C4-C6 (C5 hemisection injury with either gelfoam or bridge implantation) at time points 1 day post injury (DPI), 1week post injury (WPI), 4WPI, 8WPI and 26WPI. Spinal cord tissue was dissociated using mechanical and enzymatic methods as we previously described [85]. Next, we removed myelin debris from the cell suspension using Myelin Removal Magnetic Beads II kit (Miltenyi Biotec, Auburn, CA) using auto-MACS Pro Separator according to manufacturer instructions (Miltenyi Biotec, Auburn, CA). Cells collected after myelin removal were suspended in 0.85% ammonium chloride (diluted in sterile water) for five minutes to lyse red blood cells. The cell suspension was resuspended in PBS supplemented with 2% FBS (Thermo Fisher Scientific, Waltham, MA). Then the cells were stained with 7AAD viability dye (Thermo Fisher Scientific, Waltham, MA), CD45, CD11b, Ly6G, and CD68 antibodies as described [85]. The data was acquired using BD FACS Aria II Flow cytometer (BD Biosciences, Franklin Lakes, New Jersey) and analyzed with FlowJo software. To ensure detection of true positive signal for each fluorescence channel we used single stain compensation controls and fluorescence minus one (FMO) controls. Live cells (stained negative for 7AAD) were gated to analyze the number of CD45+CD11b+ myeloid events. These total myeloid cells were further gated to analyze the proportion of Ly6G+ve PMNs and CD68 +ve subpopulation. Antibody sources, and the dilutions were used as listed in **Table 1**.

### **PLG scaffold fabrication for in-vitro hNSC differentiation assays**

Poly(lactide-co-glycolide) (PLG) pellets are comprised of a 75:25 lactide : glycolide ratio, have molecular weight of 66,000-107,000, and inherent viscosity of 0.55-0.75 (Sigma-Aldrich Inc, Saint Louis, MO). PLG pellets were placed in a silicone mold (8 x 9 x 1mm diameter) and melted at high temperature (130°C). The liquid was compressed with a 1kg weight while the temperature was reduced 30°C every hour. Once the PLG cooled down to room temperature, PLG scaffolds were peeled from the mold and sterilized for in vitro experiments with 70% ethanol, followed by one wash with sterile water, and UV exposure in the laminar flow hood.

### **Generation of PMN or MØ condition media for hNSC in vitro fate analysis**

To test how immune cues impact hNSC after SCI in the Rag1 mice, we quantified the effect of innate immune cell conditioned media on hNSC fate *in vitro*. Polymorphonuclear leukocytes (PMNs) and macrophages (MØ) were isolated from peritoneal cavities of adult female Rag1 immunodeficient mice. Mice were stimulated with 12% sodium caseinate (i.p. injection) and were sacrificed either 12-16 hours (to collect PMNs) or 5-7 days (to collect MØ) post-injection (**Fig. 2.1B and Supplemental Fig. 2.2A-C**). PMNs and MØ (5,000,000 cells/ml) were cultured in hNSC differentiation media (DM). hNSC DM is X-vivo based media (Fisher Scientific, Waltham, MA) supplemented with bFGF (0.1 ng/mL), BDNF (PeproTech) (10 ng/mL), GDNF (10 ng/mL), Heparin (2 mg/mL), NAC (63 mg/mL), N2 (1:100), B27 (1:20) supplement and Ciprofloxacin (Cellgro) (10 mg/mL). PMN CM was collected only once after 24hrs in culture. MØ-CM was collected once a day for three days, and the culture was replenished with fresh media after each collection. Both condition media were diluted (1:1)

with fresh DM media and used for the hNSC differentiation experiments (UCI 161 cell line, passage 6).

### **hNSC line derivation and cell culture**

UCI 161 multipotent hNSC were derived from fetal brain tissue (gestational 16–20 weeks) and cultured as previously described [86]. Briefly, hNSC were fluorescence-activated cell sorting (FACS)-sorted to isolate the CD133+ stem cell population. The presence of the CD133 allows for enrichment of hNSC that have high neurosphere-generating capacity. After passage six the cells were grown as monolayers on poly-L-ornithine (PLO)/laminin (LAM) coated flasks. The cells were grown in hNSC growth medium (GM) consisting of X-VIVO 15 media (Fisher Scientific, Waltham, MA) supplemented with bFGF (20 ng/mL), EGF (2ng/mL), Heparin (2 µg/mL), NAC (63 µg/mL), N2 (10 µg/mL), and LIF (10 ng/mL). Cells were given fresh media twice a week and were passaged at 80% confluency.

### **hNSCs differentiation assays and fate analysis:**

hNSC were plated either on glass chamber slides coated with poly-L-ornithine (Sigma- 5 mg/mL) and laminin (Invitrogen- 10 mg/mL) (PLO/LAM) or on the PLG scaffolds were also precoated with PLO/LAM. hNSCs on both substrates were differentiated for 14 days in vitro (DIV) in presence of either PMN-CM, MØ-CM, or DM. hNSC fate analysis for neuronal marker Tubulin βIII (TubβIII), astrocytic marker glial fibrillary acidic protein (GFAP), and oligodendrocyte marker Olig2 were analyzed by immunocytochemistry (**Fig. 2.4-2.5**). hNSCs differentiated on glass and PLG scaffold were fixed with 4% paraformaldehyde at room temperature for 20 minutes. Cells were permeabilized and

blocked with 0.1% Triton X-100 (Sigma-Aldrich Inc, Saint Louis, MO) and 10% donkey serum (Jackson ImmunoResearch, West Grove, PA) in PBS. Next, cells were incubated with primary antibodies overnight and secondary antibodies for two hours in PBS supplemented with 10% Donkey serum. Antibody sources and the dilutions were used as listed in **Table 2.1**. Cells were counterstained with nuclear dye Hoechst 33342 (1:1000 dilution; Invitrogen, Waltham, MA). Images were captured using random sampling with a ZEISS Axio Imager II light microscope with an Apotome2 image processor (Zeiss, Oberkochen, Germany). Imaris software (Bitplane, Zurich, Switzerland) was used to quantify the hNSC fate. Image acquisition and quantification were conducted by researchers that were blinded. For analysis, three to five z-stack images were acquired per PLG scaffold and nine random images per PLO/LAM control. All experiments were conducted in biological quadruplicates.

### **Preincubation of PLG scaffold in MØ condition media and sequestration effect assessment**

Sterile PLG scaffold was incubated in MØ condition media (MØ-CM) at 37° C for 48 hours. Total protein concentration was quantified using Pierce BCA Protein Assay Kit (Thermo Fisher Scientific, Waltham, MA) in control groups (MØ-CM) and MØ-CM + PLG scaffold preincubation (MØ-CM-PLG). Next, we assessed how PLG scaffold affects C1q concentration in both groups using C1q ELISA kit (Hycult Biotech, Uden Netherlands) according to the manufacturer's instructions.

### **NSC transplantation**

RAG1 mice are an optimal model for xenotransplantation, as we have previously shown (FB 2020). Since CRYM-ZsGreen1 transgenic mice are immunocompetent, each animal received a combinatorial immunosuppression paradigm to ensure the donor cell engraftment as described in supplemental method 3. Four weeks post-injury/implantation (WPI), a second surgery was performed to transplant hNSCs in Rag1 mice and the mT-mNSC in CRYM-ZsGreen1 transgenic mice as previously described [56], [17], [50]. Once the location of C5 injury was re-exposed, a NanoInjector system and micromanipulator (World Precision Instruments, Sarasota, FL) and siliconized beveled glass micropipettes (bevel measurements: outer diameter = 100–110 mm and inner diameter = 70 mm) (Sutter Instruments, Novato, CA) were used for transplantation. A total of 75,000 cells or vehicle (X-Vivo media) contained in 1uL total volume was delivered at four sites, two rostral and two caudal to the injury, at 250nL per site (as shown in the schematic in **Fig. 2.1C**). All mice received post-operative care as described above. Mice within both injured groups (gelfoam and PLG bridge implantation) were randomly allocated to either receive vehicle or hNSC transplantation.

### **Pseudorabies virus (PRV) tracing**

PRV-152-GFP trans-synaptic tracer (2.48 X 10<sup>9</sup> pfu/ml; In collaboration with Dr. Xiangmin Xu laboratory, UCI) was injected into the ipsilateral (left) forelimb triceps muscle of the animals at 30 WPI. This allows for retrograde labeling of cortical pyramidal neurons and validation of functional connectivity after PLG bridge implantation. Following anesthesia (1.5% isoflurane in O<sub>2</sub> for 10 minutes), a skin incision was made to expose the left triceps forelimb muscle. Using a stereotaxic Hamilton syringe with a 26-gauge needle, 5 µL PRV was

injected into two sites of the left forelimb muscle at different depths with a five-minute wait period between each injection. The skin was closed using tissue adhesive Vetbond (St. Paul, Minnesota, USA). Animals were transferred to a Biosafety Level D room, where they received an injection of Carprofen (5mg/kg) and continued to receive bladder care twice a day. Four days post-PRV injection, mice were perfused, and the spinal cord segment (C3 to C7) and brain tissues were dissected for further analysis.

### **Perfusion, Tissue Collection, and Sectioning**

Mice were anesthetized using pentobarbital (100 mg/kg) and transcardially perfused with PBS (15 mL) and 4% paraformaldehyde (100 mL) at 16 WPT (hNSC differentiation fate and regeneration assessment) or 26 WPT (PRV connectivity tracing). Brain tissue and spinal cord segments corresponding to C3-C7 roots were dissected and post-fixed/cryoprotected overnight in 4% paraformaldehyde + 20% sucrose. The tissue was then flash frozen using -60°C isopentane and stored at -80°C. Brain tissue were transversely sectioned using a sliding microtome, and 30µm serial sections were collected in phosphate-buffered saline with 0.02% sodium azide and stored at 4°C until further use. C2-C8 spinal cord segments were embedded in Neg50 Frozen Section Medium (Fisher Scientific International, Hampton, NH) to be processed into 30µm thickness with a cryostat and Cryo-Jane tape transfer system (Leica Biosystems, Wetzlar, Germany). Spinal cords were sectioned either transversely or horizontally, and the slides were stored at -20°C until processed for immunohistochemistry.

### **Immunohistochemistry and imaging**

Spinal cord tissue sections slides (Cryo-Jane tape transfer slides) were dewaxed in Histo-Clear II clearing agent (National Diagnostics, Atlanta, Georgia) rehydrated in descending ethanol gradient (100%, 95%, 80% and 70%), and hydrated in distilled water for 10 minutes. For antigen retrieval, slides were incubated in preheated sodium citrate antigen retrieval solution (10 mM Sodium citrate, 0.05% Tween 20, pH 6.0) for 30 min at 96 deg C in water bath. Following a 20-minute cool down in room temperature, slides were rinsed in water and processed for immunohistochemistry as described below. Spinal cord sections (Cryo-Jane tape transfer slides) and brain sections (microtome, free-floating) were blocked (1.5% donkey serum and 0.1% Triton X in PBS) for 1 hour at room temperature and incubated with primary antibody (diluted in blocking solution) overnight at room temperature. Antibody information and dilutions are listed in Table 2.1. Following 3 five-minute washes (0.1% Triton-X 100 in PBS), tissue was incubated with appropriate fluorescent-dye conjugated secondary antibodies and nuclear dye Hoechst 33342 (1:1000 dilution; Invitrogen, Waltham, MA) for 2 hours at room temperature. Following 3 final five-minute washes (0.1% Triton-X 100 in PBS), slides were mounted with Fluoromount G (SouthernBiotech, Birmingham, AL). Images were captured using ZEISS Axio Imager II light microscope with an Apotome2 image processor and ZEISS LSM 900 with Airyscan 2 microscope (Zeiss, Oberkochen, Germany).

### **hNSC fate quantification in vivo**

For hNSC fate quantification, 16WPT transverse tissue sections (1/12 sampling series) were processed for immunohistochemistry for STEM121<sup>+</sup> (human cells cells), STEM121<sup>+</sup>/Olig2<sup>+</sup> (oligodendrocytes), STEM121<sup>+</sup>/DCX<sup>+</sup> (neuronal precursors) and

STEM121<sup>+</sup>/GFAP<sup>+</sup> (astrocytes) markers. An ApoTome microscope (Zeiss) microscope system and 20x objective were used to capture 30-40  $\mu\text{m}$  Z-stacks of optical slices in 2  $\mu\text{m}$  intervals. Migration of human cells in the rostral and caudal parenchyma was determined with unbiased stereology using systematic random sampling, an optical fractionator probe, and Stereo Investigator (MicroBrightField, Williston, VT). Although hNSC migration was observed throughout the isolated spinal cord section (collected from C2-C8 segments), stereological quantification was performed within a range of 2160 $\mu\text{m}$  rostral and 2160 $\mu\text{m}$  caudal to the injury epicenter (approximately C3-C7). Parameters for the analysis were as follows: grid size was 450  $\mu\text{m}$  x 450  $\mu\text{m}$ , frame size was 70  $\mu\text{m}$  x 70  $\mu\text{m}$ , and guard zone was two  $\mu\text{m}$ . Probe grid size and counting frame size were empirically determined to yield average cumulative error values <0.1. Because hNSC distribution was not homogeneous within the injury and sections were limited, individual injury section quantification was performed. All cells within the gelfoam/PLG bridge implantation injury site were manually quantified with StereoInvestigator version 2020.1.3 software (MicroBrightField, Williston, VT). On the intact, contralateral side of the injury, hNSC engraftment is robust and well distributed. Thus, applied systematic random sampling with StereoInvestigator was used for this quantification (version 2020.1.3 MicroBrightField, Williston, VT). Lastly, a Cavalieri probe (grid size, 20 x 20  $\mu\text{m}$ ) was used to estimate spinal cord lesion volume in (1/6 sampling interval) from horizontal spinal cord sections at 10x magnification.

### **Axonal regeneration and myelination quantification:**

To assess total regenerated and myelinated neurofilaments within the gelfoam and PLG bridge, we used transverse spinal cord tissue sections collected at 16 WPT. Since the

number of spinal cord sections with injury were limited, we used one section per animal n=5 to 6 animals/group collected at 16 WPT. Triple immunostaining was performed using NF-H (Neurofilament Heavy Chain, axonal marker), MBP (Myelin Basic Protein, pan myelination marker), and P0 (Myelin Protein Zero, Schwann cell myelin). For quantification, three to six random optical fields were imaged using Zeiss LSM 900 with Airyscan super-resolution microscope (Zeiss, Oberkochen, Germany). Antibody sources and the dilutions were used as listed in **Table 2.1**. For each optical field, 6  $\mu\text{m}$  Z stack images (0.4  $\mu\text{m}$  Z-step) were captured using 60X oil objective. 3D surface volume rendering was performed using Imaris v9.6 (Bitplane, Zurich, Switzerland). Briefly, all three volumes of total neurofilament, total MBP positive myelinated neurofilament, and total P0 positive myelinated neurofilament were masked using the Surface feature. To exclude excess noise, a filter was made to a minimum voxel size of around 1000 for each image. when masking the surface volumes. Next, the NF-H positive surface volume of neurofilament that was associated with the oligodendrocyte-derived myelin (MBP+P0- volume) and Schwann cell-derived myelin (MBP+P0+ and MBP-P0+) were masked using the object-to-object shortest distance (0.4  $\mu\text{m}$ ) filter in Imaris.

### **PRV quantification:**

Spinal cord tissue was collected at 30 WPI and sectioned horizontally at 30 $\mu\text{m}$  thickness using CryoJane. Immunostaining (1/6 sampling interval) was performed to detect PRV-GFP labeled fibers. All PRV+ fibers within the gelfoam/PLG bridge were counted manually. Brain sections were sectioned coronally at 30 $\mu\text{m}$  using a sliding microtome. Immunostaining (all sections containing motor cortex, no sampling) was performed to detect PRV-GFP cell bodies. All PRV+ cell bodies within the motor cortex were counted

manually. All quantifications were performed at 40X magnification using ZEISS Axio Imager II light microscope with an Apotome2 image processor by the investigators blinded to the experimental groups

### **Behavioral Testing and Locomotor Recovery Assessment**

All behavioral data were collected and analyzed by blinded observers. Mice were handled daily for two weeks prior to pre-injury behavioral testing to acclimate animals to human contact. Horizontal ladder beam and CatWalk Gait Acquisition were performed to quantify any changes in motor recovery and kinetic parameters after injury. For Rag1 mice, locomotor assessments were acquired at pre-injury and 16 WPT timepoints. The CRYM-ZsGreen1 transgenic mice locomotor assessments were acquired at pre-injury, 4 WPI (Pre-transplantation), and 12 WPT. Horizontal ladder beam: Following a five-minute acclimation to the environment, mice were recorded walking across a horizontal ladder beam for three trials. Video analysis quantified each left paw placement error, as previously described [87]. CatWalk Gait Acquisition: Following a five-minute acclimation, each animal performed three runs across the LED lighted glass stage of CatWalk XT (Noldus Information Technology Inc., Leesburg, VA). A successful run must contain ten consecutive steps, a consistent walking speed, and no paw placement on the stage walls. Runs were auto-classified using the CatWalk software version 10.1 [88]. Statistical Analysis of CatWalk data was conducted in R. Univariate two-way ANOVAS for the effect of bridge vs. gelfoam and hNSC vs. vehicle were performed using the aov function. Then, results were screened for variables that had a p-value  $\leq 0.05$  for either the effect of the bridge or the cells.

## **RESULTS**

### **Quantitative innate immune cell profiling in the presence of PLG bridge following SCI.**

We have previously shown that SCI is associated with a multiphasic immune cell response [58]. We have also shown that innate immune cells and immune proteins in the injury microenvironment modulate hNSC fate, migration, and potential for repair after *in vivo* transplantation [57], [56]. In parallel, consistent with its role as a biodegradable biomaterial, we have reported macrophages migrate to and help biodegrade the implanted PLG bridge. Critically, no deleterious effects of PLG are observed *in vitro* or *in vivo* after bridge implantation. Indeed, lactate, a PLG biodegradation product, has been implicated in polarizing immune cells towards tolerogenic phenotypes [88]. Accordingly, we first tested how PLG bridge implantation modulates the innate immune cell response within the bridge and surrounding spared spinal cord tissue at different time points following injury. We utilized a quantitative flow cytometry-based method to characterize this multiphasic response in a hemisection injury model for PLG bridge and gelfoam control implanted animals. **Figure 2.1A** shows how the injured spinal cord of C57BL/6 and in Rag1 mice (C4 to C6 cervical segment) was dissected and labeled for the myeloid population. Representative flow cytometry plots show the CD45+CD11b+ myeloid cells are further gated into the Ly6G+ neutrophils/PMNs and CD68+ macrophages/microglia subpopulations.

We investigated the numbers of total CD45+CD11b+ myeloid cells at 1 day post injury (DPI), as well as 1, 4, 8, and 24 weeks post injury (WPI). PLG bridge and gelfoam groups behaved similarly until 8 WPI; however, myeloid cells were significantly reduced in PLG vs. gelfoam mice at 24 WPI (**Fig. 2.2A**). We next investigated the proportion of neutrophils/PMN and MØ/microglia in the total myeloid population. As demonstrated previously after contusion

SCI in rodents [58], the epicenter environment was dominated by PMN in both gelfoam and PLG groups at 1 DPI (**Fig. 2.2B**) and PMN were dramatically reduced at 1 and 4 WPI. Similarly, there was a delayed re-emergence of the PMN population was observed at 8 and 24 WPI. This second phase of PMN infiltration was significantly reduced in PLG bridge vs. gelfoam mice (**Fig. 2.2B**). As expected from previous analysis in contusion SCI, MØ/microglia populations were sparsely detected at the 1 DPI (**Fig. 2.2C**) and exhibited a later peak in response. However, while the PLG bridge and gelfoam groups were similar at 1 WPI, the MØ/microglia subpopulation peak was significantly extended in PLG bridge vs. gelfoam control mice (**Fig. 2.2C**), consistent with the known role of macrophages/monocytes in PLG bridge degradation. Analysis of neutrophil and MØ/microglia populations as a ratio is a useful way to visualize the dynamic balance of these immune populations within the spinal cord [58], highlighting an enhanced neutrophil response in the gelfoam group (**Fig. 2.2D**) and an extended phase of macrophage/microglia recruitment in the PLG bridge group (**Fig. 2.2E**). Thus, the subacute/chronic injury time point of 4-24 WPI represents a window in which the PLG bridge modulates the cellular inflammatory response.

### **Modulation of hNSC fate in presence of PLG substrate and immune cues in vitro**

Studies have shown that the physical, mechanical, and biochemical properties of biomaterial scaffolds can influence NSC differentiation, neurite extension, and cell morphology, as well as change actin structure and focal adhesion molecules [89] [90] [91]. The potential for multipotent donor hNSC to elicit repair after transplantation is strongly linked to fate selection [17] [50] [57] [56]. Accordingly, we tested the effect of PLG vs.

PLO/LAM control substrate on hNSC fate, analyzing oligodendroglial (nuclear Olig2+), astroglial (GFAP+), and neuronal (Tubulin  $\beta$ III+) lineage selection (**Fig. 2.1B**).

In addition to physical, mechanical, and biochemical factors, innate immune cells and their secreted components within the microenvironment have been shown to influence the outcome of hNSC transplantation, resulting in changes in fate, migration, and efficacy [57] [56] [55]. We therefore also tested the effect of PLG on hNSC fate in the presence of innate immune cues, utilizing PMN and macrophage (M $\emptyset$ ) conditioned media (CM) (**Fig. 2.1B & Supplemental Fig. 2.2A-C**). In the presence of PLG, hNSC selectively clustered on the scaffold, and were not observed in the intervening spaces, leading to an alteration of the appearance of nuclei distribution (**Fig 2.3A-T**). However, PLG showed no significant effect vs. PLO/LAM on the total number of cells after 14 DIV in DM via nuclei count (Hoechst; mean $\pm$ SEM, PLO/LAM 219.4 $\pm$ 33.5, PLG 248.7 $\pm$ 30.3, unpaired t-test two-tailed P=0.5404; **Supplemental Fig. 2.2D**). Because of the effect of the PLG bridge on distribution of nuclei, cell fate was compared via analysis of fate proportion in captured images. As reported previously, both PMN- and M $\emptyset$ -CM suppressed oligodendroglial fate on PLO/LAM (**Figs. 2.3A-C, Fig. 2.3G**). While hNSC cultured on PLG scaffold exhibited a similar effect, PLG drove a highly significant increase in oligodendroglial fate under baseline conditions and rescued oligodendroglial fate under PMN- and M $\emptyset$ -CM conditions. Consistent with our previous observations [56], PMN-CM enhanced astroglial fate and suppressed neuronal fate, while M $\emptyset$ -CM had no effect on astroglial fate and enhanced neuronal fate. hNSC culture on PLG substrate modulated these effects, reducing astroglial fate at baseline and in response to PMN- and M $\emptyset$ -CM, and enhancing neuronal fate in response to PMN- and M $\emptyset$ -CM (**Fig. 2.3H-U**). In the presence of PLG, hNSC selectively clustered on the scaffold, and were not observed

in the intervening spaces, leading to an alteration of the appearance of nuclei distribution (**Fig 2.3A-T**). However, PLG showed no significant effect vs. PLO/LAM on the total number of cells after 14 DIV in DM via nuclei count (**Fig. 2.3V**). Collectively, these data indicate that PLG substrate alters hNSC fate at baseline and in response to immune cues.

The enhancement of baseline oligodendroglial fate, and suppression of astroglial fate, by culture on PLG scaffold vs. PLO/LAM suggests that direct signaling to hNSC via cell-substrate contact plays an important role in modulation of differentiation. However, PLG could also sequester soluble molecules contained within the differentiation media as well as in CM derived from these immune cell populations. We tested this possibility via a pre-incubation paradigm, focusing on oligodendroglial fate in response to MØ-CM as a read out. Treatment of hNSC cultured on PLO/LAM with MØ-CM collected after pre-incubation with PLG scaffold (MØ-CM-PI) produced a partial restoration of oligodendroglial fate (**Fig. 2.3Y**). In parallel, quantification of protein concentration in MØ-CM and MØ-CM-PI showed a reduction in total protein concentration (**Fig. 2.1W**). We have previously demonstrated that complement component C1q is a key mediator of the effects of PMN- and MØ-CM on hNSC fate, and that C1q neutralizing antibodies reverse the effect of CM on hNSC fate [57]. We therefore further tested for sequestration of soluble molecules by ELISA analysis of C1q protein levels present in MØ-CM cultures on PLG substrate, identifying an approximately 60% reduction in available C1q (**Fig. 2.3X**). Together, these data suggest that PLG scaffold modulates hNSC fate via both contact-mediated mechanisms as well as alteration of soluble components in the microenvironment.

**PLG bridge implantation supports robust hNSC engraftment in the spared tissue parenchyma rostral and caudal to the injury site.**

We have reported that immunodeficient models lacking T cells are required to enable both xenogeneic and allogeneic CNS engraftment at levels sufficient to analyze sustained effects of donor NSC in the host environment [17] [92]. These models are similar to the translational setting, in which allogeneic stem cell transplantation requires long-term administration of pharmacological immunosuppressants in humans, which similarly target lymphoid cells. Accordingly, these studies utilize Rag1 mice, which lack mature T and B cells but retain a functional innate immune cell response [93].

We first confirmed that the innate immune cell profile in Rag1 mice for the hemisection injury is similar to the profile of the C57BL/6 mice as shown in Figure 1 (**Supplemental Fig. 2.1**). As expected, Rag1 mice have fewer innate immune cells (CD45+CD11b+ cells) in comparison to C57BL/6 mice, since they lack T-cells which orchestrate the innate immune response (**Fig. 2.2A, Supplemental Fig. 2.1A**). Importantly however, PMN and MØ/microglia cell proportions closely paralleled that of C57BL/6 mice (**Fig. 2. 2D-E, Supplemental Fig. 2.1B-C**) after SCI, from 1 DPI through 24 WPI.

hNSC were transplanted into the spared parenchyma rostral and caudal to the gelfoam- or PLG bridge- implanted injury site, we therefore first evaluated hNSC engraftment, migration, and fate in these regions (**Fig. 2.4**), comparing these groups. Spinal cord transverse sections were aligned relative to the SCI epicenter and the distribution of transplanted cells at defined section distances was analyzed using unbiased stereology (**Methods, Fig. 2. 4A**). Coronal sections were stained for SC121 (human stem cell marker) to

reveal the distribution of transplanted cells (**Fig. 2.4B-B1**). There were no significant differences in the total number of engrafted donor hNSCs detected within the rostral and caudal segments or between the PLG and gelfoam groups (**Fig. 2.4C**). However, because the unilateral hemisection injury is localized to the left (ipsilateral) side of the spinal cord at the cervical C5 segment, the ipsilateral and contralateral sides of the tissue were further analyzed separately. In section analysis, the PLG group showed a trend towards an increased total number of transplanted donor hNSC, which reached significance at -720um rostral to the injury epicenter (**Fig. 2.4D**). This trend could be attributed to a consistent change in ipsilateral SC121+ human cell number in the PLG group (**Fig. 2.4E**). Conversely, analysis of contralateral SC121+ cell engraftment did not reveal consistent differences between the PLG and gelfoam groups (**Fig. 2.4F**). We investigated the effect of PLG bridge implantation on hNSC fate by quantifying the number of donor cells differentiating into oligodendrocytes (SC121+/Olig2+, **Fig. 2.4G**), neuronal precursors (SC121+/DCX+, **Fig. 2.4J**), mature neurons (SC121+/NeuN+, **Fig. 2.4M**), and astrocytes (SC121+/GFAP+, **Fig. 2.4P**). The PLG group showed significant ipsilateral increases in the total number of oligodendrocytes (**Figs. 4H-I**) and neuronal precursors (**Figs. 2.4K-L**). Ipsilateral increases in mature NeuN+ neurons were less pronounced, with a significant increase in the PLG group only at -720µM rostral to the injury (**Figs. 2.4N-O**). Interestingly, a significant ipsilateral increase in SC121+ human astrocytes was observed in the PLG group caudal to the lesion epicenter (**Figs. 2.4Q-R**). No consistent differences were observed for any of these human cell makers contralaterally (**Figs. 2.4I, L, O & R**). Overall, our results suggest that there is a selective ipsilateral increase in the number of transplanted hNSCs in the PLG group and that the combination of PLG scaffold implantation with hNSC transplantation results in a modulation of cell fate.

**hNSC preferentially localize within PLG bridge channels and exhibit tri-lineage differentiation.**

We investigated whether donor hNSC were competent to migrate into the gelfoam- or PLG bridge-implanted injury site (**Figs. 2.5A and B**). Because donor cell distribution was not homogenous within the gel foam and PLG bridge, we performed manual quantification for each tissue section. Few human cells were detected in the injury site of the gelfoam group (mean = 9 SC121+ cells/section; **Figs. 2.5A, A1 and C**). In contrast, the number of engrafted SC121+ cells quantified within the injury site exhibited a striking increase in the PLG group (mean = 145 SC121+ cells/section; **Figs. 2.5B, B1, and C**). SC121+ hNSC in the PLG group also exhibited differentiation into all three lineages (oligodendrocytes, neurons, and astrocytes) by 16 WPT. There were too few engrafted human cells for fate quantification in the gelfoam group. However, in the PLG group, cell fate analysis of SC121+ cells within the injury site identified 21.6% Olig2+ cells (**Figs. 2.5D and E**), 27.7% DCX+ cells (**Figs. 2.5D and F**), 8.45% NeuN+ (**Figs. 2.5D and G**) cells, and 24.9% GFAP+ cells (**Figs. 2.5D and H**). 17.19% of SC121+ cells were unlabeled for the tested markers (**Fig. 2.5D**). The combined percentages of the DCX+ and NeuN+ cells totaled to 36.25% (**Fig. 2.5D**), demonstrating that a majority of SC121+ cells in the PLG bridge differentiated along the neuronal lineage. hNSC were highly localized within the channels of the PLG bridge where the bundles of regenerated axons are present (**Fig. 2.5B, B1-2, and E**). While other cell types (e.g. fibroblasts, macrophages, Schwann cells, oligodendrocytes, and endothelial cells) localize to the porous bridge structure [48], as seen by the distribution of Hoechst 33342 labeling in Figure 5B, hNSC avoided these regions. These data demonstrate that hNSC in the bridge

differentiate into all three neural lineages, and that hNSC migrate into the PLG bridge along the same track as regenerating axons.

**Both total hNSC engraftment and the number of hNSC-derived oligodendrocytes are increased in the contralateral spared tissue in PLG bridge vs. gelfoam implanted mice.**

We have previously shown that PLG bridge implantation stabilizes adjacent spinal cord tissues [48]. We therefore sought to test whether spared spinal cord tissues exhibited differences in hNSC engraftment or fate, analyzing hNSC that engrafted in the spared tissue directly contralateral to the site of PLG bridge or gelfoam implantation. We applied systematic random sampling using the Stereoinvestigator optical fractionator probe and measurement of tissue area to estimate total cell number and corresponding differentiation fate. We identified a significant increase in the number of total engrafted SC121+ hNSC in the PLG group compared to the Gelfoam control (**Fig. 2.5I**). Similarly, there was a significant increase in the number of STEM121+/Olig2+ cells in the PLG group (**Fig. 2.5J**). While there was a parallel trend for an increase in the number of immature STEM121+/DCX+ cells ( $p$  value =0.06, **Fig. 2.5K**), this was not observed for either mature STEM121+/NeuN+ cells (**Fig. 2.5L**) or STEM121+/GFAP+ hNSC (**Fig. 2.5M**). Critically, the proportion of hNSC adopting different lineages was not significantly different between the PLG bridge vs. gelfoam groups (data not shown). These data suggest that the principal effect of the PLG bridge was on overall survival/engraftment of hNSC in the spared tissue, which is consistent with the stabilization of this region in the acute period after injury. This difference in engraftment cannot be ascribed to an increased volume but may rather reflect a change in the molecular microenvironment and/or mechanostability of this region.

## **hNSC within PLG bridge channels exhibit altered fate vs. contralateral spared tissue in SCI epicenter sections.**

In previous studies using contusion SCI models, we have shown that hNSC do not exhibit migration into the SCI epicenter; hNSC that are localized adjacent to the SCI epicenter are directed towards the astroglial lineage [56], [17], [50]. As described above, hNSC that migrated along the PLG channels exhibited differentiation into human oligodendrocytes, neurons, and astrocytes, retaining tri-lineage potential. Here, we asked whether the fate of hNSC that migrated into the PLG bridge and inflammatory environment of the SCI epicenter was similar to or different from the adjacent spared tissue. hNSC that migrated into the PLG bridge were less likely to exhibit oligodendroglial lineage selection (STEM121+/Olig2+; **Fig 2.5N**), and more likely to exhibit neuronal lineage selection (STEM121+/DCX+; **Fig 2.5O**), than hNSC the engrafted in contralateral spared tissue in the same tissue sections. In contrast, mature neuron (STEM121+/NeuN+) and astroglial (STEM121+/GFAP+) proportions were unchanged (**Fig. 2.5P-Q**). These data are consistent with the observation that the PLG bridge is dominated by macrophages in the chronic post-SCI phase (**Fig. 2.2; Supplemental Fig. 2.1**), and the influence of PLG and macrophage-derived immune factors on hNSC fate selection (**Fig. 2.3**).

## **hNSC transplantation combined with PLG bridge implantation enhances axonal regeneration and evidence of myelination by human oligodendrocytes**

We next investigated axon regeneration and myelination status in these mice by immunostaining gelfoam and PLG-implanted spinal cord tissues for neurofilament (NF-H).

Consistent with our previous reports describing regeneration of both descending motor and ascending sensory axons, NF-H+ fibers were readily observed entering bridge channels at both the rostral (**Fig. 2.6A & 6A1**) and caudal (**Fig. 2.6A & 6A2**) margins by 6 weeks post-injury and bridge implantation (WPI). In contrast, even by 20 WPI, gelfoam implantation failed to support significant growth of NF-H+ fibers into the injury site (**Fig. 2.6B-6B1**), whereas PLG bridge implantation resulted in robust regeneration of NF-H+ axons within the bridge (**Fig. 2.6C-2.6C1**). We used triple label immunohistochemistry (**Fig. 2.6D and 2.6E**; NF-H green, MBP red, P0 blue) and Imaris 3D surface rendering to quantify the total volume of NF-H+ axons (**Fig. 2.6E and E2 inset**), as well as the proportions of axons which were either unmyelinated (**Fig. 2.6D and D1 inset**) or myelinated by MBP+P0- oligodendrocyte (**Fig. 2.6E and E1 inset**), MBP+P0+ Schwann cell (**Fig. 2.6D and D2 inset**) and P0+ Schwann cell (**Fig. 2.6E and E1 inset**) populations. Proportional analysis of NF-H+ axon volume suggested that hNSC transplantation altered both total NF-H+ and the myelination status of these axons (**Fig. 2.6F**). To quantitatively assess this effect, Imaris volumetric data for the PLG bridge alone vs. PLG bridge + cell groups were normalized to gelfoam + vehicle controls (**Fig. 2.6G-I**). The presence of hNSCs enhanced total axonal regeneration (**Fig. 2.6G**), and significantly increased both oligodendrocyte-derived (**Fig. 2.6H**; MBP+P0-) and Schwann cell-derived (**Fig. 2.6I**; MBP+P0+ plus MBP-P0+) myelination.

Although histological quantification was predominantly performed at 16 WPT, a subset of animals was assessed at 26 WPT. We hypothesized that this additional engraftment time would optimize for the maturation and integration of transplanted hNSC as myelinating cells within the PLG bridge. We therefore tested whether hNSC that entered the bridge channels (white dotted lines in **Fig. 2.6J**) were capable of myelinating regenerated axons. Indeed,

there was an abundant association of SC121+ hNSC labeling aligned with and in close proximity to NF-H+ axons (**Figs. 2.6J, arrowheads**). Further, high magnification clearly identifies MBP+/STEM121+ co-labeling of NF-H+ axons (**Figure 2.6K**), indicating that hNSC contributes to myelination of axons that regenerate into PLG bridge channels.

We sought to confirm this observation, as well as to test whether donor hNSC myelinated regenerating descending motor axons. We previously reported that CRYM reporter mice can be used to specifically visualize CST axons in the spinal cord [16], including in the PLG bridge after SCI. Here we used CRYM-ZsGreen1 transgenic mice for this purpose (**Supplemental Fig. 2.3A**, see supplemental methods). Because fully functional myelin is compact, resulting in the exclusion of oligodendrocyte cytoplasm [17], we derived NSC from mice that ubiquitously express a membrane-targeted fluorescent tandem dimer Tomato (tdTomato) reporter (mT-mNSC) [42] (**Supplemental Fig. 2.3B, see supplemental methods**). This approach allowed mature, compact myelin from donor mT-mNSC to be visualized in association with regenerated CST axon targets within the PLG bridge. We employed pharmacological immunosuppression for these allogeneic transplants because CST-GFP reporter mice were not on a constitutively immunodeficient background. While this resulted in reduced mT-mNSC survival and migration in comparison with transplantation into Rag-1 mice, we were able to identify mT-mNSC aligning with and ensheathing NF-H+ (**Figure 2.6L**) and GFP+ CST (**Figure 2.6M**) axons in the PLG bridge. Orthogonal projection clearly indicated that mT-mNSC fully surrounds GFP+ CST fibers (**Figure 2.6M**, blue arrowhead).

## **Connectivity assessment of CST tract regeneration using transsynaptic pseudorabies virus (PRV) tracing (or transneuronal circuit analysis using pseudorabies virus)**

An advantage of this model is that axons detected within the implanted PLG bridge cannot represent spared fibers, they must regenerate into the channels. However, observation of axons, even CST reporter axons, in this region does not mean that these fibers have integrated into synaptic circuitry. We sought to test this key aspect of regeneration via pseudorabies virus (PRV) transsynaptic tracing. We injected GFP-reporter PRV virus into the forelimb triceps muscle ipsilateral to the SCI hemisection (**Figure 2.1C**). PRV is retrogradely transported from the neuromuscular junction, sequentially infecting synaptically connected neurons to enable circuit tracing; we sought to use this method to identify whether neuronal wiring between injected muscle cells, spinal motor neurons, and sensorimotor cortical pyramidal neurons is re-established in this paradigm. Approximately 90% of CST axons originating from sensorimotor cortical pyramidal neurons decussate at the level of the pyramids. Thus, if CST motor axons have regenerated through the implanted PLG bridge and formed synaptic connections with spinal motor neurons, PRV should be visualized in the contralateral motor cortex. In contrast, some brain nuclei (e.g. the paraventricular nucleus of the hypothalamus, PVN), would be expected to exhibit ipsilateral predominance of retrogradely labeled axons.

PRV transsynaptic tracing was validated by injection into the triceps of 2 month old naive (uninjured) mice, demonstrating a majority of labeling in contralateral motor cortex pyramidal neurons (**Supplemental Fig. 2.4A, A2**), sparse labeling in ipsilateral cortex pyramidal neurons (**Supplemental Fig. 2.4A and A1**), and predominant ipsilateral labeling

of the PVN (**Supplemental Fig. 2.4A, A3-4**). These data are consistent with previous reports of PRV circuit tracing [94], [95], [96], [97], [98]. Because of the chronic nature of the stem cell transplants and analyses in these experiments, we further validated PRV tracing in this injection paradigm in 10 month old naive mice (**Supplemental Fig. 2.4B**). Surprisingly, we found a reduction of retrograde PRV labeling in 10 month old naive mice (**Supplemental Fig. 2.4B, B1-3**), suggesting that age impacts PRV labeling efficiency. This result could reflect a loss of initial viral infection efficiency at the muscle, shift in the efficiency or timeline of retrograde viral transport, weakening of synaptic connections in the spinal cord, or other factors [99].

We next assessed PRV transsynaptic tracing in lateral hemisectioned spinal cords within the injury site as well as in the contralateral and ipsilateral motor cortex at 26 WPT (30WPI). At this experimental time point, the mice are ~10 months of age. Similar to NF-H staining (**Fig. 2.6B**), PRV labeling was not detected in the spinal cord injury site of the gelfoam group (**Fig. 2.7A, A1**). In contrast, robust PRV labeling was detected in regenerated axons within the channels of the bridge itself (**Fig. 2.7B, B1-3**), as well as crossing the rostral and caudal margins of spared spinal tissue in apposition with the PLG bridge (**Fig. 2.7B, B4-5**). Critically, GFP+ PRV labeling was identified in choline acetyltransferase (ChAT) motor neurons (**Supplemental Fig. 2.4D**), consistent with formation of a spinal motor neuron relay circuit. Finally, GFP+ PRV labeling was not observed in CGRP+ sensory fibers (**Supplemental. Fig2. 4E**). Quantification of PRV labeled axons within the injury site identified a significant number of GFP+ PRV fibers in both PLG bridge groups vs. gelfoam groups (**Fig. 2.7C**). Parallel analysis in the motor cortex revealed a significant number of

GFP+ PRV labeled cell bodies in the contralateral motor cortex in PLG bridge vs. gelfoam groups (**Figs. 2.7D & E**). Occasional GFP+ PRV labeling was observed in the ipsilateral motor cortex of PLG bridge, but not in gelfoam, groups (data not shown). Surprisingly, transplanted hNSC in the spinal cord were also identified by GFP+ PRV labeling, suggesting stable integration of these donor cells into host circuitry (**Fig. 2.7G**). Overall, these data confirm the connectivity of the regenerated axons from the motor cortex through the PLG bridge and caudal to the injury epicenter and connected to the forelimb muscle.

### **Locomotor recovery assessment using CatWalk and ladder beam analysis**

Lastly, we tested the effect of PLG bridge implantation alone or in combination with hNSC on the recovery of forelimb function. Mice were assessed for locomotor recovery using the horizontal ladder beam and CatWalk kinematic function tasks as previously described [16] [87] [100] [101]. Missed placements of the left (ipsilateral) forelimb on a horizontal ladder (**Figure 2.8A**) was quantified at pre-injury, 4WPI (pre-transplantation), and 20WPI (16 WPT) timepoints. As described under methods, mice were randomly distributed into gelfoam vs. PLG bridge groups at the time of initial surgery, and into the PLG alone vs. PLG + hNSC groups on the day of transplantation. No significant differences in ladder beam performance were observed between any groups either pre-injury (group means  $\pm$ SEM:  $8.0 \pm 0.66$ ,  $7.6 \pm 0.52$ ,  $8.9 \pm 0.65$ , and  $8.3 \pm 0.51$  for Gelfoam + Vehicle, Gelfoam + Cells, Bridge + Vehicle, and Bridge + Cells group respectively; One-way ANOVA  $P=0.4199$ ) or pre-transplant (group means  $\pm$ SEM:  $87.53 \pm 1.2$ ,  $88.2 \pm 1.5$ ,  $85 \pm 3.4$ , and  $83.6 \pm 2.7$  for Gelfoam + Vehicle, Gelfoam + Cells, Bridge + Vehicle, and Bridge + Cells group respectively; One-way ANOVA  $P=0.4879$ ). We have previously reported that PLG bridge implantation requires a minimum

of 10-12 weeks post-implantation to observe functional recovery on this task, consistent with a requirement for regeneration into and through the bridge [16]. Similarly, we have also reported that hNSC transplantation requires a minimum of 12-16 weeks to observe functional recovery on this task, consistent with a requirement for donor cell migration and differentiation to enable repair [17], [102], [103]. We were therefore most interested in locomotor function at 16 WPT, at which time both the PLG bridge alone and hNSC alone groups showed a significant decrease in errors (**Fig. 2.8B**). Mice receiving the combination of PLG bridge and hNSC transplantation demonstrated tremendous improvements in the number of ipsilateral paw placements (**Fig. 2.8B**). The combinatorial approach significantly enhanced locomotor recovery compared to the hNSC only group and showed a similar trend towards enhancement compared to the bridge alone (**Fig. 2.8B**). These data suggest that bridge implantation combined with hNSC transplantation could exert a synergistic effect on functional recovery since the presence of PLG bridge to support the axonal regeneration and stem cells to myelinate the regenerating axons are both required. Critically, while behavioral data were collected at 16 WPT, a small number of animals were carried to 26 WPT for analysis of histology and PRV (**Fig. 2.1C**). Identification of evidence for hNSC myelination of host axons in PLG bridge channels (**Fig. 2.6J-K**) and hNSC integration into host circuitry (**Fig. 2.7F**) at this later time suggests that later time points of locomotor analysis could capture the full potential for synergistic repair; however, age-related health declines in the constitutively immunodeficient mouse model required for these experiments is a limiting factor.

We also conducted a kinematic stepping assessment using CatWalk gait analysis, applying an unbiased multivariate approach to test whether the effect of PLG bridge implantation on

locomotion could be separated from that of hNSC transplantation on locomotion. This approach avoids a priori assumptions about which variables are meaningful to recovery. Univariate two-way ANOVAS were conducted in R using the aov function to analyze the independent effects of bridge implantation and cells transplantation, identifying variables that had a p-value  $\leq 0.05$  (**Fig. 2.8C**). Bridge implantation and hNSC transplantation exhibited no overlap in the subset of variables identified in this analysis. hNSC transplantation altered four variables, three of which related to contralateral (right) forepaw movement. In contrast, PLG bridge implantation altered six variables, five of which related to ipsilateral (left) hind or forepaw movement. These data suggest distinct and parallel mechanisms for locomotor recovery, in which PLG bridge implantation exerts a predominant effect at the injury site, whereas hNSC transplantation exerts a predominant effect on the intact side of the spinal cord.

## **DISCUSSION**

In the present study, we show that PLG alters the infiltration and time course of innate immune cell recruitment to the injured spinal cord *in vivo* and modulates hNSC fate in response to these cues *in vitro*. We further show that the presence of a PLG bridge affects hNSC engraftment, migration, survival, and differentiation *in vivo*. Ultimately, this study highlights the impact of hNSC engraftment on regeneration and myelination, the importance of PLG bridge on the reestablishment of synaptic circuitry, and the effect of the combinatorial approach on improvement in locomotor recovery.

PLG bridge implantation altered the innate immune response after SCI. Overall, we identified an enhanced neutrophil response in gelfoam controls and an extended phase of

macrophage/microglia recruitment in the PLG bridge group, consistent with the known role of the MØ population in phagocytosis and biodegradation of PLG in vivo [88] [104].

Analysis of myeloid cell infiltration in both C57BL/6 and Rag1 mice enabled comparison of the innate immune response in intact vs adaptive immune response suppressed models. PMN and MØ proportions were similar between the C57BL/6 and Rag1 mice in both gelfoam control and PLG bridge groups, demonstrating that innate immune responses are in essence conserved between these models, which would be similar to pharmacological immunosuppression in humans.

Given the impact of PLG bridge on innate immune cell time course, and the effect of innate immune cells on hNSC fate in vitro and in vivo [57] [56], we next assessed the effect of PLG bridge on hNSC fate in the absence or presence of immune cues. Consistent with the goal of testing hNSC transplantation as a means to enhance the remyelination of regenerated axons in the PLG bridge, PLG enhanced oligodendrocytic fate both in baseline media and in the presence of inhibitory immune cues. In parallel, PLG increased neuronal fate and decreased astrocytic fate under these conditions. The effect of PLG scaffold on hNSC fate could be mediated by several mechanisms. One of these could be by altering the bioavailability of factors secreted by immune cells or hNSCs in the condition media, as we demonstrate for C1q. However, the physical, mechanical, and biochemical properties of biomaterial scaffolds may also affect NSC differentiation and behavior [105] [106] [89] [90] [91]. For example, scaffold physical cues, such as stiffness, peptide affinity, and peptide density have been shown to affect key cellular properties such as morphology, neurite extension, change in actin structure and focal adhesion assembly that may lead to alterations

in fate decision [88] [107]. Together, these data suggest that the PLG bridge supports an immune microenvironment that is conducive to not only regeneration, but an adventitious modulation of stem cell fate

The presence of the bridge creates a novel niche at the SCI epicenter for both regenerating axons and infiltrating cells. We have shown that the bridge channels and porous micro-textured walls cellularized the injury site by enabling ingrowth of endogenous cells such as macrophages, Schwann cells, fibroblasts, and endothelial cells that integrate the PLG bridge with the spinal cord [48]. These cells in the PLG bridge deposit growth-promoting ECM and growth factors in the channels [18], providing directional cues for axons that traverse the channels. While this is a regeneration supporting environment, it does not appear to be a robustly remyelination supporting environment, and we observed only ~6.5% of axons in the PLG bridge to be associated with oligodendrocyte derived myelin. In contrast, the proportion of myelinated axons in healthy rodent spinal cord has been estimated at 40-60% ([88] [44]). Consistent with the need for efficient conduction and functionality in long tract projections, CST axons exhibit an even higher myelination proportion, with approximately 86% myelinated in rodents, and 99% in humans [88], [108]. Critically, even though the endogenous stem cell pool contains cells capable of myelination and that are distributed throughout the spinal cord, become activated and divide extensively in response to the SCI [81], these cell populations steadily decline by 4WPI [88] [109] [83]. This timeline suggests that the endogenous progenitor response to the injury goes quiescent before axonal regeneration is achieved through the PLG bridge, identifying a temporal mismatch that would require either reactivation of the progenitor pool or addition of an exogenous myelinating cell.

Therefore, we strategized to target chronic transplantation of a very active and highly migratory NSC enriched population (not progenitor cells). We transplanted NSCs at 4WPI for the following reasons, Firstly, by 4WPI axons enter and extended into the channels of the PLG bridge and we predicted that these newly formed axons would strongly cue hNSC to migrate and undergo oligodendroglial lineage selection, enabling myelination of axons in the PLG bridge [88]. Second, at four weeks, the injury environment is dominated by the macrophage population rather than PMNs, as seen in Figure 2.2. As discussed above, macrophage cues, when combined with PLG, promote neuronal and oligodendrocytic fates while reducing the scar-forming astrocytic fate (**Fig. 2.3**). Finally, this a more clinically relevant time period for delivery of cellular therapies in humans, enabling both improved informed consent and a more medically stable population given the requirement for immunosuppression in an allogeneic transplant setting, minimizing serious adverse effects [110].

Consistent with our previous studies, transplanted hNSC migrated extensively in the spared parenchyma. PLG bridge implantation increased the total number of engrafted hNSC ipsilateral to the bridge for all three lineages vs. gelfoam control. This increase in ipsilateral engraftment may be due to increased mechanostability and tissue sparing adjacent to the injury site after bridge implantation, as we have reported previously. It is also possible that the pro-regenerative environment driving axon regeneration into the PLG bridge influenced hNSC engraftment. Most importantly, donor hNSC preferentially associated with regenerating axons, migrating selectively within PLG bridge channels, and distributing throughout the length of the bridge. hNSC transplantation improved axonal regeneration as well as both Oligo- and Schwann-derived myelination in the PLG bridge. Our data show that

hNSC-derived oligodendrocytes contributed directly to myelination of mouse host axons; we confirmed this finding using membrane reporter mT-mNSC transplantation in transgenic CRYM-CST reporter mice, identifying migration of mT-mNSC into the channels of PLG bridge and ensheathment of CST axons. Importantly, however, hNSC do not generate Schwann cells, thus the presence of Schwann-cell derived myelin demonstrates that participation of endogenous progenitors in the baseline myelination response, In this regard, enhancement of both axon number and Schwann cell-derived myelin in hNSC transplanted animals suggests that these cells may also secrete trophic factors that promote host axon regeneration and myelination by endogenous progenitor cells [110], [111], [49], [112]. This is the first report illustrating that donor NSC are capable of migrating along axons regenerating into a biomaterial scaffold and contributing to myelination of those axons. Critically, we have previously shown that hNSC transplanted directly into the SCI epicenter become fate locked to generate astrocytes inside and proximal to the lesion site [113]. In contrast, few human astrocytes were observed within or adjacent to the PLG bridge. These data thus also suggest that multipotent hNSC that enter the PLG bridge follow a beneficial developmental program after transplantation, exhibiting the capacity to follow newly grown axons long distances and differentiation in a lineage appropriate manner.

We previously reported CST axons can regenerate through an implanted PLG bridge. Here, PRV tracing demonstrates CST axons that traverse the PLG bridge become synaptically connected to the ipsilateral forelimb muscle below the level of injury. This is the first report demonstrating the reestablishment of synaptic neural circuitry of any kind between the brain and neuromuscular junction after SCI via regeneration through a biomaterial bridge alone; previous electrophysiology studies have not demonstrated evidence of a synaptic

circuit after long term bridge implantation without either cell transplants or pharmacological manipulations [27] [114]. Critically, analysis of PRV also identified that hNSC-derived neurons also integrated into mouse host spinal synaptic circuitry by 26WPT. These data again suggest that multipotent hNSC that enter the PLG bridge do not become fate locked to the astroglial lineage, but rather exhibit the potential to integrate in host circuitry via differentiation to not only myelinating oligodendrocytes and neurons.

Intriguingly, while hNSC transplantation resulted in an increase in the NF-H volume of axons within the PLG bridge, the number of PRV-labeled axons within the bridge and PRV-labeled cell bodies in the motor cortex was unchanged. Several parameters are important to consider in interpreting these results: 1) hNSC may not enhance the synaptic connectivity of these fibers but instead contribute to the improvement in myelinating these functional axons in the PLG bridge; 2) The presence of hNSC in the spinal circuitry may led to an increase in the number of synapses formation below the level of injury, which may need a longer period of mice survival after PRV injection for the virus to sequentially infect the synaptically-connected neurons and reach the motor cortex, 3) factors secreted by the engrafted hNSC may enhance the recruitment of descending axons from brainstem areas into the bridge. Brainstem motor pathways including reticulospinal- and rubrospinal tracts play a major part in controlling rodent locomotion [115].

Achieving efficacy after hNSC transplantation in the chronic period post-SCI is generally thought to be a challenging target. A key question is the functional impact of combined acute PLG bridge implantation and chronic hNSC transplantation on locomotor recovery. The observed motor recovery in the bridge implantation only group is consistent

with our previous reports, and the pro-regenerative impact of the PLG bridge and rewiring the severed circuitry. We have not previously tested the potential for hNSC to mediate locomotor recovery in a partial transection SCI model, however the observed improvement is consistent with our previous reports in contusion SCI. While the chronic hNSC transplantation paradigm employed in this study is not consistent with acute sparing as a mechanism for repair, these data do suggest that hNSC contribute to repair via pleiotropic mechanisms.

hNSC transplanted in the absence of a PLG bridge were confined to the spared tissue above and below the lesion, and the region contralateral to the lesion site. Similarly, no axonal regeneration occurred through the injury site in the absence of bridge implantation. Thus, recovery in this group had to have been mediated by mechanisms that did not involve either regeneration of axons or myelination of those axons. In this context, alternative mechanisms of repair could include: (i) Strengthening of undamaged intact motor circuitry rostral to the lesion. Spinal motor neuron columns innervating the forelimb muscles range from C2-T1, with a majority spanning the C5 spinal segment [116]. As we show, this leads to significant motor function deficits (90% loss of placement in gelfoam + vehicle control animals) after a C4/C5 lesion. However, while insufficient to maintain function in animals that receive neither a bridge or cell transplants, there will be motor neuron sparing within the C2-C3 region; hNSC in the absence of bridge implantation could potentially enhance this spared circuitry. (ii) While there is a failure of regeneration through the lesion site in the absence of an implanted PLG bridge, it is known that this lesion produces significant sprouting and reorganization of descending motor tracts, including increases in crossing fibers by CST [117, 118]. Thus, enhancement or modulation of these compensatory

connections by transplanted hNSC contralateral to the lesion, or in the ipsilateral regions above and below the lesion, could also improve outcome. In this regard, studies have shown that as a consequence of secondary tissue degeneration following hemisection spinal cord injury, oligodendrocytes die due to apoptosis and spontaneous demyelination of intact axons on the contralateral side, and a decline in conduction of these axons [119, 120]. Our results indicate an increase in oligodendrocytic fate in the tissue contralateral to the injury suggesting that hNSC may in part support motor recovery by remyelinating and strengthening these spared axons. Consistent with a pleiotropic effect of hNSC in this model, kinematic analysis suggested that motor recovery in the combination group is mediated in part through parallel mechanisms, in which bridge implantation supported recovery of the ipsilateral side whereas hNSC treatment supported improvement on the contralateral side. Critically, motor recovery observed in the hNSC transplantation group was further improved by combination with acute PLG bridge implantation, suggesting an additive or synergistic effect, perhaps via remyelination of regenerating axons. Importantly, PRV synaptic tracing indicated evidence of hNSC integration into synaptic circuitry at 26WPT, as well as additional evidence of donor myelin in the host axons. Together, these data suggest that an extended study timecourse may be necessary in order to the full potential for synergistic repair.

Overall, this study provides insight into the dynamics of the SCI innate inflammatory milieu in presence of an implanted PLG bridge, identifying modulation of the cellular inflammatory response. We demonstrated that PLG scaffold can influence hNSC fate choice and the response of these cells to inflammatory cues derived from innate immune cells, specifically by PMN & M $\phi$ . hNSC transplantation into the spared parenchyma in the chronic post-SCI period supported robust engraftment, migration, and differentiation, and revealed

novel evidence for the extensive capacity of these cells to migrate into PLG bridge channels along regenerating axons, demonstrating integration into the host spinal cord as both myelinating oligodendrocytes and synaptically connected neurons. Beyond axon regeneration into and through the PLG bridge, we show novel evidence that axons in the PLG bridge form a synaptically connected circuit that includes ipsilateral forelimb muscle and is associated with motor recovery. hNSC transplantation significantly enhanced the total number of regenerating and myelinated axons identified within the PLG bridge. Furthermore, CRYM-GFP mice with reporter mT-mNSC transplantation showed evidence of donor cell-mediated CST myelination within the PLG bridge. Finally, the combination of acute bridge implantation and hNSC transplantation improved ipsilateral forelimb recovery vs. hNSC transplant alone at 16 WPT. Together these data represent a highly novel approach to enhance neurorepair through a temporally layered approach using acute bridge implantation and chronic cell transplantation to spare tissue, promote regeneration, and maximize the function of new axonal connections.

## **SUPPLEMENTAL METHODS**

### **CRYM-ZsGreen1 transgenic mice derivation**

The transgenic CRYM-ZsGreen1 mice were generated by crossing the *Crym*<sup>cre</sup> transgenic mice (MMRRC\_036627-UCD) with the Ai6 mice that contain a CAG promoter-driven enhanced green fluorescent protein variant (ZsGreen1) (JAXmice # 007906, The Jackson Laboratory, Bar Harbor, ME). Mu-Crystallin (*Crym*) is expressed in a diverse array of tissues, including layer V-VI of motor cortex in the brain; we have demonstrated that reporter expression is localized exclusively to CST axons in the spinal cord [16]. Cre

recombinase-mediated excision of a floxed STOP enabled the expression of CrymCre:ZsGreen1 specifically in CST axons in the spinal cord.

### **mT-mNSC Line Generation and Cell Culture**

mT-mNSC were collected from 24 Gt(ROSA) 26 Sor tm4(ACTB-tdTomato,-EGFP)Luo/J mice (JAXmice #007576, The Jackson Laboratory, Bar Harbor, ME). mT-mNSC were isolated from the embryo cortices of embryonic day 11-12 (E.11-12) mice as previously described [55]. mT-mNSC ubiquitously expresses a membrane-targeted tdTomato reporter [42], which allows for visualization and identification of donor cell-derived myelin within the PLG bridge. mT-mNSCs were cultured as previously described (**Fig. 2.6**) [55].

### **Immune suppression in CRYM-ZsGreen1 transgenic mice:**

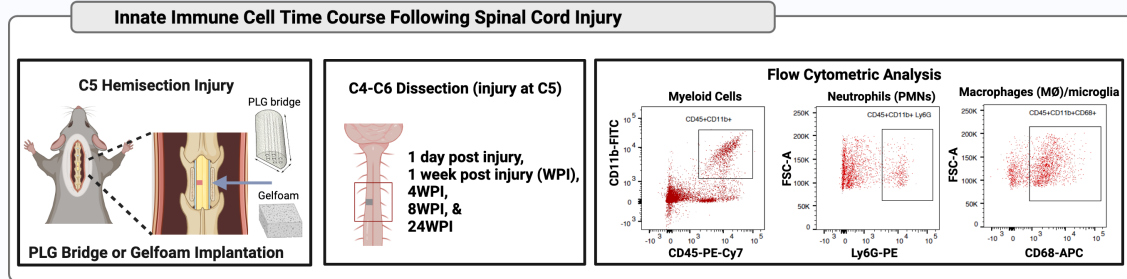
To block the T-cells mediated allograft rejection of mT-NSCs in the CRYM-GFP immunocompetent mice, we used the combinatorial immunosuppression agents Cyclosporine A and Anti-CD4 antibody. Cyclosporine A (CsA) (10 mg/kg, subcutaneous injection; Perrigo, Minneapolis, MN) was administered two days prior to transplantation and daily after the injury until sacrifice. The Anti-CD4 antibody (5 mg/kg, Intraperitoneal injection; Invitrogen, Waltham, MA) was injected one day prior to transplantation and bi-weekly thereafter until sacrifice.

To optimize the anti-CD4 antibody dosage and administration interval, we tested three different amounts of dosage: 1 mg/kg, 5 mg/kg and 10 mg/kg. In this study, all mice received either one of the doses or the vehicle intraperitoneal injection of one day prior to the C5 hemisection SCI. The tail vein blood was collected and analyzed for the presence of CD45+/CD4+ cells daily until 14 DPI and once at 21 DPI using flow cytometric analysis.

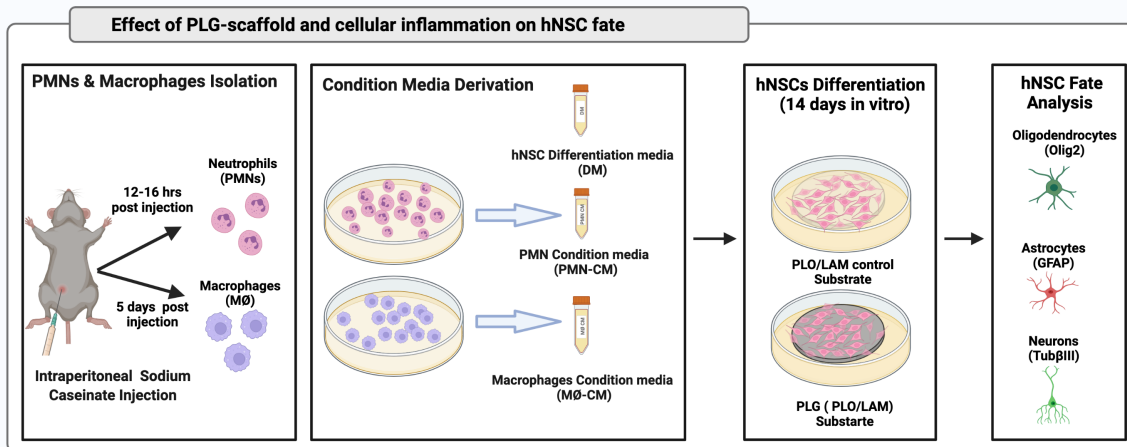
Antibody sources, and the dilutions were used as listed in Table 1. For the result, 1 mg/kg dosage started to have CD4+ cells rise at only five DPI; the 5 mg/kg and 10 mg/kg doses suppressed the number of CD4+ Th-cells for 14 DPI (Supli Fig.2.3). Since 5 mg/kg dose showed similar suppression as 10 mg/kg dose of CD4+ cells, we used 5 mg/kg dose of anti-CD4 antibody for injection one day prior to mT-mNSCs transplantation and then bi-weekly until sacrifice. [For the period anti-CD4 dosage optimization study mice were administered CsA (10 mg/kg, subcutaneous injection; Perrigo, Minneapolis, MN) two days prior to C5 hemisection SCI and daily after the injury until 21 DPI].

# FIGURES

A



B



C

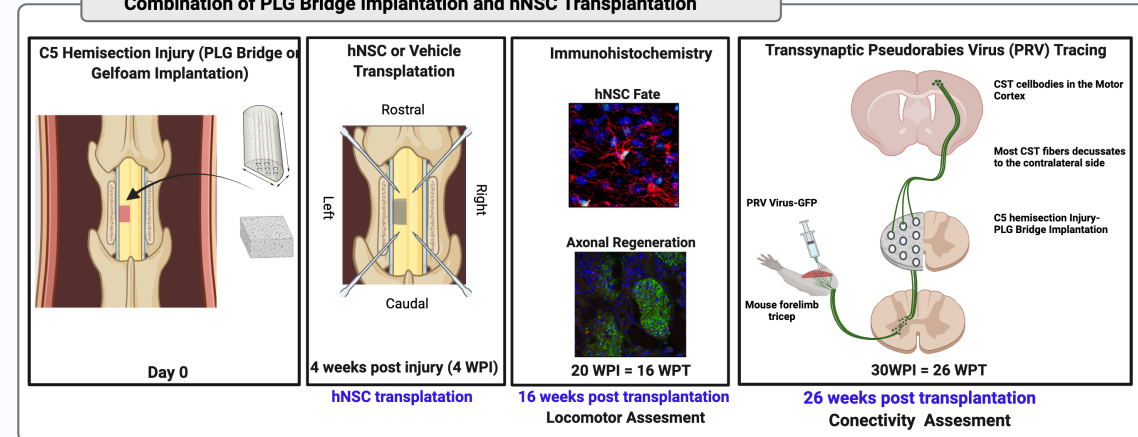


**Figure 2.1: Experimental design Schematic/Schematic diagram. (A)** Quantitative innate immune cell profiling in the presence of PLG bridge following SCI. Schematic shows C5 hemisection injury and implantation of PLG bridge or gelfoam (control) at the injury site. Next, C4 to C6 spinal cord segments (injury at C5) were dissected at different time points post-injury. Dissected spinal cord tissues were processed for flow cytometric analysis and a representative flow cytometry plot shows the gating for the total myeloid population (CD45+ CD11b+). Within this myeloid population, we further gated for neutrophils/PMNs (Ly6G+) and MØ/microglia (CD68+) subpopulations. The proportions of these innate immune cells were profiled at different timepoints in C57 BLK6 (Fig. 2.2) and Rag1 (Supp Fig 2.1) mice. **(B)** In vitro analysis of PLG-scaffold and innate immune cues on hNSC cell fate. PMNs and MØ were isolated from peritoneal cavities of Rag1 immunodeficient mice stimulated with 12% sodium caseinate (i.p. injection). PMNs and MØ were subsequently cultured in hNSC differentiation medium (DM) and respective condition media were collected. Next, hNSC were differentiated on PLO/LAM (control substrate) and PLG scaffold in the presence of DM, PMN-CM, and MØ-CM. hNSC fate was quantified using imaris software following immunocytochemistry. **(C)** Timeline for the combinatorial approach of PLG bridge implantation and hNSC transplantation in vivo. Rag1 immunodeficient mice received C5 left hemisection injury and immediate PLG bridge or gelfoam implantation. After four weeks post-injury (WPI), transplantation of hNSC or vehicle was conducted. hNSC were transplanted into the spared tissue parenchyma at two sites rostral and caudal to the injury. hNSCs fate and distribution, host axonal regeneration, myelination status, and locomotor recovery were analyzed at 16 weeks post-transplantation (WPT). Finally, transsynaptic PRV retrograde tracing was performed at 26 WPT (equivalent to 30 WPI) to investigate if the regenerated axons in the PLG bridge are synaptically connected below the level of injury.

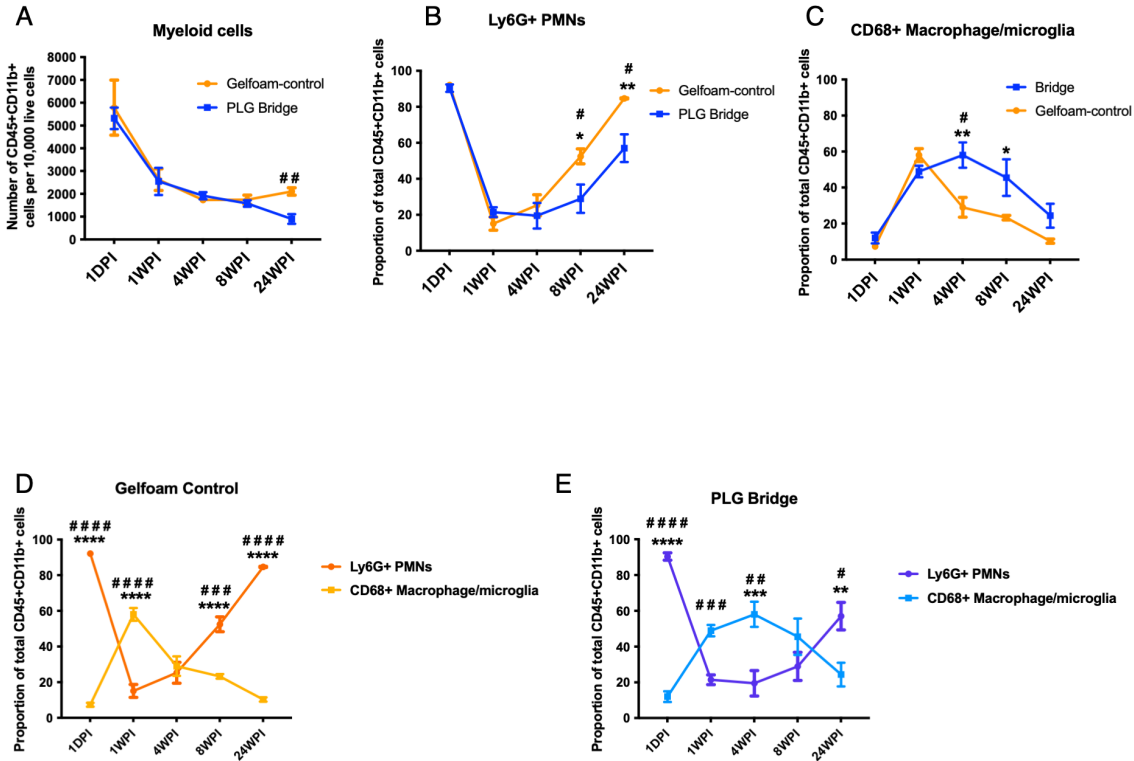


**Figure 2.2: Innate Immune Cell Time Course in C57BL/6 Mice Injured Spinal Cord. (A)** The total myeloid cell population infiltration in the gelfoam (orange) group and PLG (blue) groups over time. **(B-C)** Proportions of neutrophil/PMN (B) and MØ/microglia (C) subpopulations shown over time. **(D)** Comparison of the Ly6G+ PMNs (dark orange circle line) and MØ/microglia (light orange square line) ratios in the gelfoam group. **(E)** Comparison of the Ly6G+ PMNs (dark blue circle line) and MØ/microglia (light blue square line) ratios in the PLG group. Comparisons showing \* are using 2-way ANOVA, followed by Sidak test (\*\*\*\* $p \leq 0.0001$ , \*\*\* $P \leq 0.001$ , \*\* $P \leq 0.01$ , \* $P \leq 0.05$ ). Comparisons showing # are using unpaired t-tests at each time point (#### $p \leq 0.0001$ , ### $P \leq 0.001$ , ## $P \leq 0.01$ , # $P \leq 0.05$ ). Mean  $\pm$  SEM,  $n=3-5$  per group.

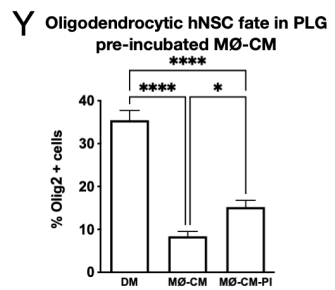
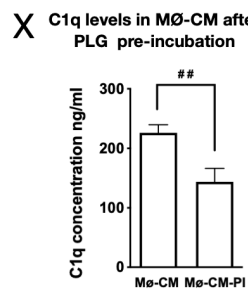
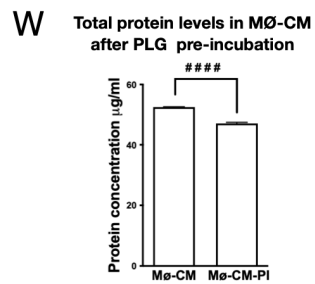
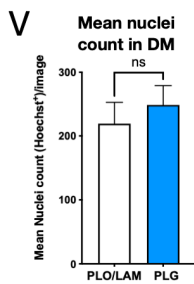
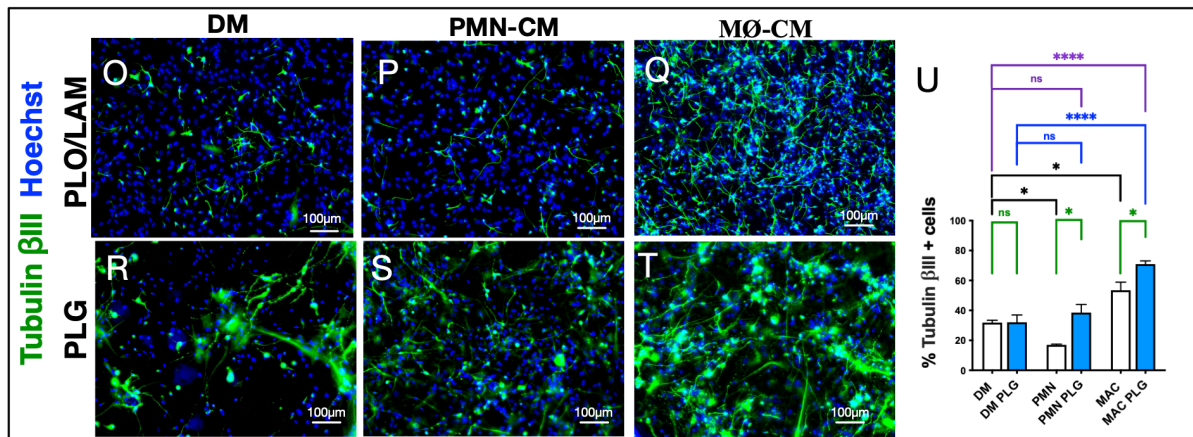
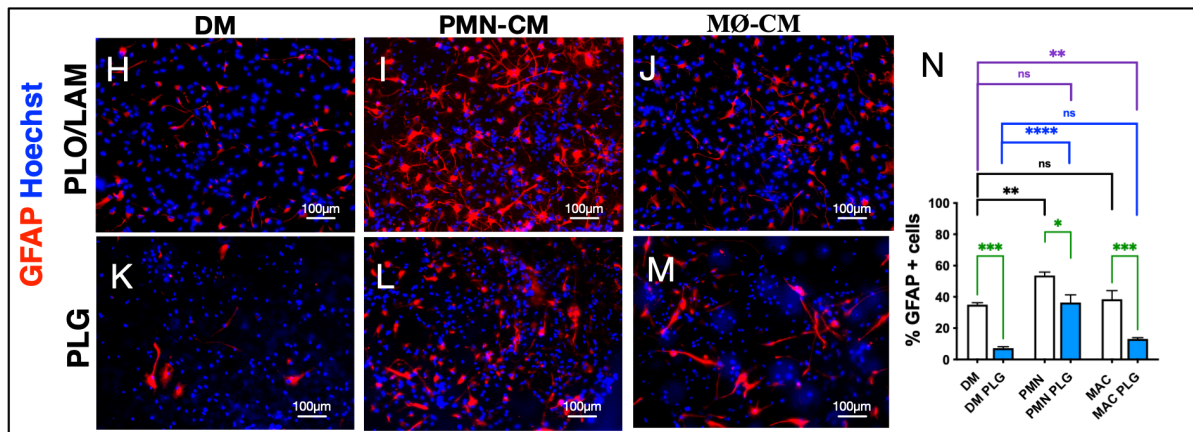
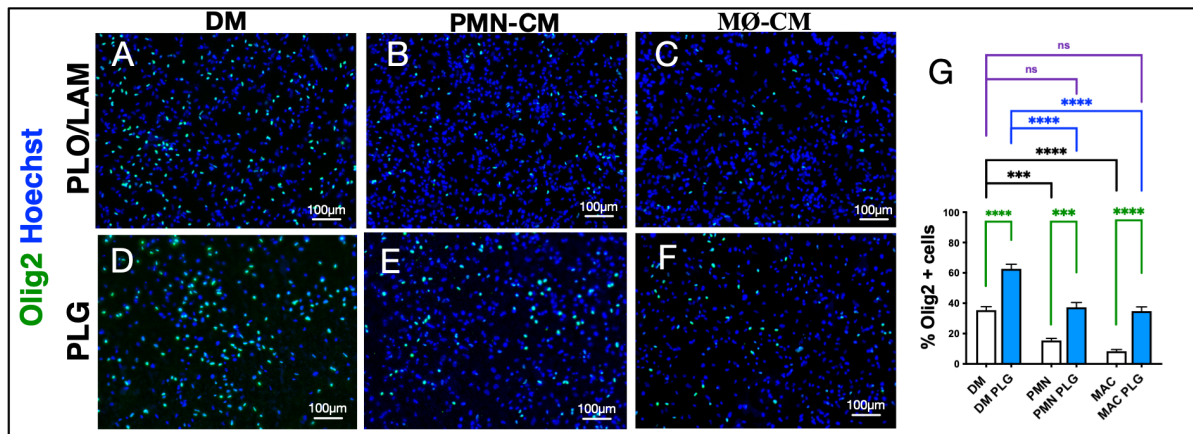


**Figure 2.3: In Vitro Assessment of hNSC Fate in the Presence of PLG Substrate and Immune Cues.** Representative images and quantification of hNSCs differentiation profile on either a PLO/LAM or PLG substrates with differentiation medium (DM), PMN conditioned medium (PMN-CM), and macrophage conditioned medium (MØ-CM) for oligodendrocyte marker (Olig2; A-F), astrocytic marker (GFAP; H-M), and neuronal marker (Tubulin  $\beta$ III; O-T). Quantitative comparisons were performed for oligodendrocytic fate (G), astrocytic fate (N), and neuronal fate (U). Black lines and \* show comparisons between DM control, PMN-CM, and MØ-CM groups on the PLO/LAM substrate. Blue lines and \* show comparisons between DM control, PMN-CM, and MØ-CM groups on the PLG substrate. Green lines and \* shows significant changes between PLO/LAM and PLG substrates. Purple lines and \* comparing the two PLG/CM groups to the PLO/LAM-DM control group. (V) Nuclei count of hNSCs differentiated in the presence of PLG scaffold versus the control PLO/LAM in the hNSC differentiation media. There was no significant difference in the total number of cells grown on the two substrates. (X-Y) PLG modulation of hNSC fate by sequestering immune cues in the conditioned media. Total protein levels (W) and C1q levels (X) were significantly reduced in MØ-CM after 48hr pre-incubation with PLG (MØ-CM-PI). (Y) Oligodendrocytic fate was partially restored in hNSC grown on PLO/LAM substrate in the presence of MØ-CM-PI. Comparisons showing \* are using one-way ANOVA, followed by Tukey post hoc tests for all comparisons. (\*\*\*\* $p \leq 0.0001$ , \*\*\* $P \leq 0.001$ , \*\* $P \leq 0.01$ , and \* $P \leq 0.05$ ). Comparisons showing # are using unpaired t-tests (#### $p \leq 0.0001$  and ## $P \leq 0.01$ ). Mean  $\pm$ SEM, N = 3-4 biological replicates/condition with a minimum of two technical replicates per condition.

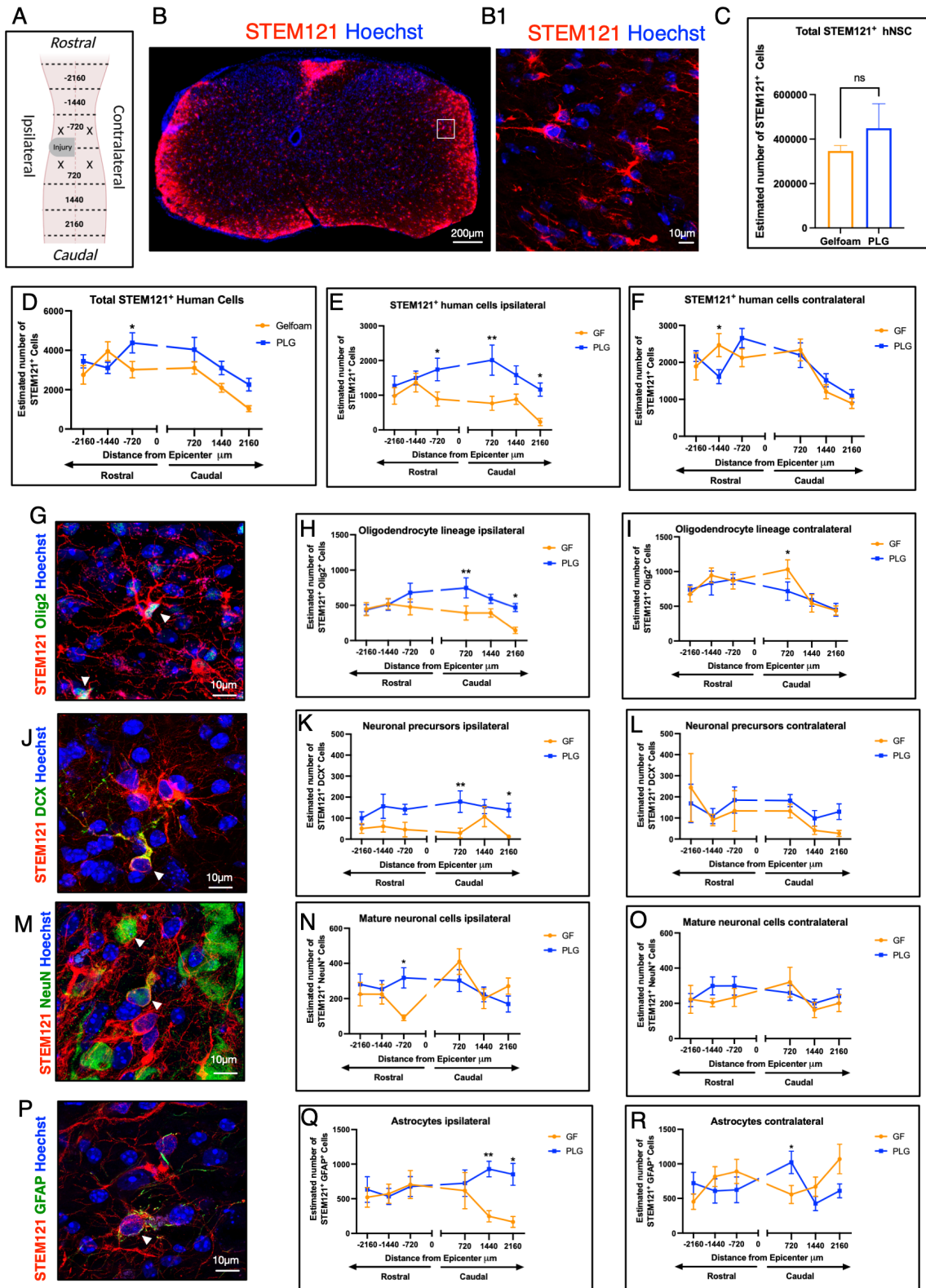
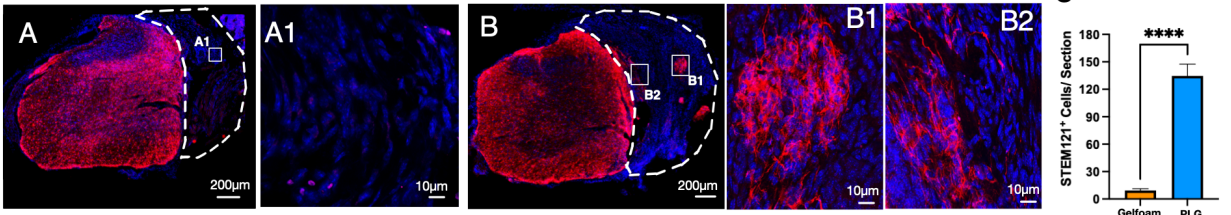


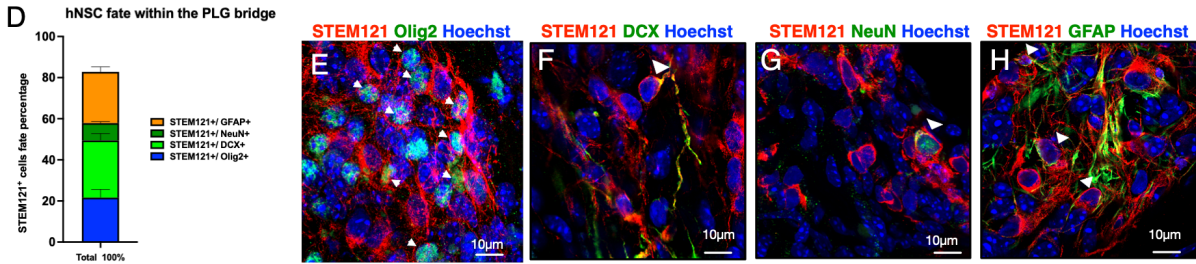
**Figure 2.4: Stereological analysis of hNSC fate and distribution along the spinal cord.**

(A) Schematic of spinal cord injury, showing the injury epicenter at C5 and indications of coordinate in  $\mu\text{m}$ . 'X' represents locations of hNSC transplantation at two injection sites rostral and two sites caudal to the injury epicenter. Ipsilateral refers to the same side as the injury, and contralateral refers to the opposite side. Dashed lines represent rostral-caudal axis binning used for histological quantifications (720, 1440, 2160 microns from injury epicenter). (B) Representative image of a coronal spinal cord section showing distribution of SC121+ transplanted human hNSC (red) and total cell nuclei (blue). (B1) shows a magnified insert of B. (C) Stereological estimation of the number of SC121+ cells in rostral and caudal regions in PLG and gelfoam groups. (D-F) Quantification of transplanted SC121+ hNSC in the total spinal cord (D), ipsilateral to the injury (E), and contralateral to the injury (F). (G-R) Representative images and quantification for (G) SC121+/OLIG2+ oligodendrocytes, (J) SC121+/DCX+ neuronal precursors, (M) SC121+/NeuN+ mature neurons, and (P) SC121+/GFAP+ astrocytes. Total numbers of stereologically quantified lineage specific cells for oligodendrocytes (H, ipsilateral side; I, contralateral side), neuronal precursors (K, ipsilateral side; L, contralateral side), mature neurons (N, ipsilateral side; O, contralateral side), and astrocytes (Q, ipsilateral side; R, contralateral side). Statistical analysis by unpaired two-tailed t-tests (\* $p \leq 0.05$ , \*\* $p \leq 0.005$ , Mean  $\pm$ SEM, N=5-6/group).

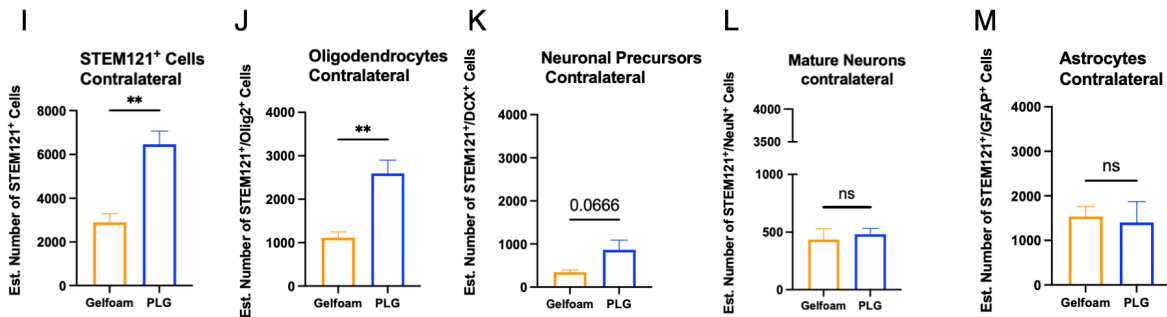
### STEM121 Hoechst



### hNSC Fate Within The PLG Bridge



### hNSC Engraftment & Fate Assessment in the Contralateral Tissue: PLG Bridge vs. Gelfoam Groups



### hNSCs Fate Assessment Within the PLG bridge vs. Contralateral Spared Tissue in PLG Group

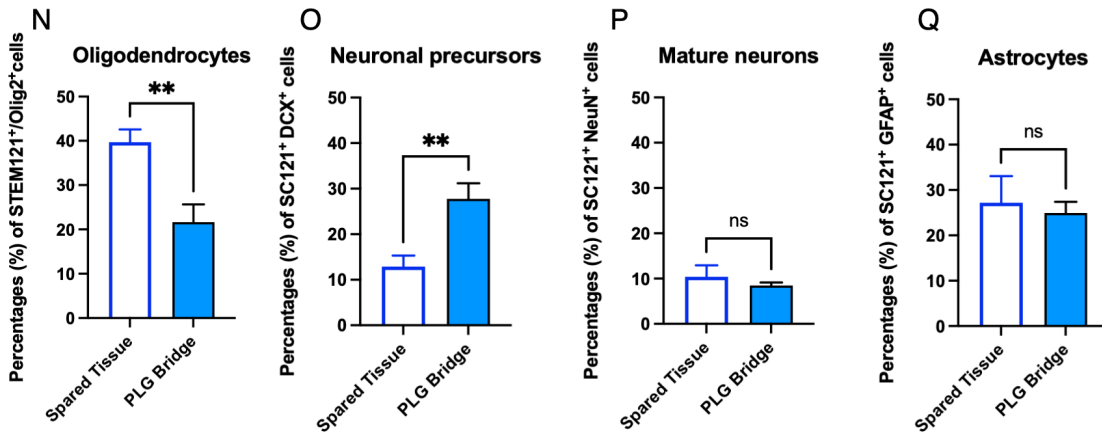


**Figure 2.5: PLG bridge creates a permissive injury environment for hNSC engraftment and influences hNSC fate.** (A-A1) Representative images of spinal cord section at the injury side for the Gelfoam group. A1 shows no hNSCs engrafted. (B-B1 & B2) Representative images of spinal cord section at the injury side for the PLG group. B1 and B2 show numerous hNSCs migrated inside the PLG channel. White dotted lines outline the injury side (ipsilateral side) in both gelfoam and PLG groups. Inserts FigA1 and B1-B2 show higher magnification images. (C) Quantification of total SC121+ hNSC comparing gelfoam and PLG groups (data represents number of cells per 30 $\mu$ m section). (D) Quantification of hNSC fate within the PLG bridge (data represents percentage of each cell fate) (E-H) Representative images of hNSC fate in the PLG bridge for SC121+/OLIG2+ oligodendrocytes (E), SC121+/DCX+ neuronal precursors (F), SC121+/NeuN+ mature neurons (G), and SC121+/GFAP+ astrocytes (H). (I) Quantification of total SC121+ hNSCs in the contralateral side comparing gelfoam and PLG groups. (J-M) Quantification of hNSC fate in the contralateral side comparing gelfoam and PLG groups. (N-Q) Data was replotted to show a proportional shift in hNSC fate by comparing injury side (data from D) versus estimated percentage contralateral side (data from I-M) for the PLG group. Statistical analysis by unpaired two-tailed t-tests. (\*\* $p \leq 0.005$ , \*\*\*\* $p \leq 0.0001$ , Mean  $\pm$ SEM, N=5-6/group).

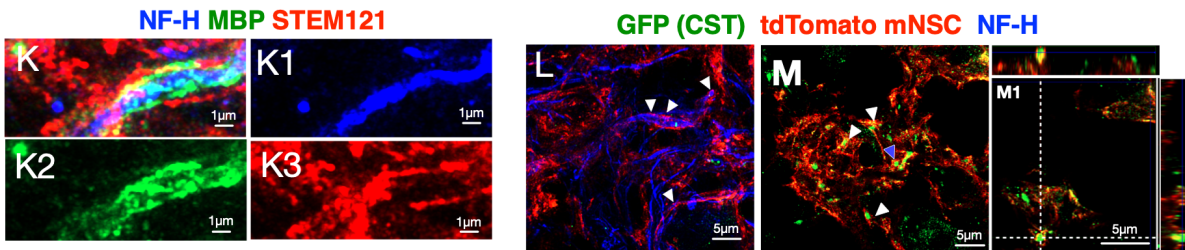
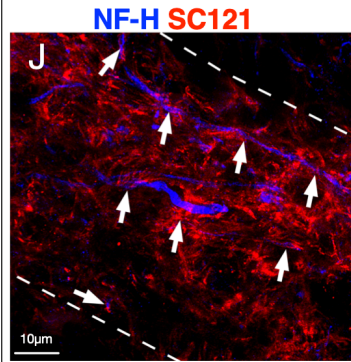
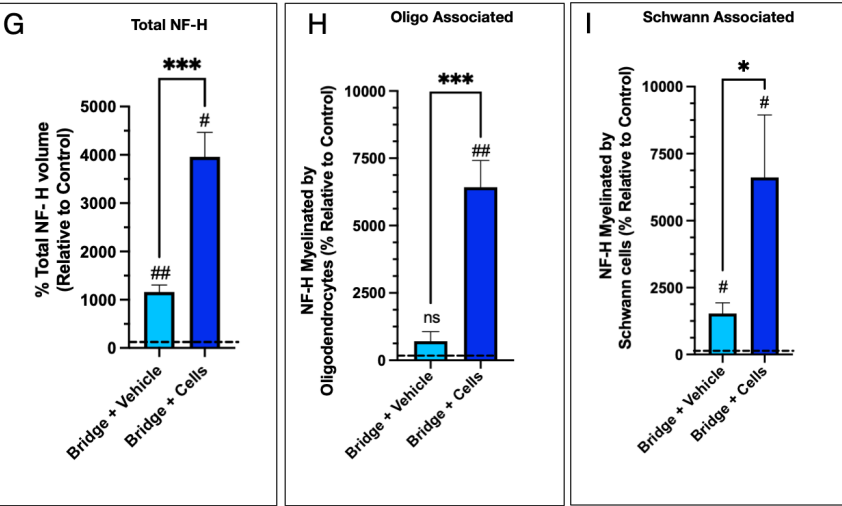
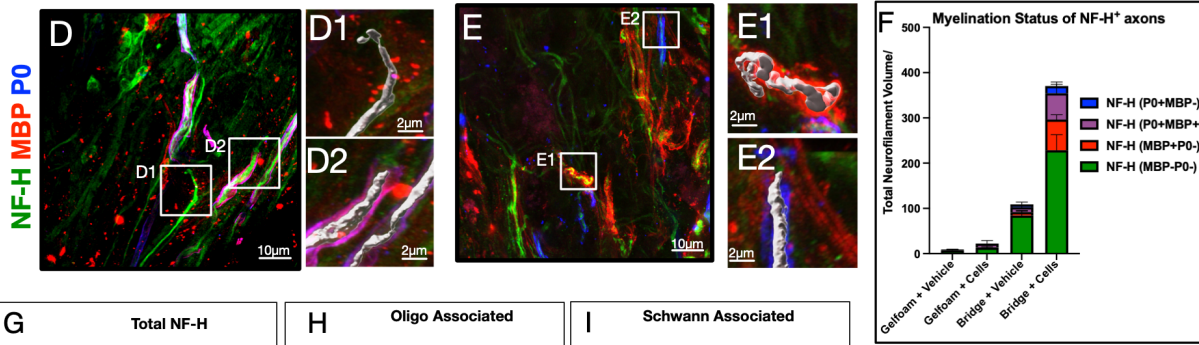
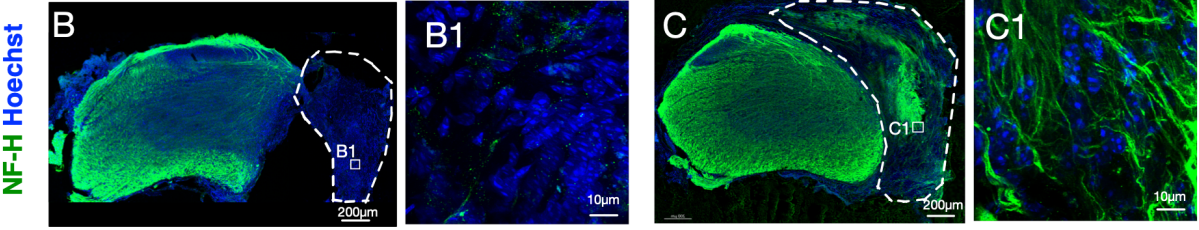
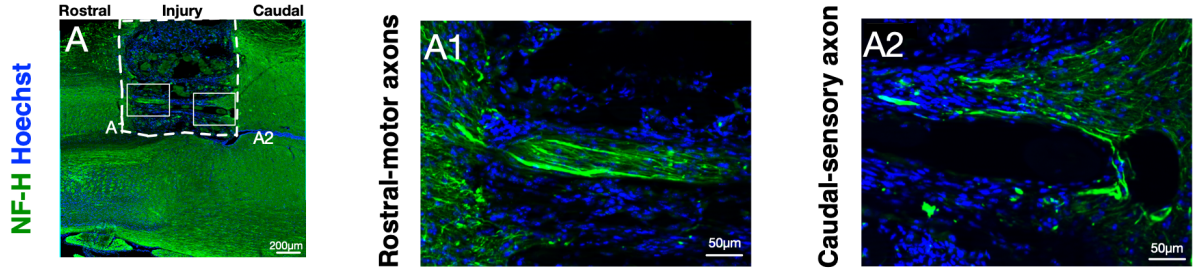
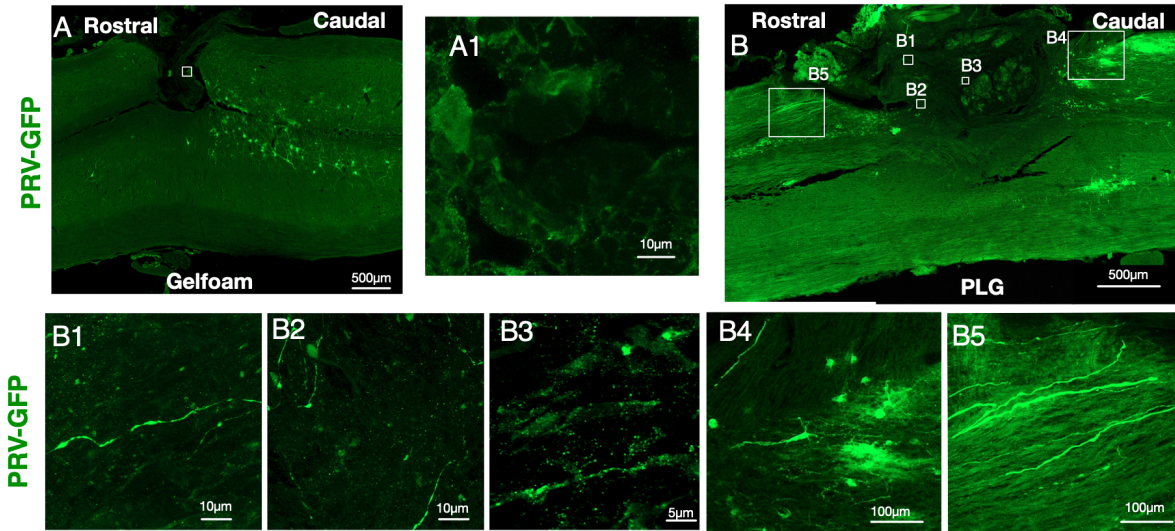
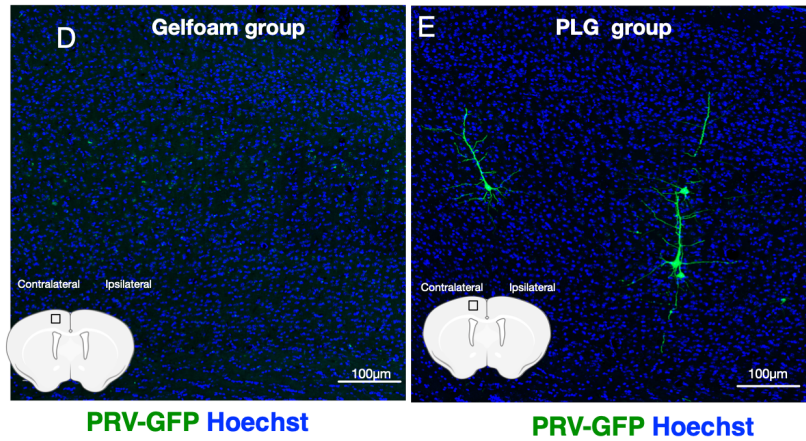
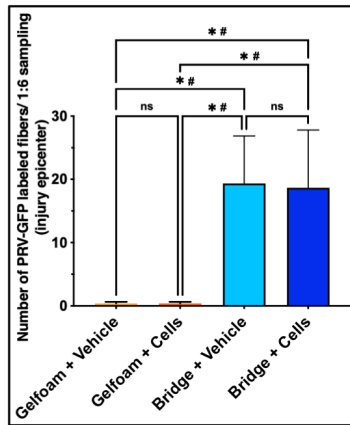


**Figure 2.6: Combination of PLG bridge implantation and hNSC transplantation enhances axonal regeneration and oligodendrocytic myelination.** (A) Immunograph of horizontal plane mouse spinal cord section (C5 left hemisection injury) with PLG bridge at the injury site showing axonal regeneration from both rostral and caudal parenchyma at 6 weeks post-SCI and bridge implantation. White dashed lines marking the bridge-tissue interface. (A1-A2) Higher magnification image of (A); (A1) NF-H+ descending motor axons (A2) NF-H+ ascending sensory axons within the channels of PLG bridge. (B & C) Representative images of transverse plane mouse spinal cord section receiving gelfoam implantation (B, B1) and PLG bridge implantation (C, C1) at 20 weeks post-SCI and bridge implantation (16WPI). White dashed lines outline the injury side (ipsilateral side) in both gelfoam and PLG groups. Boxes B1 and C1 indicate regions shown at high magnification. Gelfoam implantation shows minimal to no axonal growth, whereas PLG implantation supported robust axonal regeneration. (A-C) Sections were counterstained with a nuclear marker (Hoechst, blue). (D-E) Triple immunostaining shows NF-H labeled axons (NF-H; green), oligodendrocyte derived myelin (MBP; red) and Schwann cell myelin (P0; blue). Boxes indicate the region shown at higher magnification with 3D surface masks representing unmyelinated axon (D1), Schwann cell myelinated axon (D2, and E2) and oligodendrocyte myelinated axons (E1). (F) Data represents the total NF-H volume and the myelination status of the NF-H+ axons. (G-I) Total NF-H volume (G), NF-H volume associated with oligodendrocyte myelin (H), and NF-H volume associated with Schwann cell myelin (I) were normalized to Gelfoam + Vehicle control (dashed line) and statistical comparisons were conducted using unpaired two-tailed t-tests (\* $p < 0.05$  and \*\*\* $p \leq 0.001$ ) and one sample t and Wilcoxon test (# $p \leq 0.05$  and ## $p \leq 0.01$ ).  $n = 5-6$  mice/group, one spinal cord section per mouse and 3 to 6 images within the injury site (Mean  $\pm$  SEM). (J) SC121 + processes (red) warping around NF-H axons (blue). (K) High power merge image and (K1-K3) Individual channel images representing SC121+ human cytoplasm in the outermost layer of myelin. (L-M) mT-mNSCs showing close alignment with regenerated axons in the PLG bridge NF-H+ axons (L) and CRYM-GFP+ CST axons (M) at 12 WPT.



**C** PRV labeling within the injury site



**F** PRV labeling in the contralateral motor cortex

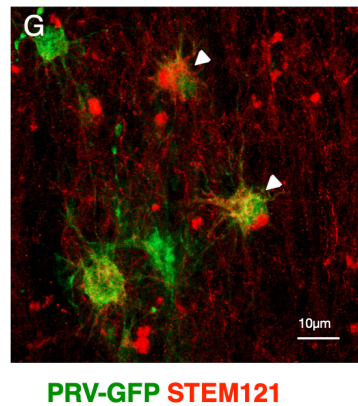
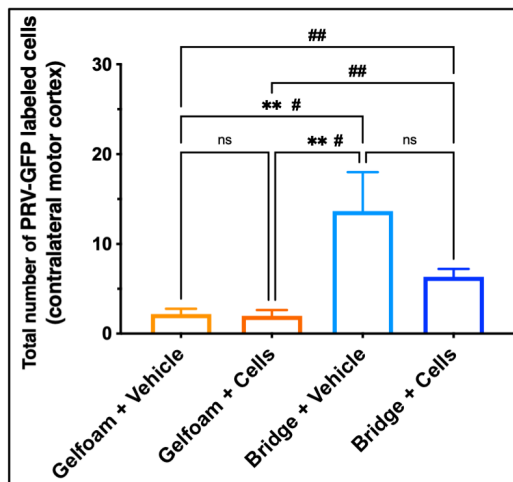
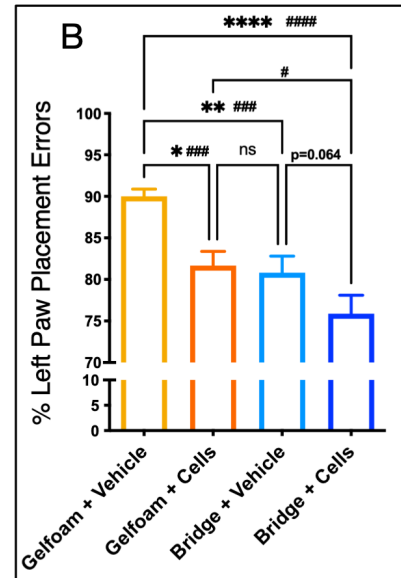
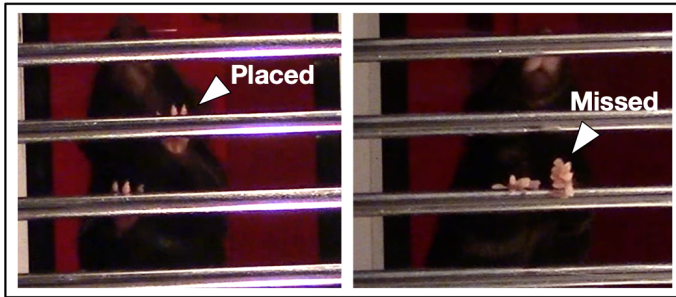


**Figure 2.7: Transsynaptic pseudorabies virus (PRV) tracing indicates that the regenerated CST axons through the PLG bridge are synaptic connected.** (A-A1) Horizontal section showing PRV labeling (green) in the gelfoam group; A1 insert shows that PRV fibers were not observed in the gelfoam implantation site. (B) Horizontal section showing PRV labeling in the PLG group. (B1-B3) Higher magnification inserts show PRV+ regenerated fibers inside the PLG bridge. (B4-B5) PRV+ fibers rostral to the PLG bridge. (B6) PRV+ fibers caudal to the PLG bridge. (C) Quantification of PRV labeling in the injury site (quantification performed for one in every six sections). (D-E) Representative image of PRV labeling in the contralateral motor cortex gelfoam group (D) and PLG group (E). (F) Quantification of total PRV-labeled CST cell bodies in the motor cortex. (G) STEM121+ cells stained positive to GFP+PRV suggest stable integration into host circuitry. Groups were compared using one-way ANOVA, followed by Tukey post hoc tests (\* $P \leq 0.05$ , \*\* $P \leq 0.01$ ). Statistical analysis by multiple unpaired t-tests. (# $p \leq 0.05$ , ## $p \leq 0.01$ ). n = 3-5 biological replicates/group. Mean  $\pm$ SEM.

**A Ladder Beam Analysis**



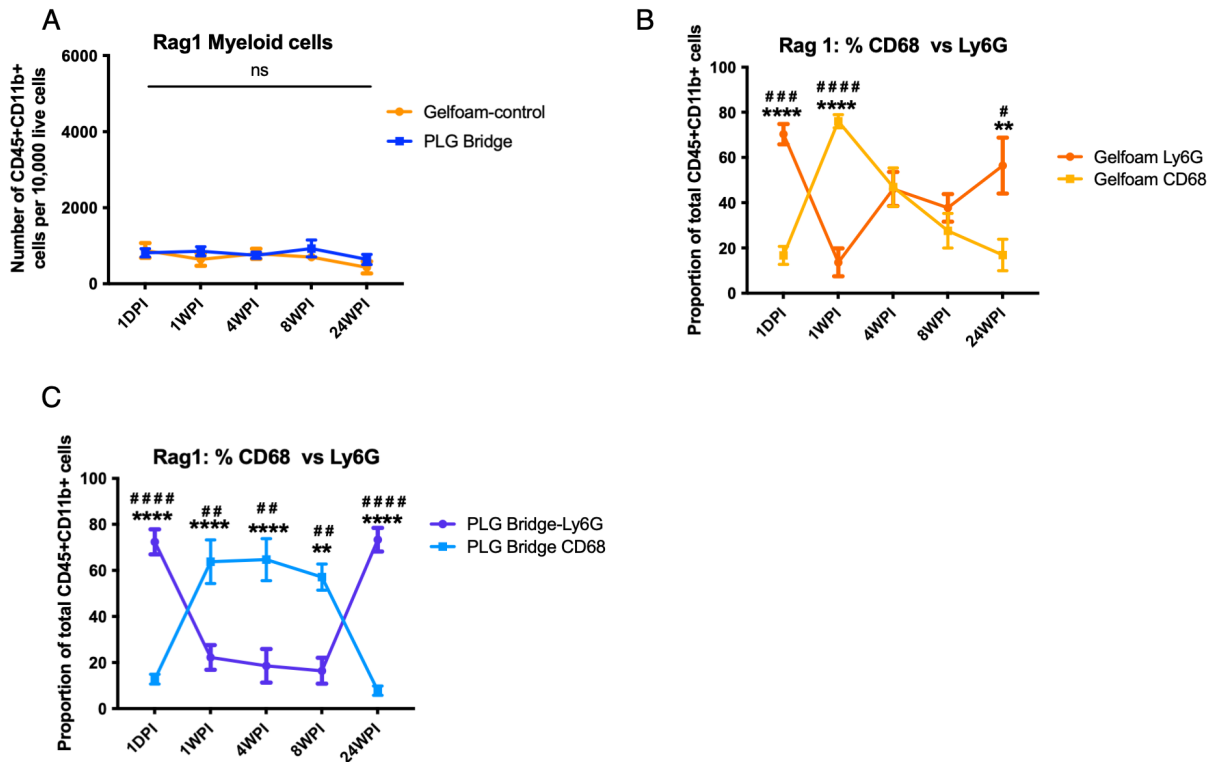
**C CatWalk Gait Analysis**

| Catwalk Parameters                   | Cells       | Bridge      |
|--------------------------------------|-------------|-------------|
| RF_Stand_.s._Mean                    | 0.013248194 | 0.975532342 |
| Couplings_LH..LF_CStat_Mean          | 0.015601257 | 0.948971728 |
| RF_DutyCycle_..._Mean                | 0.020300083 | 0.806560169 |
| RF_StandIndex_Mean                   | 0.025747088 | 0.181256606 |
| LH_StandIndex_Mean                   | 0.233679866 | 0.045553678 |
| RH_BodySpeedVariation_..._Mean       | 0.289635776 | 0.030419585 |
| LF_MinIntensity_Mean                 | 0.474304921 | 0.012787487 |
| LF_BodySpeedVariation_..._Mean       | 0.665900405 | 0.037140399 |
| LF_MaxIntensityAt_..._Mean           | 0.683832754 | 0.014452937 |
| LF_PrintArea_.cm <sup>2</sup> ._Mean | 0.842000474 | 0.045673847 |

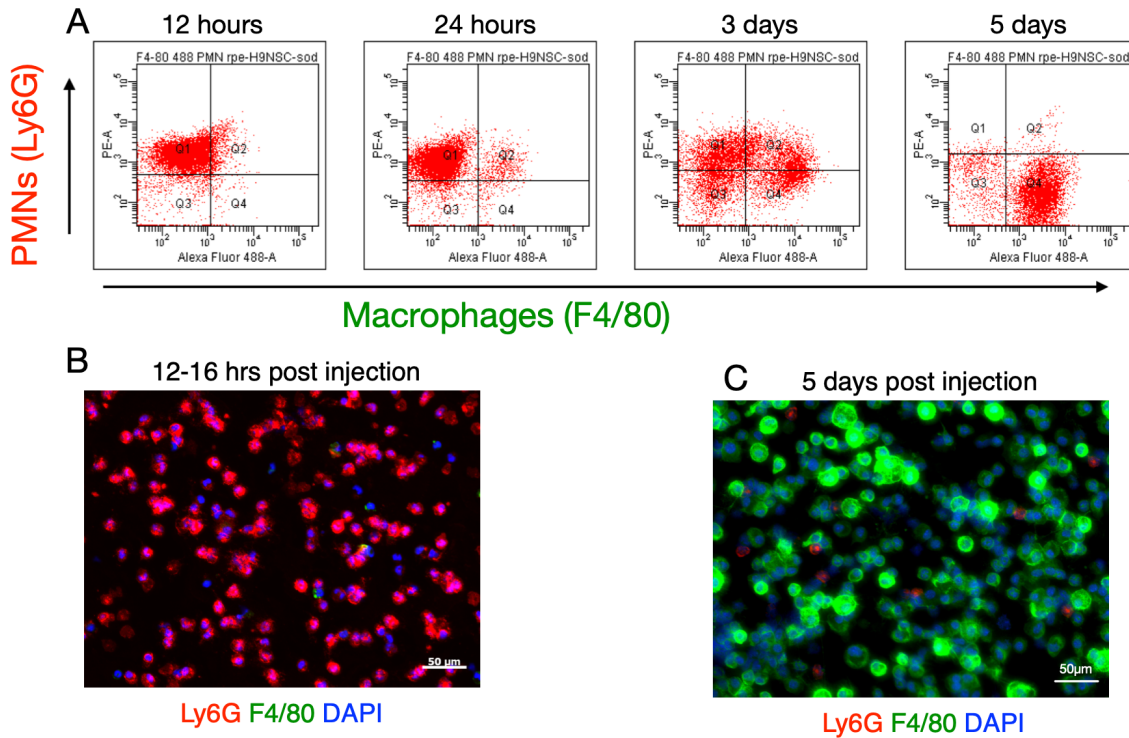
**Figure 2.8: PLG bridge**

**Locomotor behavior assessment of paw placement errors on the horizontal ladder beam and Catwalk gait analysis.** (A) Images depicting mice performing the horizontal ladder beam task. Arrows pointing a good versus missed ipsilateral (left forelimb) paw placement. (B) Quantification results of ipsilateral paw placement showed a significant reduction in errors for all three treatment groups 20 weeks after injury (16WPT). Groups were compared using one-way ANOVA, followed by Tukey post hoc tests (\*\*\*\* $p \leq 0.0001$ , \*\* $P \leq 0.01$ , and \* $P \leq 0.05$ ) and unpaired t-tests (#### $p \leq 0.0001$ , ### $p \leq 0.001$ , and # $p < 0.05$ ) mean  $\pm$ SEM and N= 9-13 animals per group (or Gelfoam + Vehicle (n=11), Gelfoam + Cells (n=10), Bridge + Vehicle (n=10), and Bridge + cells (n=12)). (C) Table of p-values for two-way ANOVAs. Variables highlighted in gray have  $p$  value  $\leq 0.05$  for the effect of hNSC transplantation and bridge implant.

## SUPPLEMENTAL FIGURES

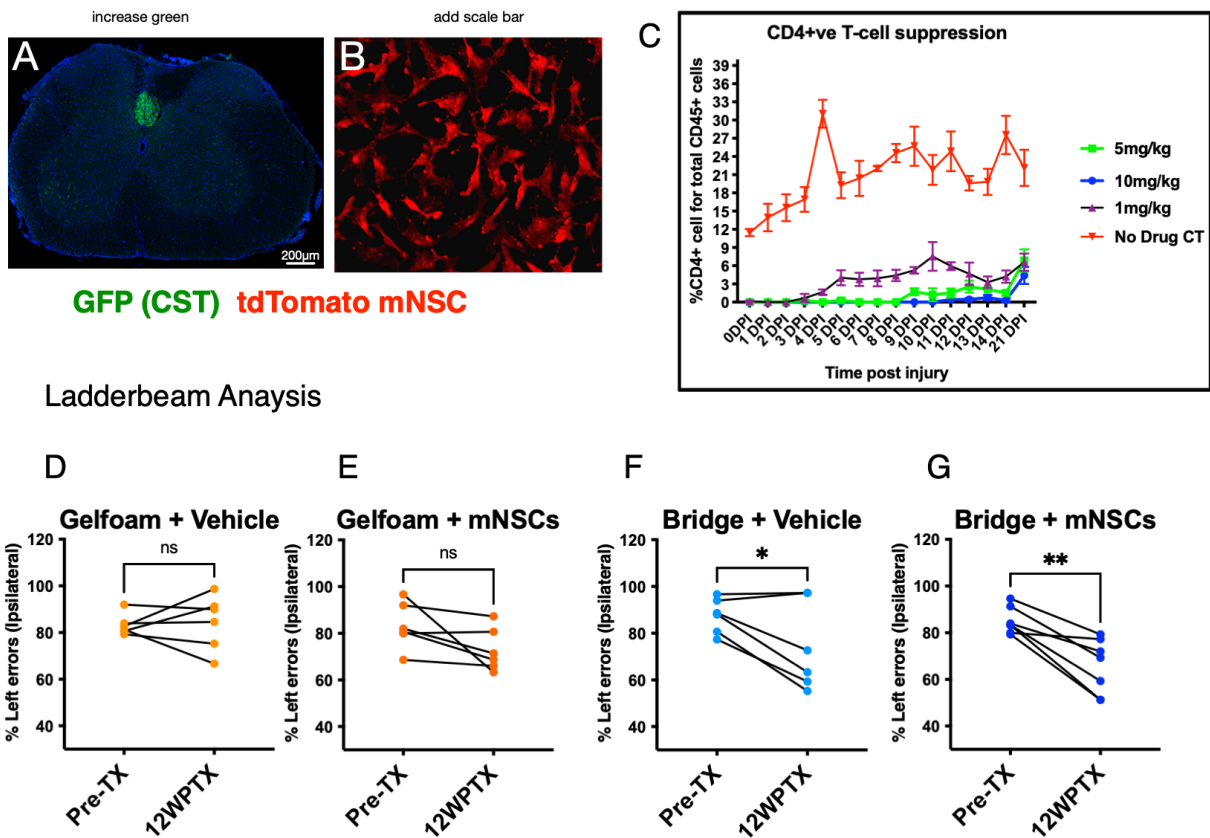


**Supplemental Figure 2.1: Innate immune cell time course in Rag1 immunodeficient mice injured spinal cord. (A)** The total myeloid cell population infiltration in the gelfoam (orange) group and PLG (blue) groups over time in Rag1 mice. **(B)** Comparison of the Ly6G+ PMNs (dark orange circle line) and MØ/microglia (light orange square line) ratios in the gelfoam group of Rag1 mice. **(C)** Comparison of the Ly6G+ PMNs (dark blue circle line) and MØ/microglia (light blue square line) ratios in the PLG group of Rag1 mice. Similar to C57BL/6 mice, the neutrophil population peaked acutely at 1DPI and re-emerged by 24WPI. Similar to the trend noted in C57BL/6 mice, the PLG bridge retained the MØ/microglia population over a prolonged time (up until 8 WPI); whereas, in the gelfoam group MØ/microglia drops after 1 WPI. Comparisons showing \* are using 2-way ANOVA, followed by Sidak test (\*\*\*\* $p \leq 0.0001$ , \*\*\* $P \leq 0.001$ , \*\* $P \leq 0.01$ , \* $P \leq 0.05$ ). Comparisons showing # are using unpaired t-tests at each time point (#### $p \leq 0.0001$ , ### $P \leq 0.001$ , ## $P \leq 0.01$ , #  $P \leq 0.05$ ). Mean  $\pm$ SEM,  $n=4-5$  per group.



**Supplemental Figure 2.2: Peritoneal PMN or macrophages (MØ) cell profiling to generate condition media for hNSC In vitro fate analysis.**

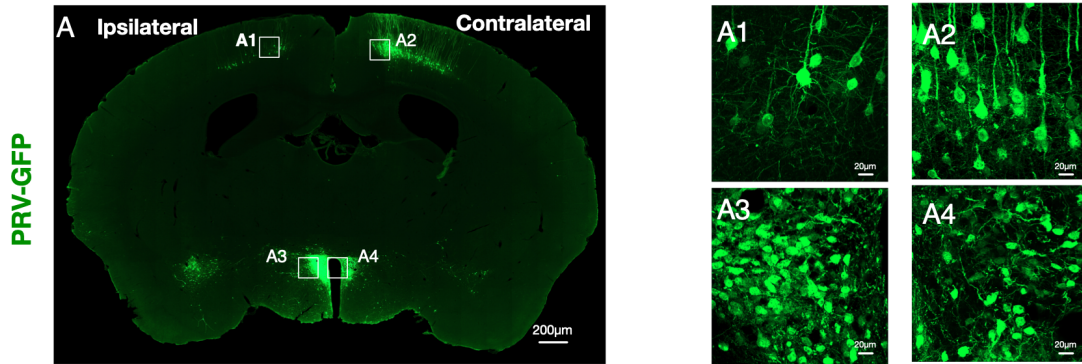
(A) Peritoneal derived PMNs and MØ were isolated from Rag1 mice after 12 hours, 24 hours, 3 days, and 5 days post 12% sodium caseinate (i.p. injection) and profiled using BD FACSCalibur flow cytometry device (Nguyen and Tidball 2003). We confirmed that Ly6G+ve PMNs are the predominant population at 12-24 hours post injection; whereas F4/80+ve macrophages emerge starting around 24 hours and dominate by 7 days post injection. Isolated cells were analyzed after labeling with antibodies to Ly6G (PMNs) and F4/80 (macrophages). (B-C) Representative images of peritoneal cells post flow analysis, depicting the predominant Ly6G+-PMNs population at 14 hours post injection (B), and the F4/80+-macrophages population at 5 days post injection.



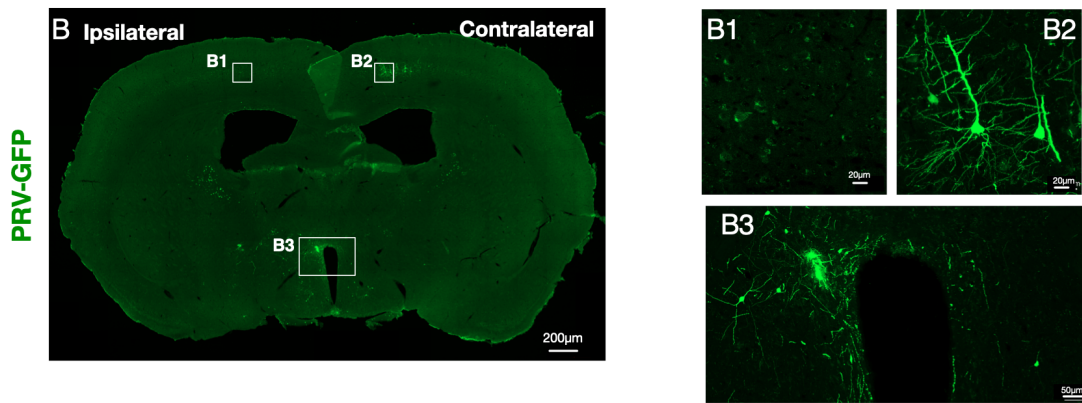
**Supplemental Figure 2.3: CRYM-ZsGreen1 mice showing GFP expression in CST and tdTomato membrane reporter expression in mT-mNSC, optimization of anti-CD4 immunosuppression paradigm, and motor recovery assessment.** (A) To answer the question of whether donor NSC myelinates the regenerating CST axons, we generated a CRYM-ZsGreen1 transgenic mice colony that expresses GFP in the CST axons (A, see **Supplemental Methods. 1**). (B) Mouse NSC (mT-mNSC) were derived from the embryonic day 12 (E12) pups cortices of tdTomato transgenic mice and cultured and expanded in vitro (see **Supplemental Methods. 2**). Transplantation was conducted at passage 4 (P4). These mT-mNSC ubiquitously express membrane-targeted fluorescent tandem dimer Tomato (tdTomato). This fluorescent labeling will enable the detection of donor mT-mNSC in the mouse-to-mouse transplantation paradigm [42]. The tdTomato membrane reporter allows for the identification of myelinated regions of the donor cells, as cytoplasmic labels may be lost when myelin is compacted. CRYM-ZsGreen1 mice received C5 hemisection SCI with immediate PLG bridge implantation and chronic mT-mNSC transplantation (4WPI) into the rostral and caudal parenchyma. (C) Immunosuppression regimen includes the combined administration of Cyclosporine A (CsA) (10 mg/kg, subcutaneous injection) two days prior to transplantation followed by daily after the injury until sacrifice and Anti-CD4 antibody (5

mg/kg, Intraperitoneal injection) one day prior to transplantation and bi-weekly thereafter until sacrifice. To optimize the anti-CD4 antibody dosage and administration interval, we tested three different amounts of dosage: 1 mg/kg, 5 mg/kg and 10 mg/kg. In this study, all mice received either one of the doses or the vehicle intraperitoneal injection of one day prior to the C5 hemisection SCI. CsA (10 mg/kg, subcutaneous injection; Perrigo, Minneapolis, MN) was administered two days prior to transplantation and daily after the injury until 21 DPI. The tail vein blood was collected and analyzed for the presence of CD45+/CD4+ cells daily until 14 DPI and once at 21 DPI using flow cytometric analysis. For the result, 1 mg/kg dosage started to have CD4+ cells rise at only five DPI; the 5 mg/kg and 10 mg/kg doses suppressed the number of CD4+ Th-cells for 14 DPI (Supl Fig.2.3). Since 5 mg/kg dose showed similar suppression of CD4+ cells, we used 5 mg/kg dose of anti-CD4 antibody for injection one day prior to mT-mNSC transplantation and then bi-weekly until sacrifice. (D-G) Locomotor functional recovery after mT-mNSC transplantation. Ladder beam analysis at 12 weeks post-transplantation data showed no significant difference observed between the treatment groups with one-way ANOVA due to small sample size (Data not shown). (D-G) Comparison of paw placement errors for pre-transplantation (Pre-TX) versus 12WPT. Gelfoam+Vehicle and Gelfoam + mT-mNSC groups showed no significant improvement in recovery over time (D, E). Whereas the Bridge+Vehicle (\*p =0.0466) and Bridge + mT-mNSC group (\*\*p=0.0022) groups showed further significant improvement in paw placement on the horizontal ladder beam by 12WPT. (Statistical analysis conducted using Paired t-test, n = 6 animals/group, Mean  $\pm$ SEM

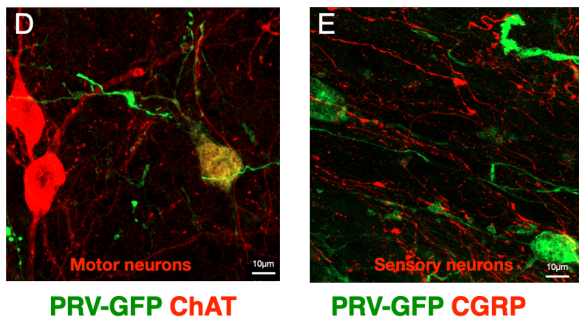
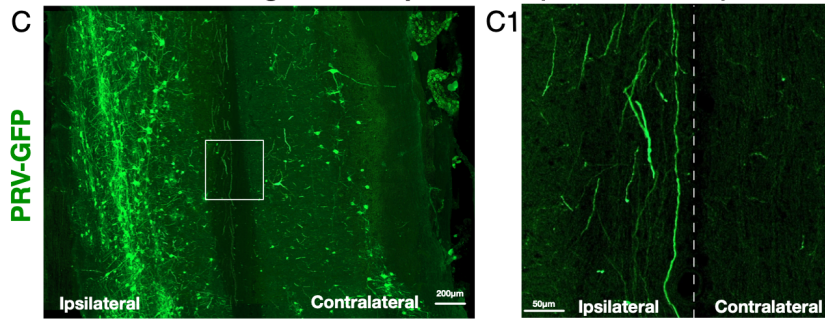
**PRV-GFP labeling in the Motor cortex and PVN of hypothalamus (2 months old mice)**



**PRV-GFP labeling in the Motor cortex and PVN of hypothalamus (10 months old mice)**



**PRV-GFP labeling in naive spinal cord (10 months old)**



**Supplemental Figure 2.4: Validation of PRV labeling in young and aged naive mice.**

(A-B) PRV was injected in the forelimb triceps of intact naive mice and was retrogradely traced to the motor cortex and hypothalamus in the brain. PRV labeling was validated in both young (2 months, A) and aged (10 months, B) old mice. (A) Representative image in 2 month-old young mice demonstrating PRV retrograde tracing. The majority of the PRV labeled neurons were detected in the contralateral motor cortex, with a lesser amount of labeling in the ipsilateral cortex (same side as tricep injection site) (A1-A2). In contrast, in the paraventricular nucleus (PVN) of the hypothalamus, the predominant portion of labeling is shown on the ipsilateral side (A3-A4). (B) To keep the age of the mice parallel to the duration of the SCI and hNSC transplantation experimental model, PRV labeling efficiency was validated in 10 months old mice. The overall load of PRV tracing was drastically reduced, suggesting weakening of synaptic connections in the aged mice. A similar pattern is detected in the contralateral/ipsilateral motor cortex (B1-B2) and hypothalamus (B3). (C) PRV-GFP labeling in the spinal cord, depicting the majority of the PRV signal on the ipsilateral side. Multiple cervical spinal cord sections (1: 6th sampling) in the naive spinal cord were overlaid to generate a maximum projection image. The image illustrates the PRV labeled neurons and axons in the cervical spinal cord; the predominant labeling in the ipsilateral side and few propriospinal neurons labeled on the contralateral side due to decussation of fibers at multiple segments across the spinal cord. (C1) High magnification image showing the CST fibers (long tract motor axons) in the ipsilateral side. (D) Colabeling with choline acetyltransferase (ChAT) showed some PRV+ cell bodies are primary motor neurons. (E) PRV labeled neurons and axons were stained negative for calcitonin gene-related peptide (CGRP) sensory markers. Critically, this suggests that PRV is specific to motor neurons, and not sensory neurons.

**Table 2.1. List of primary antibodies, sources, and dilutions.**

| <b>Primary Antibody</b> | <b>Host</b> | <b>Dilution</b> | <b>Manufacturer</b>      | <b>Specificity</b>                      |
|-------------------------|-------------|-----------------|--------------------------|---|
| Olig2                   | Rabbit      | 1:250           | Abcam                    | Oligodendrocytes                        |
| GFAP (in vitro)         | Rabbit      | 1:1000          | Dako                     | Astrocytes                              |
| Tubulin $\beta$ III     | Mouse       | 1:1000          | Biolegend                | Neuron                                  |
| STEM121                 | Mouse       | 1:500           | Takara                   | Human Neural Stem Cell                  |
| DCX                     | Goat        | 1:500           | Santa Cruz Biotechnology | Immature neurons                        |
| NeuN                    | Rabbit      | 1:500           | Millipore                | Mature neurons                          |
| GFAP (in vivo)          | Goat        | 1:1000          | Abcam                    | Astrocytes                              |
| NF-H                    | Rabbit      | 1:500           | Millipore                | Axons and processes                     |
| MBP                     | Mouse       | 1:250           | R&D Systems              | Myelin basic protein                    |
| P0                      | Chicken     | 1:500           | Aves                     | Schwann cell myelin                     |
| GFP                     | Goat        | 1:250           | Abcam                    | Green fluorescent protein (CST and PRV) |
| RFP                     | Rabbit      | 1:500           | Rockland                 | Red fluorescent protein (mT-mNSC)       |
| ChAT                    | Rabbit      | 1:200           | Abcam                    | Motor neurons                           |
| CGRP                    | Rabbit      | 1:200           | Sigma                    | Sensory fibers                          |
| CD45                    | Rat         | 1:100           | Biolegend                | Hematopoietic cells                     |
| CD11b                   | Rat         | 1:100           | bd biosciences           | Myeloid Cells                           |
| Ly6G                    | Rat         | 1:100           | Biolegend                | Neutrophils (PMNs)                      |
| CD68                    | Rat         | 1:100           | Biolegend                | Macrophages                             |
| F4/80                   | Rat         | 1:100           | SeroTec                  | Macrophages                             |

## CHAPTER 3

### **Combination of Biomaterial Bridge Implantation and Interleukin-10 Expression to Modulate the Inflammatory Response and Promote Neural Regeneration and Connectivity after Spinal Cord Injury**

#### **ABSTRACT**

Spinal cord injury (SCI) is caused by an initial trauma that leads to immune cell infiltration and initiation of an inflammatory cascade that mediates axon degeneration, demyelination, neural cell loss including apoptosis of oligodendrocytes, and the formation of inhibitory barriers for regeneration. Macrophages are the key players in the neuroimmune niche following SCI, playing divergent roles based on their surrounding stimuli. Anti-inflammatory cytokines such as interleukin-10 (IL-10) can induce neuroprotective and pro-regenerative activation states in macrophages. In this study, we investigated the effect of localized lentiviral expression of IL-10 with or without multi-channel poly(lactide-co-glycolide) (PLG) bridge implantation on outcome after spinal cord injury. Combinatorial IL-10 delivery and PLG bridge implantation resulted in a synergistic improvement in ipsilateral paw function. Transsynaptic pseudorabies virus (PRV) retrograde tracing demonstrated that axons regenerate through the PLG bridge and form a synaptic relay between corticospinal neurons as well as the paraventricular nucleus of the thalamus and the neuromuscular junction, and that the number of connected neurons in the PVN was increased by combined treatment with IL-10 and Bridge implant. Our findings support the combination of PLG bridge implantation and IL-10 expression as a novel therapeutic strategy for modulating

neuroinflammation and promoting motor recovery after SCI by reestablishing the damaged circuitry.

## **INTRODUCTION**

SCI is a complex and devastating condition that can impair motor-sensory and autonomic functions, resulting in paralysis below the level of injury. The pathophysiology of SCI is characterized by primary and secondary injury phases. Primary injury results from the initial impact, whereas secondary injury results from subsequent tissue damage caused by the interplay of environmental factors at the injury site. Injury to the spinal cord initiates a progressive inflammatory cascade that includes activation of resident immune cells (microglia) and a rapid influx of peripheral immune cells (neutrophils and macrophages) via a broken blood-spinal barrier [2].

Biomaterials have shown great promise for fostering axonal regeneration following SCI [24] [14] [26] [18] [27] [28] [29] [30]. Poly (lactide-co-glycolide) (PLG) is a widely used biomaterial for tissue repair, with a good biodegradability and biocompatibility profile. We have shown that implantation of a multi-channel PLG-bridge at the SCI site limits scar formation and promotes robust axonal regeneration [16] [40] [121] [26] [18] [122]. While the CST is generally considered to exhibit minimal long tract regeneration after SCI [123], CST axons are also capable of entering, traversing, and exiting an implanted PLG bridge [16], and regeneration of these axons is associated with locomotor improvements. However, although PLG bridge implantation supports axonal regeneration, regenerated axons in the bridge are poorly myelinated, identifying a need for supplemental strategies for repair [22].

Implanted PLG bridges exhibit robust infiltration and prolonged retention of host immune cells and other cell types, with macrophages the predominant cell type observed in the channels at 2 and 6 weeks post bridge implantation [48], where these cells contribute to the biodegradation of the bridge polymer structure [124]. Macrophages/microglia are primary orchestrators of the secondary injury phase and have been shown to play multiple roles following SCI [125] [126] [127] [128]. The acute injury microenvironment is dominated by pro-inflammatory macrophages (M1), which can release neurotoxic factors including cytokines (e.g. interleukin -6, TNF $\alpha$ , and IFN), chemokines, and free radicals (nitric oxide), all of which contribute to extended tissue damage within the spinal cord [2] [129] [59]. Macrophages/microglia can also take on a pro-regenerative neuroprotective (M2) state. Indeed, microglia play an important role in stabilizing the extent of tissue degeneration, instructing by contributing to the formation of the glial scar, which sequesters blood-derived immune cells in the lesion core and helps to preserve intact neural tissue [60, 130, 131]. Further, M2 macrophages/microglia contribute to repair by phagocytizing dead cells/debris and promoting neuro-regeneration by the release of neurotrophic factors and anti-inflammatory factors [132] [61].

Critically, macrophage/microglial phenotype can be modulated by cytokine exposure, even when these cells are biased by the early injury environment [133] [134]. Park et al showed that the combination of PLG bridge implantation with IL-10 delivery in a thoracic SCI model shifts the macrophage response from a pro-inflammatory to a pro-regenerative state, robustly enhances axon regeneration into the bridge and improves locomotor recovery. Critically, IL-10 also increased the proportion of regenerated axons that exhibited oligodendrocyte myelination in the PLG bridge [14]. Despite this enhancement,

more than 50% of regenerated axons in the PLG bridges failed to show evidence of oligodendroglial myelination, leaving significant room for improvement in this response.

One possibility to build on these data in future studies could be to combine these approaches with delivery of a myelinating stem cell population. However, both allogeneic and xenogeneic NSC transplants require constitutively immunodeficient animal models to achieve long-term cell engraftment. Data from Park et al. also leave a critical gap in understanding whether motor recovery is mediated through synaptic connectivity of regenerated motor fibers below the injury [14] [73]. In this paper, we therefore address two crucial gaps. First, we test the combination of PLG bridge implantation and IL-10 delivery in an immunodeficient (Rag1) mouse cervical SCI model, analyzing both regeneration and recovery of function. Second, we test whether recovery is associated with re-establishment of synaptic connections below the injury site, and the influence of IL-10 treatment on the number of connected neurons.

Overall, this study demonstrates the potential for combination therapy to modulate macrophage response, promote motor recovery, axonal regeneration, and myelination. Furthermore, we evaluated the association between motor recovery and synaptic connectivity and integration of robustly regenerated axons. This research paves the way for future studies that combine cell transplantation with PLG and IL-10 therapy to further enhance myelination and functional integration of regenerated axons.

## **MATERIALS & METHODS**

### **Animal Welfare**

Animal surgery procedures were performed in accordance with the Institutional Animal Care and Use Committee at the University of California, Irvine, and in consistency with U.S. Federal guidelines.

### **Fabrication PLG for in vitro studies**

We prepared a 5% Poly(lactide-co-glycolide) (comprised of a 75:25 lactide: glycolide ratio; Sigma-Aldrich Inc, Saint Louis, MO) in chloroform solution and dispersed it in a glass petri dish covered with 1mm sodium chloride crystals. Following chloroform evaporation (2 hours), water was added to the dried salt/polymer and allowed to sit for twenty-four hours to leach out sodium chloride. Petri dishes with PLG scaffold were sterilized with 70% ethanol, one sterile water wash, and UV exposure in the laminar flow hood.

### **Macrophage isolation and anti-inflammatory cytokine hIL-10 treatment**

As previously described, macrophages (MØ) were isolated from peritoneal cavities of adult female Rag1 immunodeficient mice, as previously described (**Fig. 3.1A**) [135]. Mice were given an i.p. injection of 12% sodium caseinate and MØ were collected at 5 post-injections. Isolated MØ were seeded with X-vivo media (X-vivo based media (Fisher Scientific, Waltham, MA) supplemented with bFGF (0.1 ng/mL), BDNF (PeproTech) (10 ng/mL), GDNF (10 ng/mL), Heparin (2 mg/mL), NAC (63 mg/mL), N2 (1:100), B27 (1:20) supplement and Ciprofloxacin (Cellgro) (10 mg/mL). MØ were cultured for 4 days on PLG or plain glass substrate and received either human recombinant IL-10 protein (10 ng/mL; R&D Systems) treatment or vehicle (PBS). Media was replaced 48 hours following treatment.

### **Quantitative PCR**

RNeasy Mini Kit (Qiagen, Chatsworth, CA) was used to isolate RNA from MØ samples following treatment. RNA samples were treated with DNA-free DNase I to eliminate traces of genomic DNA (Ambion, Austin, TX). cDNA was generated using High-Capacity cDNA Reverse Transcription Kit per the manufacturer's instructions (Life Technologies, Carlsbad, CA). Quantitative Real-Time PCR reactions were performed using Taqman Universal Master Mix and Taqman gene expression assays (Thermo Fisher Scientific, Waltham, MA), according to manufacturer's protocol, in Applied Biosystems ViiA 7 Real-Time PCR System (Thermo Fisher Scientific, Waltham, MA). Housekeeping gene GAPDH was used to normalize all target genes and fold changes in expression were calculated using the DD<sub>Ct</sub> method. Results presented in technical replicates and biological quadruplets. List of Taqman gene expression assays used for RT-PCR are listed in **Table 3.1**.

### **Fabrication of multiple channel PLG bridges for in vivo implantation studies**

Poly(lactide-co-glycolide) (PLG) bridges were generated using a gas foaming/particulate leaching method as previously described [40] [18]. The final bridge dimensions were 1.15 mm in length, 1.25 mm in width, and 2 mm in height, containing 9 channels.

### **Lentivirus production**

Lentivirus containing pLenti-CMV-Luciferase or pLenti-CMV-IL10 was produced from HEK293T cells as previously described [15]. Virus titers were determined by a Lentivirus qPCR Titer Kit (Applied Biological Materials, Richmond, BC, Canada) and 2E9 IU/mL was used in this study.

### **Lentivirus loading into the multiple channel PLG bridge and gelfoam**

PLG bridge and gelfoam were disinfected (70% ethanol and sterile water wash). 2  $\mu$ L of lentivirus was added onto the material and, after a 2-minute incubation at room temperature, excess moisture was removed with sterile filter paper and the process was repeated three times. Lentivirus loaded bridge and gelfoam samples were stored on ice and implanted within 3 hours. Lentivirus conditions included Interleukin 10 (IL-10) and Firefly luciferase (FLuc; control)

### **Spinal cord injury**

Cervical hemisection injury and postoperative care was performed as previously described (Pawar, Cummings, et al. 2015). Briefly, the mice were anesthetized using 2% isoflurane and the mice received C4-C5 laminectomies to reach the C5 vertebrae of the spinal cord. All mice received left sided unilateral hemisection of 1-1.1 mm in length. Spinal cord tissue was removed and immediately replaced with a lentivirus loaded either PLG bridge or gelfoam (Pfizer, New York, NY). The exposed muscle was sutured using 5-0 chromic gut, and the skin was closed using wound clips. All mice were placed in cages with clean Alpha-Dri bedding on top of heating pads at 37°C overnight. The following subcutaneous injections were administered post-op: Baytril (2.5mg/kg) once a day for two weeks, lactated ringers (50mL/kg) once a day for five days, and buprenorphine (0.05mg/kg) every 12 hours for three days. Expression of bladders was done manually twice a day for the study duration. Oral antibiotics [ciprofloxacin (10mg/100mL), Sulfamethoxazole/Trimethoprim (2mL/100mL), and ampicillin (20mg/mL)] were rotated every two weeks for the duration of the study to avoid bladder infection.

### **Pseudorabies Virus (PRV) tracing**

PRV-152-GFP trans-synaptic tracer ( $2.48 \times 10^9$  pfu/ml; In collaboration with Dr. Xiangmin Xu's laboratory, UCI) was injected into the ipsilateral (left) forelimb triceps muscle of animals 30 WPI. This enables retrograde labeling of pyramidal neurons in the cortex and validation of functional connectivity after PLG bridge implantation. After 10 minutes of anesthesia (1.5 percent isoflurane in O<sub>2</sub>), a skin incision was made to expose the left triceps forelimb muscle. 5  $\mu$ L PRV was injected at different depths into two sites of the left forelimb muscle using a stereotaxic Hamilton syringe with a 26-gauge needle, with a five-minute interval between each injection. Using tissue adhesive Vetbond, the skin was sewn shut (St. Paul, Minnesota, USA). The animals were transferred to a Biosafety Level D room, where they received a Carprofen (5mg/kg) injection and continued to receive bladder care twice daily. Four days after PRV injection, the spinal cord segment (C3 to C7) and brain tissues of mice were perfused and dissected for further examination.

### **Perfusion, Tissue Collection, and Sectioning**

Mice were anesthetized with 100 mg/kg pentobarbital and transcardially perfused with PBS (15 mL) and 4% paraformaldehyde (100 mL) at 16 WPT (hNSC differentiation fate and regeneration assessment) or 26 WPT (PRV connectivity tracing). Brain tissue and spinal cord segments corresponding to C3-C7 roots were dissected and post-fixed/cryoprotected overnight in 4% paraformaldehyde + 20% sucrose. The tissue was then flash frozen using -60°C isopentane and stored at -80°C. Using a sliding microtome, brain tissue was sectioned transversely, and 30 $\mu$ m serial sections were collected in phosphate-buffered saline with 0.02 percent sodium azide and stored at 4 C until further use. C2-C8 spinal cord segments were embedded in Neg50 Frozen Section Medium (Fisher Scientific International, Hampton, NH) to be processed into 30  $\mu$ m thickness with a cryostat and Cryo-Jane tape transfer system

(Leica Biosystems, Wetzlar, Germany). Transversely or horizontally sectioned spinal cords were stored at -20 degrees Celsius until immunohistochemistry processing.

### **Immunohistochemistry and imaging**

Spinal cord tissue sections slides (Cryo-Jane tape transfer slides) were dewaxed in Histo-Clear II clearing agent (National Diagnostics, Atlanta, Georgia) rehydrated in descending ethanol gradient (100%, 95%, 80% and 70%), and hydrated in distilled water for 10 minutes. For antigen retrieval, slides were incubated in preheated sodium citrate antigen retrieval solution (10 mM Sodium citrate, 0.05% Tween 20, pH 6.0) for 30 min at 96 deg C in water bath. After 20 minutes at room temperature, the slides were rinsed with water and immunohistochemistry was performed as described below. Spinal cord sections (Cryo-Jane tape transfer slides) and brain sections (microtome, free-floating) were blocked (1.5% donkey serum and 0.1% Triton X in PBS) for 1 hour at room temperature and incubated with primary antibody (diluted in blocking solution) overnight at room temperature. Antibody information and dilutions are listed in **Table 2.1**. Following 3 five-minute washes (0.1% Triton-X 100 in PBS), tissue was incubated with appropriate fluorescent-dye conjugated secondary antibodies and nuclear dye Hoechst 33342 (1:1000 dilution; Invitrogen, Waltham, MA) for 2 hours at room temperature. After three final five-minute Triton-X 100 in PBS washes, the slides were mounted with Fluoromount G. (SouthernBiotech, Birmingham, AL). Images were captured using ZEISS Axio Imager II light microscope with an Apotome2 image processor and ZEISS LSM 900 with Airyscan 2 microscope (Zeiss, Oberkochen, Germany).

### **PRV quantification:**

Spinal cord tissue was collected at 30 WPI and sectioned horizontally at 30um thickness using CryoJane. Immunostaining ( $\frac{1}{4}$  sampling interval) was performed to detect

PRV-GFP labeled fibers. All PRV+ fibers within the gelfoam/PLG bridge were counted manually. Brain sections were sectioned coronally at 30um using a sliding microtome. Immunostaining (all sections containing motor cortex, no sampling) was performed to detect PRV-GFP cell bodies. All PRV+ cell bodies within the motor cortex were counted manually. All quantifications were performed at 40X magnification using ZEISS Axio Imager II light microscope with an Apotome2 image processor by the investigators blinded to the experimental groups

### **Ladder beam analysis**

All behavioral data were collected and analyzed by blinded observers. Mice were handled daily for two weeks prior to pre-injury behavioral testing to acclimate animals to human contact. Following a five-minute acclimation to the environment, mice were recorded walking across a horizontal ladder beam for three trials. Video analysis quantified each left paw placement error, as previously described [87].

## **RESULTS**

### **PLG Scaffold and IL-10 Polarize Macrophages Towards an M2 Phenotype**

We have previously shown that IL-10 and PLG bridge-implantation alter the bulk-sequencing transcriptome of spinal cord host tissue after a thoracic hemisection injury [14]. Here, we sought to establish whether a shift in macrophage activation state could also be achieved in the Rag-1 mouse model, in which we expect innate immune cell responses to be attenuated. We examined the effect of IL-10 and PLG bridge on M1/M2 markers using quantitative RT-PCR analysis on peritoneal-derived macrophages, as summarized in the schematic in Figure 3.1A. Macrophage inflammatory state was assessed using three anti-inflammatory markers for M2: IL-10, CD206, and Arginase 1 and two inflammatory markers

for M1: TNF alpha, and IL-6 (**Fig. 3.1B-F**). Culture of macrophages on PLG scaffold alone increased Arg1 expression (2-fold), and decreased IL-6 expression (0.48), but did not alter the other markers analyzed. In contrast, culture of macrophages in the presence of IL-10 alone increased Arginase 1 (5.4-fold), CD206 (2.3-fold) and IL-10 (2.4-fold), and decreased TNF alpha (0.26-fold), identifying a consistent shift towards an anti-inflammatory state. The combination of PLG and IL-10 retained these effects and produced a synergistic effect on CD206 (3.1-fold) (**Fig 3.1C**). Our findings indicate that IL-10 treatment decreases the pro-inflammatory M1 phenotype while increasing the pro-regenerative M2 phenotype in Rag1 peritoneal macrophages.

### **Locomotor assessment revealed that PLG bridge and IL-10 supported motor recovery and combinatorial therapy resulted in a synergistic outcome**

Given that IL-10 enhances pro-regenerative gene expression and reduces pro-inflammatory gene expression, we next tested the effect of PLG bridge implantation and IL-10 delivery on locomotor recovery. We implanted the following treatment groups: 1) gelfoam + plenti-CMV-Firefly luciferase (FLuc) lentivirus control, 2) gelfoam + IL-10 lentivirus, 3) PLG + FLuc control, and 4) PLG + IL10 lentivirus. As published previously, we compared epicenter implantation of the PLG bridge to gelfoam control, which we have shown to be inert and identical to an 'empty' condition for axonal regeneration [16]. A left-sided cervical segment C5 hemisection injury induces motor deficits in the left forelimb. To investigate the effect of bridge implantation, as well as the combination of bridge + IL-10, on locomotor recovery. We used the horizontal ladder beam task at 20 WPI, analyzing left (ipsilateral) forelimb placement errors as previously described [16], [87], [100], [101]. Mice

were randomly assigned to each experimental group and the acquisition and analysis were performed by observers blinded to experimental conditions as described under methods. At the pre-injury time point, no significant differences were observed between experimental groups (percentage error means:  $8.0 \pm 0.66$ ,  $7.6 \pm 0.52$ ,  $8.9 \pm 0.65$ , and  $8.3 \pm 0.51$  for Gelfoam + FLuc, Gelfoam + IL10, Bridge + FLuc, and Bridge + IL10 group respectively; One-way ANOVA  $P=0.4199$ ). At 20 WPI, both the PLG bridge and IL10 alone groups showed a significant decrease in placement errors (**Fig. 3.2**). Error reduction in IL-10 alone is consistent with a previously published, neuroprotective effect of IL-10 treatment using this same vector in a thoracic SCI model [14]. Similarly, the reduction of errors by PLG bridge implantation alone is consistent with Pawar et al., in which we demonstrated the first evidence for CST regeneration into and through an implanted PLG bridge in this ipsilateral cervical SCI paradigm [16]. Critically, the PLG bridge + IL10 groups showed further enhanced motor recovery in comparison to each individual treatment, supporting a combinatorial effect.

### **Combination of PLG bridge and IL-10 significantly enhanced axonal regeneration and myelination.**

To investigate the effect of IL-10 in combination with PLG bridge implantation on axonal growth and myelination in an immunodeficient mouse model we compared epicenter implantation of the PLG bridge to gelfoam control, which we have shown to be inert and identical to an 'empty' condition for axonal regeneration [16]. Spinal cord tissues were harvested and sectioned 20 weeks post-SCI, and sections were immunostained with neurofilament heavy polypeptide (NF-H) to identify regenerated axons. PLG bridge groups exhibited robust regeneration of NF-H+ axons into the lesion site, whereas control groups

did not (**Fig. 3.3A-D, G**). Total axonal regeneration as well as the proportion of axons that were unmyelinated, myelinated by oligodendrocytes (MBP+P0-), or myelinated by Schwann cells (MBP+P0+ and MBP-P0+) was determined using Imaris's 3D volume rendering in triple immunolabeled high magnification images (**Fig. 3.3E**). PLG bridge alone significantly increased NF-H+ axon regeneration, which was further enhanced by IL-10 (**Fig. 3.3F-G**). Both Schwann cell-derived (**Fig. 3.3H**; MBP+P0+ plus MBP-P0+) and oligodendrocyte-derived (**Fig. 3.3I**; MBP+P0-) myelination of regenerated axons in the PLG bridge were also increased by IL-10. This increased myelination reflects an increase in total axon regeneration in the bridge; however, in addition to increased myelination, we observed an increase in the proportion of axons myelinated by oligodendrocytes (**Fig. 3.3F**). PLG+IL-10 group: 32% of total regenerated axons associated with myelin (~18% oligodendrocyte- and ~14% Schwann cell-derived myelin). PLG bridge alone (naive): 21% of total regenerated axons is associated with myelin (~6.5% oligodendrocyte- and ~14.8% Schwann cell-derived myelin).

Clearly, however, the vast majority of axons in the PLG bridge in either condition remained unmyelinated. This represents a significant deficit, as 40 to 60% of total axons, and as much as, and CST axons as an example, only ~86% of CST axons, in healthy rodent spinal cord are myelinated by oligodendrocytes. Together, these data demonstrate a benefit for IL-10 for regeneration and myelination in combination with PLG bridge implantation, but also support the need for an additional or more effective means by which to improve connectivity. In this regard, these findings also validate the RAG1 model for this regeneration paradigm, which will enable future testing of cell transplantation strategies to improve myelination efficiency. While achieving robust myelination of regenerated axons remains a

challenge, the robust regeneration identified in this paradigm is a significant finding. In this regard, a key issue that has not previously been addressed, whether regenerated axons form a functional synaptic bridge circuit between brain structures and the neuromuscular junction is unknown. We therefore next investigated synaptic connectivity of regenerated fibers using transsynaptic pseudorabies virus (PRV) tracing at 30WPI.

### **Transsynaptic pseudorabies virus (PRV) tracing assessment revealed that regenerated axons in the PLG bridge are synaptically connected**

We tested whether axons that regenerate into the PLG bridge become integrated into synaptic circuitry via retrograde GFP-reporter pseudorabies virus (PRV) tracing. GFP-PRV was injected into the forelimb triceps ipsilateral to the lesion site (**Fig. 3.4A**), with analysis of axonal labeling in the bridge implantation/injury site (**Fig 3.4B-D**), in the motor cortex (**Fig. 3.5A-B**), and in PVN of the hypothalamus (**Fig 3.5A, C-D**).

As for NF-H, PRV labeling was not detected within the injury site of either gelfoam or gelfoam+IL-10 controls (**Fig. 3.4B-B1**), whereas robust PRV labeling was observed in both PLG bridge groups (**Fig. 3.4C-C1, D**). In contrast to analysis of total NF-H positive fiber volume (**Fig. 3.3**), IL-10 expression in combination with bridge implantation did not further enhance the number of PRV labeled axons identified (**Fig. 3.4D**). However, these analyses were conducted in different animals, with different methods and planes of section (NF-H volume within the PLG channels in transverse sections vs. PRV axon number in horizontal sections), based on the principal endpoints we sought to determine. Interpretation of these data is discussed in detail under Discussion. The most parsimonious interpretation of these data, however, is that IL-10 enhances axon regeneration in the PLG bridge, as demonstrated

by NF-H, but does not a priori enhance the synaptic connectivity of these axons as interrogated by PRV tracing. Most importantly, these data demonstrate that both the PLG bridge and PLG bridge + IL-10 support not only regeneration, but also reestablishment of synaptic connectivity, for axons that enter and traverse the bridge.

Based on this evidence for synaptic connectivity of axons traversing the bridge, we next analyzed PRV-labeled neurons in two brain regions, the motor cortex and PVN. The corticospinal tract (CST) is the descending tract of the motor cortex. The CST originates in the layer V-VI motor cortex pyramidal neurons; the majority (>90%) of spinal CST axons decussate at the pyramids in the medulla, continuing in the contralateral spinal cord to innervate muscle after synapsing with ventral horn motor neurons. Consistent with the anatomical organization of the CST, PRV-GFP+ neurons were predominantly detected in the motor cortex contralateral to the injury and site of bridge implantation (**Figs. 3.5A1-2**), with sparse labeling detected in ipsilateral motor cortex. Transsynaptic PRV tracing was identified only in animals receiving PLG bridge implantation, and combined treatment (bridge + IL-10) did not increase the number of PRV+ labeled motor cortex neurons. These data represent novel evidence for synaptic connectivity between the motor cortex and forelimb muscle groups after a unilateral cervical SCI with PLG bridge implantation. These data are consistent with the interpretation that at this time point, IL-10 may have enhanced regeneration into the bridge based on NF-H labeling, but not the formation of synapses by these regenerated axons.

We also investigated PRV tracing in a second brain structure that has greater capacity than the motor cortex/CST to exhibit regeneration after axon injury, the PVN. PVN

connections are critical for autonomic regulation, including thermoregulation and cardiovascular function [136], [137], [138]. PVN neurons send projection ipsilaterally to the rostral ventrolateral medulla (RVLM) and RVLM neurons project to the sympathetic intermediolateral column (IML) of the spinal cord [139], [140]. Besides PVN-RVLM connections, the PVN contains neurons that monosynaptically connect to the spinal intermediolateral cell column (IML; PVN-IML neurons). The PVN-RVLM and PVN projections enter the lateral funiculus predominantly ipsilaterally and innervate the IML, although some fibers cross to the contralateral IML in the spinal cord [141]. Consistent with this anatomical organization, the PRV-labeled neurons were predominantly detected in the PVN neurons ipsilateral to the injected forelimb and SCI site, with the identification of a smaller population in the contralateral PVN (**Fig. 3.5A3**). As for the motor cortex, transsynaptic PRV tracing was identified only in animals receiving PLG bridge implantation. However, in contrast to the motor cortex, IL-10 increased the number of PRV+ labeled neurons in both the ipsilateral and contralateral PVN circuitry (**Figs. 3.5C-D**). Together, these data suggest that IL-10 may increase the representation of descending axons from different brain regions that regenerate and exhibit synaptic connections after SCI.

## **DISCUSSION**

SCI is a multi-phasic condition that causes paralysis below the level of damage. Injury to the spinal cord elicits a strong inflammatory response, leading to substantial neural cell death, axonal degeneration and dieback, demyelination, formation of a glial scar, and deposition of growth inhibitory factors such as chondroitin sulfate proteoglycans and myelin-associated inhibitors of regeneration [75] [7] [9] [76] [77] [2] [4]. Several decades of

extensive SCI research have made it clear that this complex problem requires combinatorial solutions. In this study, we examined the potential of anti-inflammatory cytokine IL10 delivery combined with PLG bridge implantation to repair the injured spinal cord and restore locomotor recovery. Previous studies have reported that IL-10 delivery at the injury site modulates inflammation, reduced cell loss, axonal dieback, and promoted motor function [67] [68] [69] [70] [71] [72] [62]. Consistent with this, Park et al. demonstrated that IL10 delivery combined with PLG bridge implantation significantly improved functional recovery and enhanced axonal regeneration through this inhibitory milieu [14] [122] [73]. However, it is unknown whether the improvement in motor recovery associated with the PLG bridge implantation and further enhancement in the combination group is due to the strengthening of spared circuitry or synaptogenesis, where regenerated axons through the PLG bridge form new synaptic connections below the level of the injury. To address this gap in the field, we utilize retrograde PRV transsynaptic tracing methodology to investigate the connectivity of regenerated axons through the PLG bridge and into the brain motor nuclei. Additionally, in this report, we utilized the Rag1 mice that have a normal innate immune response but impaired T and B cell function, we investigate the regenerative potential of the PLG bridge/IL-10 combinatorial approach. Our experimental model allows for translation to future research studies involving xenotransplantation of human stem cells into the injured spinal cord.

Innate immune cells play a vital role in SCI inflammatory microenvironment. For example, studies have reported that macrophages take on different activation states across the pro-inflammatory to pro-regenerative spectrum based on the cues they receive [142] [143]. IL-10 is known to induce pleiotropic effects in immunoregulation and inflammation.

IL-10 induces a shift towards an anti-inflammatory state in macrophages through suppressed secretion of inflammatory cytokines [144]. For example, IL10 suppresses nuclear factor-kB (NF-kB) binding, which is a key transcription factor involved in regulating pro-inflammatory cytokine secretion [145]. We have previously reported that lentiviral mediated IL-10 expression drives macrophages towards an M2 phenotype and enhances the expression of synaptogenesis- and neurogenesis-related genes in the injured thoracic C57Bl6 spinal cord [14].

In this report, we validated this phenotype shift in the injured cervical Rag-1 mouse spinal cord using a targeted set of markers for gene expression analysis. We demonstrate that IL-10 upregulated M2 pro-regenerative gene expression (Arginase-1 and CD206) and decreased M1 pro-inflammatory genes (IL-6 and TNF alpha). Arginase1 is an enzyme that enhances the expression of polyamines, which are associated with elevated cyclic AMP (cAMP) levels. Elevated cAMP levels can in turn negate the inhibitory effect of myelin-associated glycoproteins on axonal regeneration. [146, 147] [142]. CD206 binds to and facilitates the removal of apoptotic and necrotic cells without causing toxic byproducts [147], [143]. In contrast, TNF alpha and IL-6 are proinflammatory cytokines that are upregulated immediately after injury and play a pivotal role in the initiation of inflammatory cascade and secondary tissue degeneration in the injured spinal cord [148] [149] [150] [150] [151] [152]. In sum, these data support the previous publication by Park et al. in thoracic SCI, in which IL-10 induced an M2 macrophage response and pro-regenerative environment and demonstrate a comparable effect in Rag-1 cervical SCI mice, which retain innate immune cells but lack an adaptive immune response.

While IL-10 expression significantly improved both regeneration and myelination status of regenerated axons in the PLG bridge in C57Bl6 and Rag-1 mice, particularly the proportion of oligodendroglial myelin, the majority of axons in both PLG bridge and combination group remained unmyelinated. These data highlight that there is a further requirement to maximize the myelination of regenerated axons. While Smith et al. showed that NT3 in combination with IL-10 can significantly enhance oligodendroglial myelination, a majority of axons in that study also remained unmyelinated. Thus, new approaches are required. Future studies could explore the use of transplanted human neural stem cells that have the capacity to generate new oligodendrocytes (CNS myelinating cells). We and others showed the potential of NSC to differentiate into oligodendrocytes in the injured spinal cord and participate in the myelination process in the injured spinal cord [17] [50] [153]. Therefore, validation of regenerative capacity and the effect of IL-10 in the PLG bridge implantation paradigm in Rag1 mice is a critical step for future studies.

A significant gap in the literature for this paradigm has been a test of whether descending axons form a synaptic circuit connecting the brain and neuromuscular junction. We demonstrated the synaptic connectivity of regenerated axons that enter and traverse the bridge utilizing PRV transsynaptic tracing. In addition, our data suggest that IL-10 delivery may enhance the regeneration or recruitment of axons from selected brain regions into this circuitry.

As described under results, analysis of NF-H positive fiber volume at 20 WPI demonstrated an enhancement in the bridge + IL-10 group, but analysis of PRV labeled axon number at 30 WPI did not. Several parameters are important to consider in interpreting

these results: 1) method of analysis, 2) timing and 3) alternative circuitry. The method of analysis used to quantify the total number of PRV+ axons may not be directly comparable with the volumetric analysis used for total NF-H+ regenerated axons in the PLG bridge. We are currently completing Imaris 3D volumetric analysis to quantify PRV+ fibers in the PLG bridge. If these data also identify an increase in PRV+ axon volume in bridge + IL-10 vs. bridge alone, it may suggest a predominant effect of IL-10 on axon caliber or length, as opposed to number per se. In the case of timing, we performed the NF-H analysis at 20 WPI, whereas PRV tracing was performed at a later time point of 30 WPI. It is possible that the principal effect of IL-10 is not to induce the regeneration of axons that would otherwise not have entered the PLG bridge, but rather to accelerate the entry or growth of these axons. Thus, the number of axons in the PLG bridge alone vs. PLG bridge + IL-10 groups could have equalized between 20 and 30 WPI. Lastly, with respect to alternative circuitry, the brain region quantification in this report focused on the motor cortex and PVN labeling. While IL-10 did not significantly increase the number of PRV+ CST projection neurons in motor cortex, it did increase the number of PRV+ descending projection neurons in the PVN. This suggests that IL-10 enhanced recruitment of descending axons from additional brain areas into the bridge, which could have led to synergistic improvement of motor function in the combination group. Brainstem motor pathways including reticulospinal- and rubrospinal tracts play a major part in controlling rodent locomotion [115]. We are currently quantifying PRV labeling in other brain nuclei to understand the level of rewiring of spinal-brainstem-brain motor circuitry between the bridge and bridge+IL-10 group.

Collectively, this report demonstrates that PLG bridge implantation and localized IL-10 expression drive a synergistic improvement in locomotor recovery. This improved motor

recovery is associated with enhancement of axonal regeneration and myelination, particularly the proportion of oligodendroglial myelin relative to the bridge alone treatment, as well as increased synaptic connectivity between the PVN and forelimb triceps. Quantification PRV labeling in brainstem nuclei is currently underway to determine the degree of spinal-brainstem-brain motor circuitry rewiring between the bridge group and the bridge+IL-10 group. Our findings indicate that the combination of PLG bridge implantation and IL-10 expression is a promising strategy for modulating neuroinflammation and promoting motor recovery after SCI and supports enhanced synaptic connectivity as a mechanism of repair.

## FIGURES

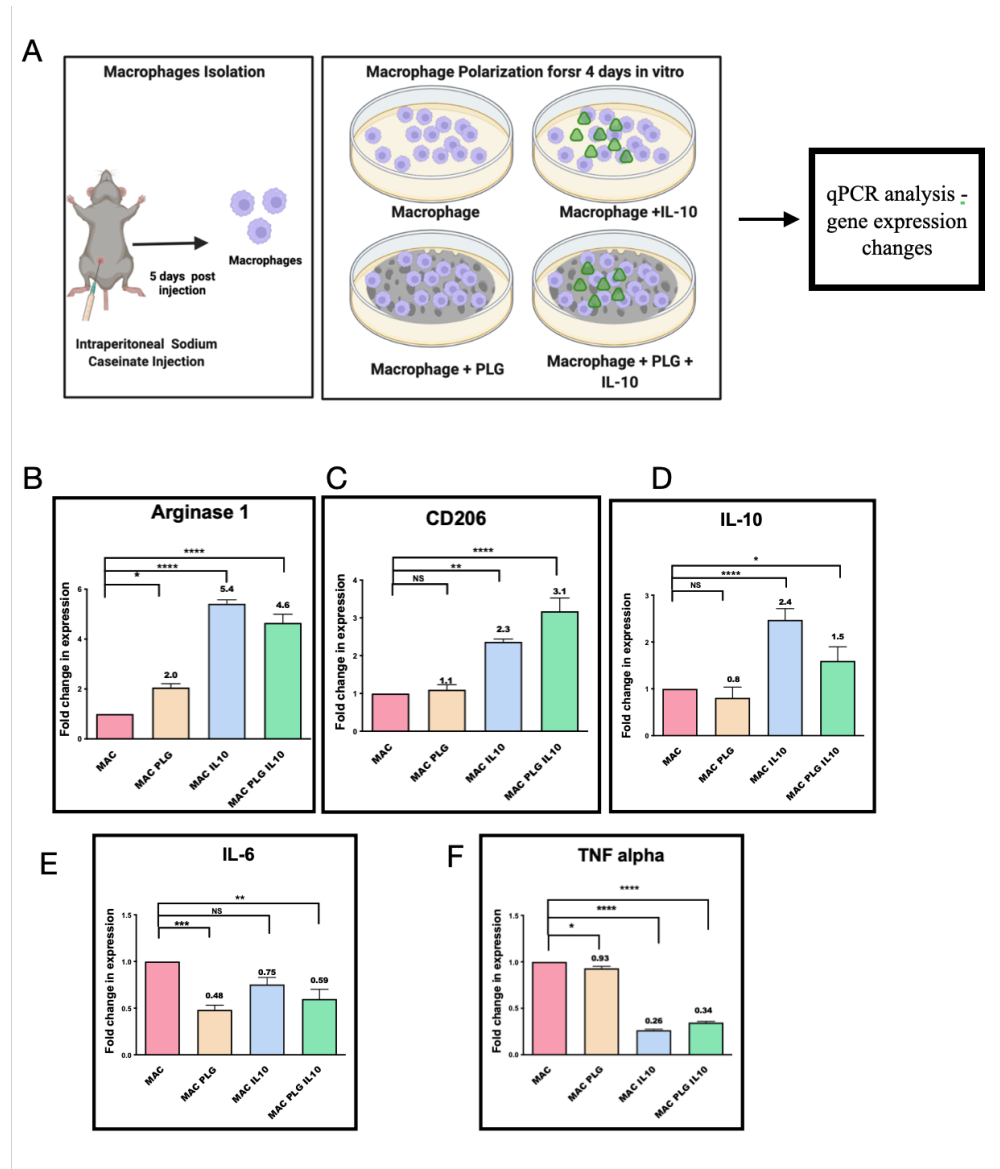


**Figure 3.1: Anti-inflammatory cytokine IL-10 and PLG alters macrophage activation state. (A)** Schematic of experimental design showing polarization of peritoneal macrophages in presence of PLG scaffold and IL-10 *in vitro*. **(B-F)** Fold change in expression of anti-inflammatory markers **(B-D)** and pro-inflammatory markers **(E and F)**. Statistical analysis was conducted using One-way ANOVA. with Dunnett's multiple comparison test, (Mean  $\pm$ SEM) n=4/group. List of Taqman gene expression assays used for RT-PCR are listed in Table 3.1

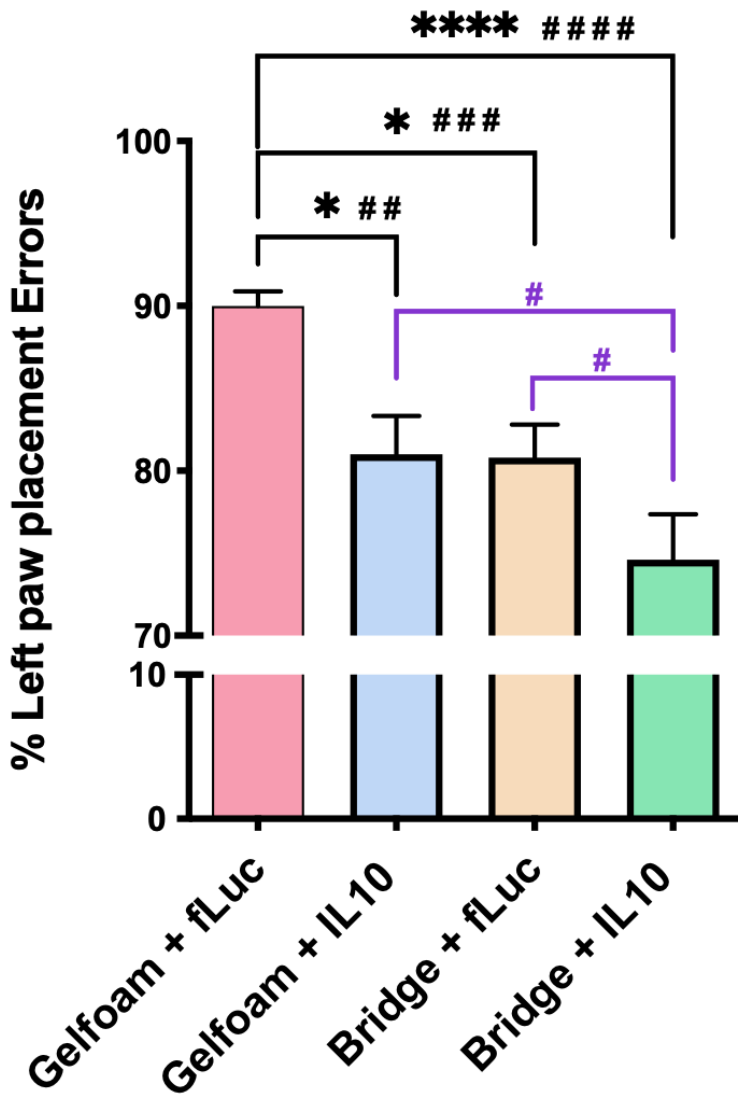


**Figure 3.2: Locomotor behavioral assessment of paw placement errors on the horizontal ladder beam.** Quantification of ipsilateral paw placement errors show a significant reduction in errors for all three treatment groups 20 weeks after injury (16WPT). Groups were compared using one-way ANOVA, followed by Tukey post hoc tests (\*\*\*\* $p \leq 0.0001$ , \*\* $P \leq 0.01$ , and \* $P \leq 0.05$ ) and unpaired t-tests (#### $p \leq 0.0001$ , ### $p \leq 0.001$ , and # $p < 0.05$ ) mean  $\pm$ SEM and N= 9-13 animals per group.

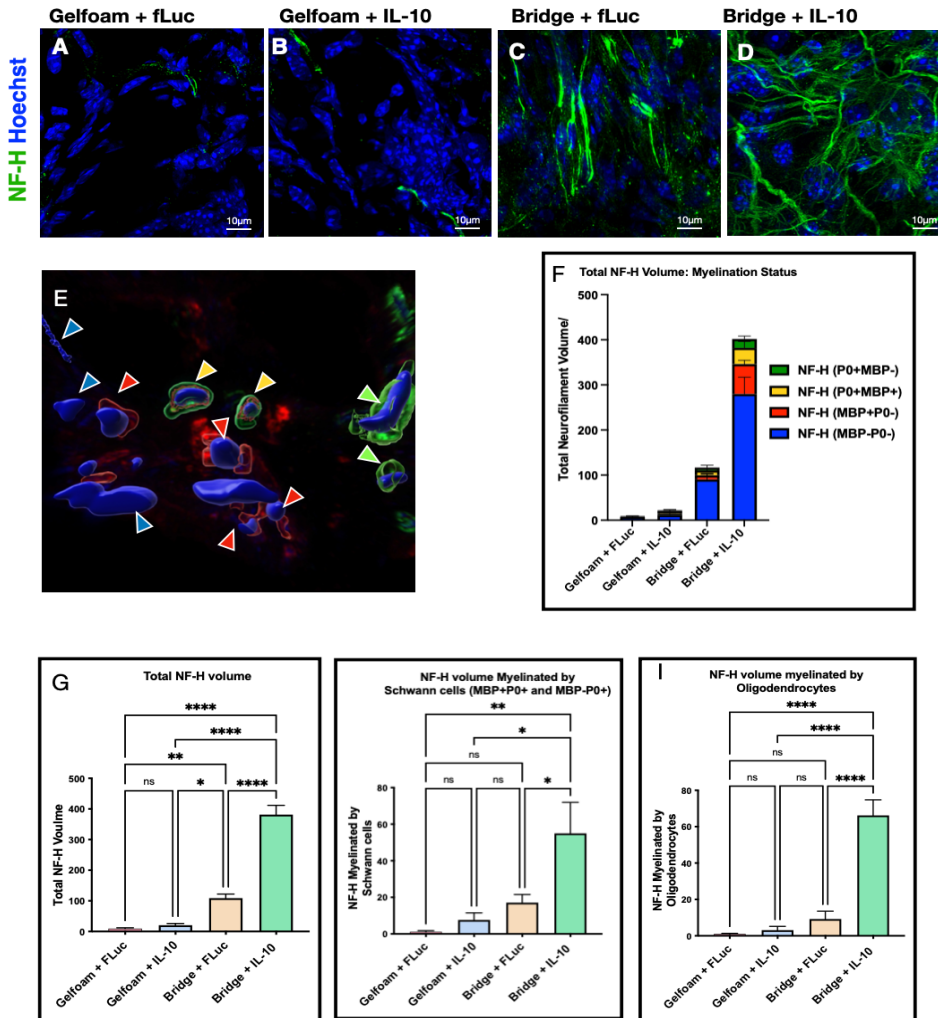


**Figure 3.3: PLG bridge implantation and localized expression of IL-10 promotes axonal growth and myelination at 20WPI. (A-D)** Immunograph of neurofilament (NF-H) labeling inside the injury epicenter in gelfoam+fLuc (control) (A), IL-10 (B), PLG bridge (C), and PLG bridge + IL-10 (D). **(E)** Representative micrograph showing Imaris 3D surface volume rendering of neurofilament fibers (NF-H, blue), oligodendrocyte-derived myelin volume (MBP, red), and Schwann cell-derived myelin volume (P0, green); blue arrowhead is pointing to unmyelinated NF-H+ filament, red arrowhead is pointing to NF-H+ filament associated with oligodendrocyte-derived myelin (MBP+P0-), Green & yellow arrowhead are pointing to NF-H+ fibers associated with Schwann cell-derived myelin (MBP+P0+, and MBP-P0+). **(F)** Grouped data represents the total NF-H volume and myelination status of the NF-H+ axons. **(G-I)** Total NF-H volume (G), NF-H volume associated with Schwann cell myelin (H) and NF-H volume associated with oligodendrocyte myelin (I) were normalized to gelfoam + fLuc control (dashed line) and statistical analysis was conducted using One-way ANOVA with Tukey's multiple comparison test. n=5-6 mice/group, one spinal cord section per mouse and 3 to 6 images within the injury site (Mean ± SEM).

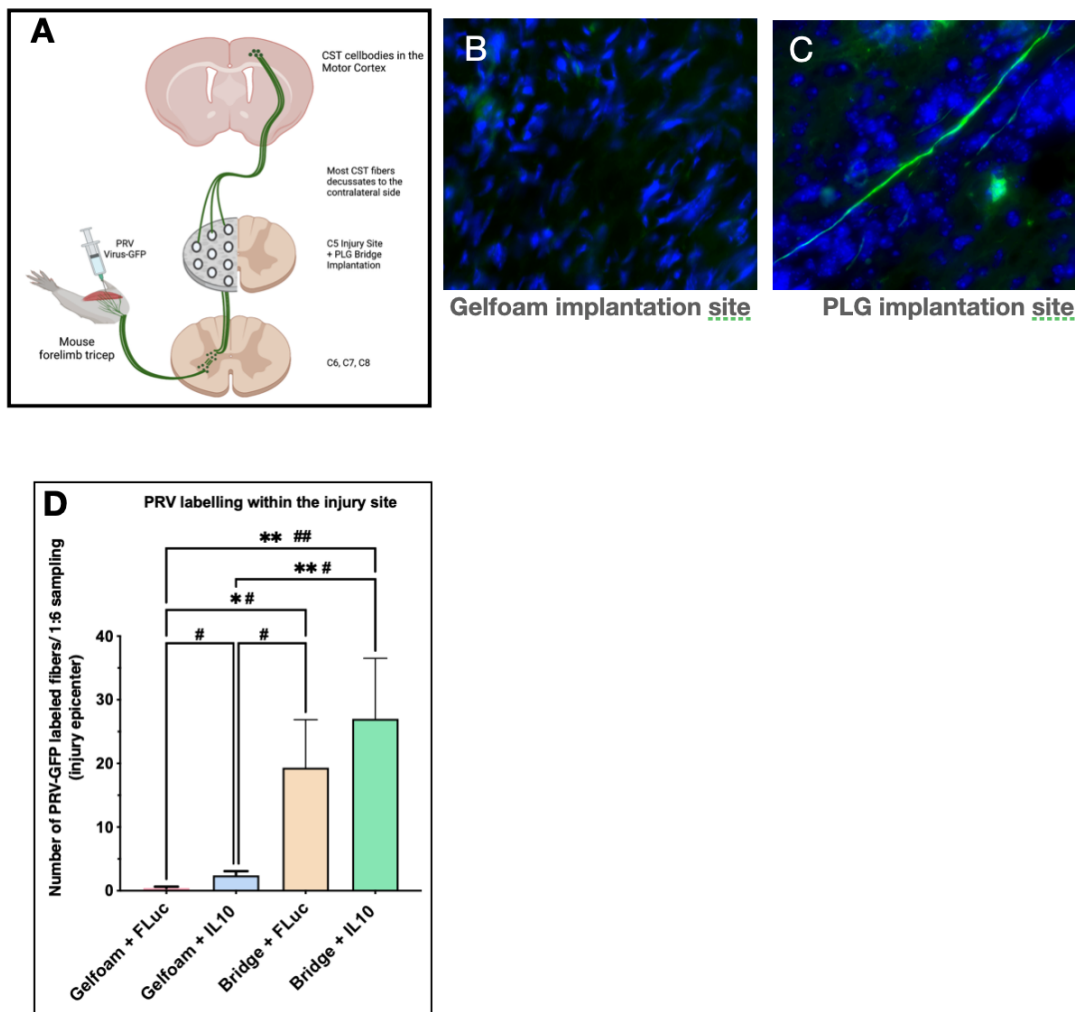


**Figure 3.4: PRV functional synaptic connectivity assessment within the injury site. (A)** Schematic of PRV retrograde tracing showing ipsilateral triceps injection and transport of PRV from lower motor neuron innervated to the forelimb muscle to the corticospinal tract cell bodies in motor cortex through synaptically connected regenerated fibers in the PLG bridge. **(B-C)** Representative image of mouse spinal cord section in horizontal plane (C5 left hemisection injury) at 30 weeks post-SCI showing PRV labeling. **(B)** PRV labeling (green) in the gelfoam group; B1 insert shows that PRV fibers were sparsely detected or not observed in the gelfoam implantation site. **(C)** PRV labeling in the PLG group. (C1) Higher magnification inserts show PRV+ regenerated fibers inside the PLG bridge. **(D)** Quantification of PRV labeling within the injury site (1 in 6 tissue section sampling was performed). Groups were compared using one-way ANOVA, followed by Tukey post hoc tests (\* $P \leq 0.05$ , \*\* $P \leq 0.01$ ) and unpaired t-test two-tail. (# $p \leq 0.05$ , ## $P \leq 0.01$ ).

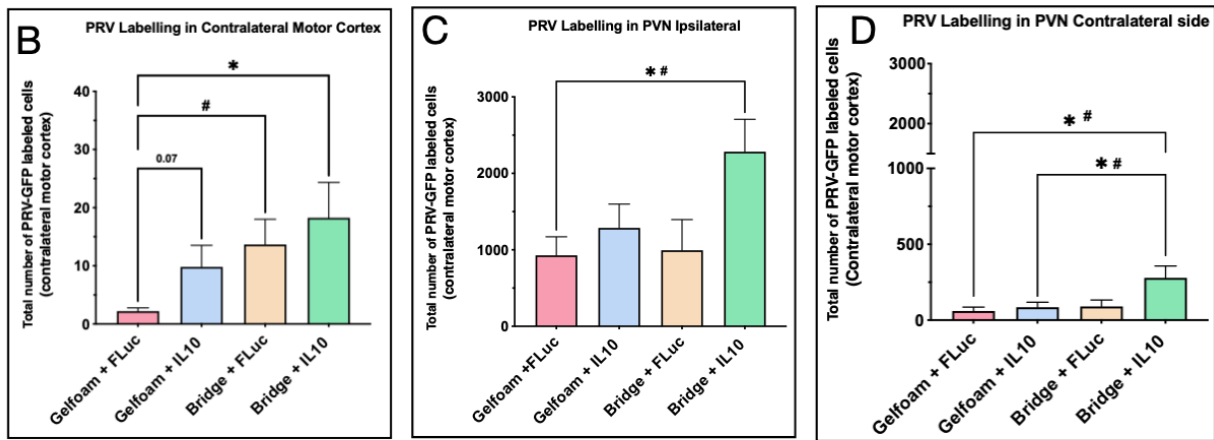
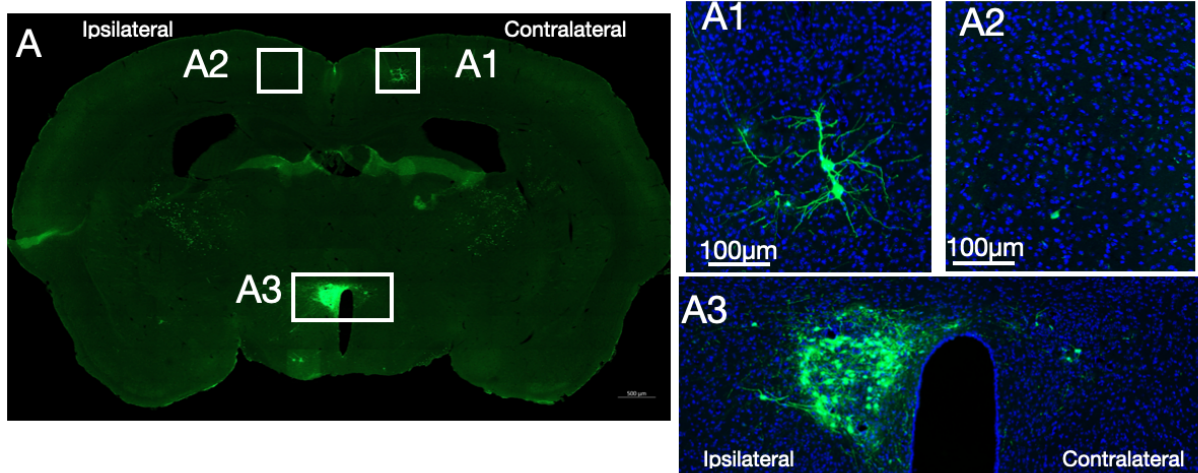


**Figure 3.5: PRV functional synaptic connectivity assessment in the motor cortex and PVN regions of the brain.** (A) Representative image showing PRV labeling in the CST cell bodies in the motor cortex. (A1-A3) High magnification image showing contralateral (A1) and ipsilateral labeling (A2) in the motor cortex, and in the PVN (A3). (B) Quantification of total PRV-labeled CST cell bodies in the contralateral motor cortex region (A1), showing connectivity in both the individual treatments and further enhancement in the combinatorial approach. (C-D) Quantification of total PRV-labeled cell bodies in the PVN ipsilateral (C) and contralateral (D). Groups were compared using one-way ANOVA, followed by Tukey post hoc tests (\* $P \leq 0.05$ , \*\* $P \leq 0.01$ ) and unpaired t-test two-tail. (# $p \leq 0.05$ ,  $p$  value=0.085).  $n = 3-5$  biological replicates/group. Mean  $\pm$  SEM.

**Table 3.1. List of Primers**

| <b>Primer</b> | <b>Assay ID</b> | <b>Specificity</b> |
|---------------|-----------------|--------------------|
| GAPDH         | Mm99999915_g1   | Endogenous Control |
| IL-6          | Mm00446190_m1   | M1 macrophages     |
| TNF-alpha     | Mm00443258-m1   | M1 macrophages     |
| Arginase-1    | Mm00475988-m1   | M2 macrophages     |
| CD206 (Mrc1)  | Mm01329362-m1   | M2 macrophages     |
| IL-10         | Mm01288386-m1   | M2 macrophages     |

## **CHAPTER 4**

### **Summary and Conclusion**

Spinal cord injury causes paralysis and significantly impacts the affected patients due to the lack of treatment to restore the lost function. There is a pressing need to address this complex multifaceted problem using combinatorial approaches. In this dissertation, I investigated combinatorial approaches for spinal cord injury. In Chapter 2, I tested acute PLG bridge implantation and chronic hNSC transplantation, employing PLG bridge implantation to support axonal regeneration through the injury site and hNSC transplantation to support regeneration and remyelination of the regenerated axons. In Chapter 3, I investigated the effect of localized expression of IL-10 with or without PLG bridge implantation to modulate neuroinflammation and promote motor recovery by reestablishing the synaptic neural circuitry through the PLG bridge. In ongoing analyses of my work, I am assessing the combination of PLG bridge implantation, hNSC transplantation, and IL-10 delivery to further enhance functional improvement, regeneration, and synapse formation.

#### **Chapter 2: Acute Biomaterial Bridge Implantation and Chronic Neural Stem Cell Transplantation to Facilitate Axonal Regeneration, Myelination, and Connectivity After Spinal Cord Injury**

Pathological events that occur post spinal cord injury exacerbate tissue damage. In particular, the presence of scar tissue and buildup of inhibitory factors prevents severed axons in the spinal cord from exhibiting an effective regeneration response. In this study, I used a PLG bridge to fill the defect, modulate the injury environment, and support axonal

regrowth. Despite the ability of the PLG bridge to support axonal growth and promote motor recovery, only a small percentage of axons that regenerate into the PLG bridge channels become myelinated, an essential factor for efficient transmission of signals from the motor cortex to the spinal cord. hNSCs transplantation is one clinically relevant alternative by which the myelination of regenerating axons could be enhanced. Accordingly, we tested the hypothesis that transplanted hNSCs have an ability to migrate into the channels of the PLG bridge and contribute to the myelination of newly formed axons to further enhance locomotor functional recovery. While NSC transplantation studies are promising in terms of functional improvement, the post-SCI immune niche has a dramatic effect on NSC fate, migration, and functional integration, and consequently the overall efficacy of these cells after SCI. Accordingly, in this study, I first tested the effect of PLG bridge on innate immune response after SCI in vivo and the subsequent effect of PLG immune niche on hNSC fate in vitro and in vivo. In the second series of experiments, I investigated the therapeutic potential of the combination of PLG bridge implantation and hNSC transplantation in vivo.

### **Key findings**

- Long-term profiling of innate immune response revealed that the presence of PLG bridge alters the innate immune response after SCI. PLG bridge modulates the cellular inflammatory response by supporting an extended phase of macrophage/microglia recruitment while delaying the re-emergence of the PMN population. Understanding the SCI inflammatory environment in presence of PLG bridge is crucial for the meaningful interpretation of hNSC fate, migration, and potential for repair after in vivo transplantation studies with PLG bridge.

- PLG modulates hNSC fate at the baseline and alters the hNSC response to the immune cues by enhancing oligodendrocytic fate and neuronal fate while decreasing astrocytic fate. These findings support the goal of testing hNSC transplantation as a means to remyelinate the regenerating axons in the PLG bridge.
- The combination of PLG bridge implantation and hNSC transplantation in vivo resulted in enhancement of hNSC engraftment and a selective ipsilateral increase in the number of all three CNS lineage cells.
- In particular, supporting our hypothesis, donor human NSC navigated along regenerated axons to migrate into the PLG bridge channels where the bundles of regenerated axons are present, differentiated into oligodendrocytes, and hNSC-derived oligodendrocytes contributed directly to myelination of mouse host axons.
- hNSC transplantation combined with PLG bridge implantation significantly improved axonal regeneration as well as both Oligo- and Schwann-derived myelination in the PLG bridge.
- Transsynaptic PRV tracing assessment revealed that hNSC-derived neurons in spared parenchyma integrated into mouse host circuitry, exhibiting synaptic connectivity.
- In this study, I showed novel evidence of reestablishment of synaptic neural circuitry between the brain and neuromuscular junction after SCI via regeneration through a biomaterial bridge.

- PLG bridge and hNSC treatment yielded individual effects on motor recovery and the combination group resulted in a synergistic outcome. Our data supports motor recovery in the bridge implantation group, which is consistent with a pro-regenerative impact of the PLG bridge and rewiring the severed circuitry [16]. Recovery in the hNSC group supports strengthening the spared circuitry and hNSC derived neuronal integration into the spared parenchyma [17]. Further enhanced recovery in the combination group suggests these additive effects and enhanced myelination status regenerated axons in the PLG bridge.
- Overall, these data show that combining PLG bridge implantation with transplanted hNSC can modify and bypass inhibitory barriers to regeneration in the injury niche, paving the way for promising translational approaches to treat SCI.

### **Chapter 3: Combination of Biomaterial Bridge Implantation and Interleukin-10 Expression to Modulate the Inflammatory Response and Promote Neural Regeneration and Connectivity after Spinal Cord Injury**

The acute SCI microenvironment is dominated by pro-inflammatory macrophages and activated microglia that can release neurotoxic factors that contribute to extensive tissue damage. In this study, I examined the potential of anti-inflammatory cytokine IL10 delivery combined with PLG bridge implantation to repair the injured spinal cord and restore locomotor recovery in the Rag-1 mouse model. I hypothesized that IL-10 expression combined with PLG bridge implantation promotes locomotor recovery, which is mediated via neuroprotection and improved synaptic connectivity of regenerated axons.

## Key findings

- Consistent with previous studies, IL-10 treatment decreases the pro-inflammatory M1 phenotype while increasing the pro-regenerative M2 phenotype in Rag1 peritoneal macrophages [14, 62].
- By 20 WPI, both the PLG bridge and IL10 alone groups showed a significant improvement in motor recovery. Improvement in IL-10 alone treatment is consistent with a neuroprotective effect of IL-10 [14]. Similarly, improvement in the bridge implantation group is consistent with the pro-regenerative impact of the PLG bridge [16]. Combinatorial IL-10 delivery and PLG bridge implantation resulted in a synergistic improvement.
- Transsynaptic PRV tracing assessment revealed that the bridge supported reestablishment of neuronal circuitry from the motor cortex, PVN of the hypothalamus, and further enhancement in PVN circuitry with IL-10 delivery
- My data indicates that improved motor recovery is associated with the enhancement of axonal regeneration and myelination as well as increased synaptic connectivity between the PVN and forelimb triceps.
- Overall, my findings support the combination of PLG bridge implantation and IL-10 expression as a novel therapeutic strategy for modulating neuroinflammation and promoting motor recovery after SCI by reestablishing the damaged circuitry.

## **BIBLIOGRAPHY**

1. Lo, V., et al., *Critical care management of patients with acute spinal cord injury*. J Neurosurg Sci, 2013. **57**(4): p. 281-92.
2. Anwar, M.A., T.S. Al Shehabi, and A.H. Eid, *Inflammogenesis of Secondary Spinal Cord Injury*. Front Cell Neurosci, 2016. **10**: p. 98.
3. Ambrozaitis, K.V., et al., [*Pathophysiology of acute spinal cord injury*]. Medicina (Kaunas), 2006. **42**(3): p. 255-61.
4. Katoh, H., K. Yokota, and M.G. Fehlings, *Regeneration of Spinal Cord Connectivity Through Stem Cell Transplantation and Biomaterial Scaffolds*. Front Cell Neurosci, 2019. **13**: p. 248.
5. Gadani, S.P., et al., *Dealing with Danger in the CNS: The Response of the Immune System to Injury*. Neuron, 2015. **87**(1): p. 47-62.
6. Silver, J. and J.H. Miller, *Regeneration beyond the glial scar*. Nat Rev Neurosci, 2004. **5**(2): p. 146-56.
7. Tsintou, M., K. Dalamagkas, and A.M. Seifalian, *Advances in regenerative therapies for spinal cord injury: a biomaterials approach*. Neural Regen Res, 2015. **10**(5): p. 726-42.
8. Hejrati, N. and M.G. Fehlings, *A review of emerging neuroprotective and neuroregenerative therapies in traumatic spinal cord injury*. Curr Opin Pharmacol, 2021. **60**: p. 331-340.
9. Richardson, P.M., U.M. McGuinness, and A.J. Aguayo, *Axons from CNS neurons regenerate into PNS grafts*. Nature, 1980. **284**(5753): p. 264-5.
10. Ahuja, C.S., et al., *Traumatic Spinal Cord Injury-Repair and Regeneration*. Neurosurgery, 2017. **80**(3S): p. S9-S22.
11. Bracken, M.B., et al., *Efficacy of methylprednisolone in acute spinal cord injury*. JAMA, 1984. **251**(1): p. 45-52.
12. Chio, J.C.T., et al., *The effects of human immunoglobulin G on enhancing tissue protection and neurobehavioral recovery after traumatic cervical spinal cord injury are mediated through the neurovascular unit*. J Neuroinflammation, 2019. **16**(1): p. 141.
13. Stirling, D.P., et al., *Minocycline treatment reduces delayed oligodendrocyte death, attenuates axonal dieback, and improves functional outcome after spinal cord injury*. J Neurosci, 2004. **24**(9): p. 2182-90.
14. Park, J., et al., *Local Immunomodulation with Anti-inflammatory Cytokine-Encoding Lentivirus Enhances Functional Recovery after Spinal Cord Injury*. Mol Ther, 2018. **26**(7): p. 1756-1770.
15. Park, J., et al., *Reducing inflammation through delivery of lentivirus encoding for anti-inflammatory cytokines attenuates neuropathic pain after spinal cord injury*. J Control Release, 2018. **290**: p. 88-101.
16. Pawar, K., et al., *Biomaterial bridges enable regeneration and re-entry of corticospinal tract axons into the caudal spinal cord after SCI: Association with recovery of forelimb function*. Biomaterials, 2015. **65**: p. 1-12.
17. Cummings, B.J., et al., *Human neural stem cells differentiate and promote locomotor recovery in spinal cord-injured mice*. Proc Natl Acad Sci U S A, 2005. **102**(39): p. 14069-74.
18. Thomas, A.M., et al., *Channel density and porosity of degradable bridging scaffolds on axon growth after spinal injury*. Biomaterials, 2013. **34**(9): p. 2213-20.
19. Gonzenbach, R.R., et al., *Delayed anti-nogo-a antibody application after spinal cord injury shows progressive loss of responsiveness*. J Neurotrauma, 2012. **29**(3): p. 567-78.
20. Bregman, B.S., et al., *Recovery from spinal cord injury mediated by antibodies to neurite growth inhibitors*. Nature, 1995. **378**(6556): p. 498-501.

21. Forgione, N. and M.G. Fehlings, *Rho-ROCK inhibition in the treatment of spinal cord injury*. World Neurosurg, 2014. **82**(3-4): p. e535-9.
22. Thomas, A.M., et al., *Sonic hedgehog and neurotrophin-3 increase oligodendrocyte numbers and myelination after spinal cord injury*. Integr Biol (Camb), 2014. **6**(7): p. 694-705.
23. Bartus, K., et al., *Large-scale chondroitin sulfate proteoglycan digestion with chondroitinase gene therapy leads to reduced pathology and modulates macrophage phenotype following spinal cord contusion injury*. J Neurosci, 2014. **34**(14): p. 4822-36.
24. Saremi, J., et al., *Advanced approaches to regenerate spinal cord injury: The development of cell and tissue engineering therapy and combinational treatments*. Biomed Pharmacother, 2022. **146**: p. 112529.
25. Bedir, T., et al., *3D bioprinting applications in neural tissue engineering for spinal cord injury repair*. Mater Sci Eng C Mater Biol Appl, 2020. **110**: p. 110741.
26. Tuinstra, H.M., et al., *Long-term characterization of axon regeneration and matrix changes using multiple channel bridges for spinal cord regeneration*. Tissue Eng Part A, 2014. **20**(5-6): p. 1027-37.
27. Koffler, J., et al., *Biomimetic 3D-printed scaffolds for spinal cord injury repair*. Nat Med, 2019. **25**(2): p. 263-269.
28. Perale, G., et al., *Hydrogels in spinal cord injury repair strategies*. ACS Chem Neurosci, 2011. **2**(7): p. 336-45.
29. Dumont, C.M., et al., *Aligned hydrogel tubes guide regeneration following spinal cord injury*. Acta Biomater, 2019. **86**: p. 312-322.
30. Hurtado, A., et al., *Robust CNS regeneration after complete spinal cord transection using aligned poly-L-lactic acid microfibers*. Biomaterials, 2011. **32**(26): p. 6068-79.
31. Abbas, W.A., et al., *Recent Advances in the Regenerative Approaches for Traumatic Spinal Cord Injury: Materials Perspective*. ACS Biomater Sci Eng, 2020. **6**(12): p. 6490-6509.
32. Sun, Y., et al., *3D printing collagen/chitosan scaffold ameliorated axon regeneration and neurological recovery after spinal cord injury*. J Biomed Mater Res A, 2019. **107**(9): p. 1898-1908.
33. Yu, Z., et al., *Application of fibrin-based hydrogels for nerve protection and regeneration after spinal cord injury*. J Biol Eng, 2020. **14**: p. 22.
34. Santhosh, K.T., A. Alizadeh, and S. Karimi-Abdolrezaee, *Design and optimization of PLGA microparticles for controlled and local delivery of Neuregulin-1 in traumatic spinal cord injury*. J Control Release, 2017. **261**: p. 147-162.
35. Jeong, H.J., et al., *Biomaterials and strategies for repairing spinal cord lesions*. Neurochem Int, 2021. **144**: p. 104973.
36. Mahoney, M.J. and K.S. Anseth, *Three-dimensional growth and function of neural tissue in degradable polyethylene glycol hydrogels*. Biomaterials, 2006. **27**(10): p. 2265-74.
37. Andreopoulos, A.G., E.C. Hatzi, and M. Doxastakis, *Controlled release systems based on poly(lactic acid). An in vitro and in vivo study*. J Mater Sci Mater Med, 2000. **11**(6): p. 393-7.
38. Straley, K.S., C.W. Foo, and S.C. Heilshorn, *Biomaterial design strategies for the treatment of spinal cord injuries*. J Neurotrauma, 2010. **27**(1): p. 1-19.
39. Gower, R.M. and L.D. Shea, *Biomaterial Scaffolds for Controlled, Localized Gene Delivery of Regenerative Factors*. Adv Wound Care (New Rochelle), 2013. **2**(3): p. 100-106.
40. Tuinstra, H.M., et al., *Multifunctional, multichannel bridges that deliver neurotrophin encoding lentivirus for regeneration following spinal cord injury*. Biomaterials, 2012. **33**(5): p. 1618-26.
41. Guest, J.D., E.D. Hiester, and R.P. Bunge, *Demyelination and Schwann cell responses adjacent to injury epicenter cavities following chronic human spinal cord injury*. Exp Neurol, 2005. **192**(2): p. 384-93.

42. Powers, B.E., et al., *Remyelination reporter reveals prolonged refinement of spontaneously regenerated myelin*. Proc Natl Acad Sci U S A, 2013. **110**(10): p. 4075-80.
43. Chung, K. and R.E. Coggeshall, *Numbers of axons in lateral and ventral funiculi of rat sacral spinal cord*. J Comp Neurol, 1983. **214**(1): p. 72-8.
44. Hsu, J.Y., S.A. Stein, and X.M. Xu, *Development of the corticospinal tract in the mouse spinal cord: a quantitative ultrastructural analysis*. Brain Res, 2006. **1084**(1): p. 16-27.
45. Jin, M.C., et al., *Stem cell therapies for acute spinal cord injury in humans: a review*. Neurosurg Focus, 2019. **46**(3): p. E10.
46. Yamazaki, K., et al., *Clinical Trials of Stem Cell Treatment for Spinal Cord Injury*. Int J Mol Sci, 2020. **21**(11).
47. Liu, W.Z., et al., *Mesenchymal stem cell-derived exosomes: therapeutic opportunities and challenges for spinal cord injury*. Stem Cell Res Ther, 2021. **12**(1): p. 102.
48. Yang, Y., et al., *Multiple channel bridges for spinal cord injury: cellular characterization of host response*. Tissue Eng Part A, 2009. **15**(11): p. 3283-95.
49. Shao, A., et al., *Crosstalk between stem cell and spinal cord injury: pathophysiology and treatment strategies*. Stem Cell Res Ther, 2019. **10**(1): p. 238.
50. Salazar, D.L., et al., *Human neural stem cells differentiate and promote locomotor recovery in an early chronic spinal cord injury NOD-scid mouse model*. PLoS One, 2010. **5**(8): p. e12272.
51. Uccelli, A., et al., *Neuroprotective features of mesenchymal stem cells*. Best Pract Res Clin Haematol, 2011. **24**(1): p. 59-64.
52. Wright, K.T., et al., *Concise review: Bone marrow for the treatment of spinal cord injury: mechanisms and clinical applications*. Stem Cells, 2011. **29**(2): p. 169-78.
53. Xu, X.M., et al., *Bridging Schwann cell transplants promote axonal regeneration from both the rostral and caudal stumps of transected adult rat spinal cord*. J Neurocytol, 1997. **26**(1): p. 1-16.
54. Novikova, L.N., et al., *Biodegradable poly-beta-hydroxybutyrate scaffold seeded with Schwann cells to promote spinal cord repair*. Biomaterials, 2008. **29**(9): p. 1198-206.
55. Benavente, F., et al., *Novel C1q receptor-mediated signaling controls neural stem cell behavior and neurorepair*. Elife, 2020. **9**.
56. Nguyen, H.X., et al., *Systemic Neutrophil Depletion Modulates the Migration and Fate of Transplanted Human Neural Stem Cells to Rescue Functional Repair*. J Neurosci, 2017. **37**(38): p. 9269-9287.
57. Hooshmand, M.J., et al., *Neutrophils Induce Astroglial Differentiation and Migration of Human Neural Stem Cells via C1q and C3a Synthesis*. J Immunol, 2017. **199**(3): p. 1069-1085.
58. Beck, K.D., et al., *Quantitative analysis of cellular inflammation after traumatic spinal cord injury: evidence for a multiphasic inflammatory response in the acute to chronic environment*. Brain, 2010. **133**(Pt 2): p. 433-47.
59. Donnelly, D.J. and P.G. Popovich, *Inflammation and its role in neuroprotection, axonal regeneration and functional recovery after spinal cord injury*. Exp Neurol, 2008. **209**(2): p. 378-88.
60. Van Broeckhoven, J., et al., *Macrophage phagocytosis after spinal cord injury: when friends become foes*. Brain, 2021. **144**(10): p. 2933-2945.
61. McMurrin, C.E., et al., *CNS Remyelination and the Innate Immune System*. Front Cell Dev Biol, 2016. **4**: p. 38.
62. Bethea, J.R., et al., *Systemically administered interleukin-10 reduces tumor necrosis factor-alpha production and significantly improves functional recovery following traumatic spinal cord injury in rats*. J Neurotrauma, 1999. **16**(10): p. 851-63.
63. Lee, J.M., et al., *Methylprednisolone protects oligodendrocytes but not neurons after spinal cord injury*. J Neurosci, 2008. **28**(12): p. 3141-9.

64. Kim, Y.T., J.M. Caldwell, and R.V. Bellamkonda, *Nanoparticle-mediated local delivery of Methylprednisolone after spinal cord injury*. *Biomaterials*, 2009. **30**(13): p. 2582-90.
65. Saville, L.R., et al., *A monoclonal antibody to CD11d reduces the inflammatory infiltrate into the injured spinal cord: a potential neuroprotective treatment*. *J Neuroimmunol*, 2004. **156**(1-2): p. 42-57.
66. Degboe, Y., et al., *Polarization of Rheumatoid Macrophages by TNF Targeting Through an IL-10/STAT3 Mechanism*. *Frontiers in Immunology*, 2019. **10**.
67. Boehler, R.M., et al., *Lentivirus delivery of IL-10 to promote and sustain macrophage polarization towards an anti-inflammatory phenotype*. *Biotechnol Bioeng*, 2014. **111**(6): p. 1210-21.
68. Ciciriello, A.J., et al., *IL-10 lentivirus-laden hydrogel tubes increase spinal progenitor survival and neuronal differentiation after spinal cord injury*. *Biotechnol Bioeng*, 2021. **118**(7): p. 2609-2625.
69. Ishii, H., et al., *ifn-gamma-dependent secretion of IL-10 from Th1 cells and microglia/macrophages contributes to functional recovery after spinal cord injury*. *Cell Death Dis*, 2013. **4**: p. e710.
70. Hellenbrand, D.J., et al., *Sustained interleukin-10 delivery reduces inflammation and improves motor function after spinal cord injury*. *J Neuroinflammation*, 2019. **16**(1): p. 93.
71. Zhou, Z., et al., *IL-10 promotes neuronal survival following spinal cord injury*. *Exp Neurol*, 2009. **220**(1): p. 183-90.
72. Oruckaptan, H.H., et al., *Systemic administration of interleukin-10 attenuates early ischemic response following spinal cord ischemia reperfusion injury in rats*. *J Surg Res*, 2009. **155**(2): p. 345-56.
73. Chen, J.Y., et al., *Lentiviral Interleukin-10 Gene Therapy Preserves Fine Motor Circuitry and Function After a Cervical Spinal Cord Injury in Male and Female Mice*. *Neurotherapeutics*, 2021. **18**(1): p. 503-514.
74. Blair, J.A., et al., *Military penetrating spine injuries compared with blunt*. *Spine J*, 2012. **12**(9): p. 762-8.
75. Fawcett, J.W., et al., *Defeating inhibition of regeneration by scar and myelin components*. *Handb Clin Neurol*, 2012. **109**: p. 503-22.
76. Bunge, M.B., *Bridging areas of injury in the spinal cord*. *Neuroscientist*, 2001. **7**(4): p. 325-39.
77. Kadoya, K., et al., *Combined intrinsic and extrinsic neuronal mechanisms facilitate bridging axonal regeneration one year after spinal cord injury*. *Neuron*, 2009. **64**(2): p. 165-72.
78. Krishna, V., et al., *Biomaterial-based interventions for neuronal regeneration and functional recovery in rodent model of spinal cord injury: a systematic review*. *J Spinal Cord Med*, 2013. **36**(3): p. 174-90.
79. Gros, T., et al., *Regeneration of long-tract axons through sites of spinal cord injury using templated agarose scaffolds*. *Biomaterials*, 2010. **31**(26): p. 6719-29.
80. Suzuki, Y., et al., *Electrophysiological and horseradish peroxidase-tracing studies of nerve regeneration through alginate-filled gap in adult rat spinal cord*. *Neurosci Lett*, 2002. **318**(3): p. 121-4.
81. Barnabe-Heider, F., et al., *Origin of new glial cells in intact and injured adult spinal cord*. *Cell Stem Cell*, 2010. **7**(4): p. 470-82.
82. Kotter, M.R., et al., *Myelin impairs CNS remyelination by inhibiting oligodendrocyte precursor cell differentiation*. *J Neurosci*, 2006. **26**(1): p. 328-32.
83. Horvath, L.L., et al., *Fate of endogenous stem/progenitor cells following spinal cord injury*. *J Comp Neurol*, 2006. **498**(4): p. 525-38.
84. Margul, D.J., et al., *Reducing neuroinflammation by delivery of IL-10 encoding lentivirus from multiple-channel bridges*. *Bioeng Transl Med*, 2016. **1**(2): p. 136-148.

85. Nguyen, H.X., K.D. Beck, and A.J. Anderson, *Quantitative assessment of immune cells in the injured spinal cord tissue by flow cytometry: a novel use for a cell purification method*. J Vis Exp, 2011(50).
86. Uchida, N., et al., *Direct isolation of human central nervous system stem cells*. Proc Natl Acad Sci U S A, 2000. **97**(26): p. 14720-5.
87. Cummings, B.J., et al., *Adaptation of a ladder beam walking task to assess locomotor recovery in mice following spinal cord injury*. Behav Brain Res, 2007. **177**(2): p. 232-41.
88. !!! INVALID CITATION !!! .
89. Ghasemi-Mobarakeh, L., et al., *Structural properties of scaffolds: Crucial parameters towards stem cells differentiation*. World J Stem Cells, 2015. **7**(4): p. 728-44.
90. Arulmoli, J., et al., *Combination scaffolds of salmon fibrin, hyaluronic acid, and laminin for human neural stem cell and vascular tissue engineering*. Acta Biomater, 2016. **43**: p. 122-138.
91. Ortinau, S., et al., *Effect of 3D-scaffold formation on differentiation and survival in human neural progenitor cells*. Biomed Eng Online, 2010. **9**: p. 70.
92. Sontag, C.J., et al., *Immunosuppressants affect human neural stem cells in vitro but not in an in vivo model of spinal cord injury*. Stem Cells Transl Med, 2013. **2**(10): p. 731-44.
93. Mombaerts, P., et al., *RAG-1-deficient mice have no mature B and T lymphocytes*. Cell, 1992. **68**(5): p. 869-77.
94. Ueno, M., et al., *Corticospinal Circuits from the Sensory and Motor Cortices Differentially Regulate Skilled Movements through Distinct Spinal Interneurons*. Cell Rep, 2018. **23**(5): p. 1286-1300 e7.
95. Vizzard, M.A., et al., *Transneuronal labeling of neurons in the adult rat brainstem and spinal cord after injection of pseudorabies virus into the urethra*. J Comp Neurol, 1995. **355**(4): p. 629-40.
96. Liu, Z., et al., *Remodeling of the corticospinal innervation and spontaneous behavioral recovery after ischemic stroke in adult mice*. Stroke, 2009. **40**(7): p. 2546-51.
97. Gu, Z., et al., *Skilled Movements Require Non-apoptotic Bax/Bak Pathway-Mediated Corticospinal Circuit Reorganization*. Neuron, 2017. **94**(3): p. 626-641 e4.
98. Li, C., et al., *The identification and neurochemical characterization of central neurons that target parasympathetic preganglionic neurons involved in the regulation of choroidal blood flow in the rat eye using pseudorabies virus, immunolabeling and conventional pathway tracing methods*. Front Neuroanat, 2015. **9**: p. 65.
99. Seidler, R.D., et al., *Motor control and aging: links to age-related brain structural, functional, and biochemical effects*. Neurosci Biobehav Rev, 2010. **34**(5): p. 721-33.
100. Koopmans, G.C., et al., *The assessment of locomotor function in spinal cord injured rats: the importance of objective analysis of coordination*. J Neurotrauma, 2005. **22**(2): p. 214-25.
101. Nishi, R.A., et al., *The effects of mouse strain and age on a model of unilateral cervical contusion spinal cord injury*. PLoS One, 2020. **15**(6): p. e0234245.
102. Cummings, B.J., et al., *Human neural stem cell differentiation following transplantation into spinal cord injured mice: association with recovery of locomotor function*. Neurol Res, 2006. **28**(5): p. 474-81.
103. Hooshmand, M.J., et al., *Analysis of host-mediated repair mechanisms after human CNS-stem cell transplantation for spinal cord injury: correlation of engraftment with recovery*. PLoS One, 2009. **4**(6): p. e5871.
104. Park, J., et al., *Intravascular innate immune cells reprogrammed via intravenous nanoparticles to promote functional recovery after spinal cord injury*. Proc Natl Acad Sci U S A, 2019. **116**(30): p. 14947-14954.
105. Siegelbaum, M.H., et al., *Congenital pelvic arteriovenous malformation with massive prostatic hemorrhage: a case report*. J Urol, 1989. **141**(2): p. 382-4.

106. Lim, S.H., et al., *The effect of nanofiber-guided cell alignment on the preferential differentiation of neural stem cells*. *Biomaterials*, 2010. **31**(34): p. 9031-9.
107. Niari, S.A., et al., *Biomaterials patterning regulates neural stem cells fate and behavior: The interface of biology and material science*. *J Biomed Mater Res A*, 2022. **110**(3): p. 725-737.
108. Olivares-Moreno, R., et al., *The rat corticospinal system is functionally and anatomically segregated*. *Brain Struct Funct*, 2017. **222**(9): p. 3945-3958.
109. Wang, Y., et al., *Migration and remyelination by oligodendrocyte progenitor cells transplanted adjacent to focal areas of spinal cord inflammation*. *J Neurosci Res*, 2011. **89**(11): p. 1737-46.
110. Riegger, T., et al., *Immune depression syndrome following human spinal cord injury (SCI): a pilot study*. *Neuroscience*, 2009. **158**(3): p. 1194-9.
111. Pajer, K., T. Bellak, and A. Nogradi, *Stem Cell Secretome for Spinal Cord Repair: Is It More than Just a Random Baseline Set of Factors?* *Cells*, 2021. **10**(11).
112. Lu, P., et al., *Neural stem cells constitutively secrete neurotrophic factors and promote extensive host axonal growth after spinal cord injury*. *Exp Neurol*, 2003. **181**(2): p. 115-29.
113. Piltti, K.M., et al., *Safety of epicenter versus intact parenchyma as a transplantation site for human neural stem cells for spinal cord injury therapy*. *Stem Cells Transl Med*, 2013. **2**(3): p. 204-16.
114. Anderson, M.A., et al., *Required growth facilitators propel axon regeneration across complete spinal cord injury*. *Nature*, 2018. **561**(7723): p. 396-400.
115. Ishida, A., et al., *Dynamic Interaction between Cortico-Brainstem Pathways during Training-Induced Recovery in Stroke Model Rats*. *J Neurosci*, 2019. **39**(37): p. 7306-7320.
116. Tosolini, A.P., R. Mohan, and R. Morris, *Targeting the full length of the motor end plate regions in the mouse forelimb increases the uptake of fluoro-gold into corresponding spinal cord motor neurons*. *Front Neurol*, 2013. **4**: p. 58.
117. Bareyre, F.M., et al., *The injured spinal cord spontaneously forms a new intraspinal circuit in adult rats*. *Nat Neurosci*, 2004. **7**(3): p. 269-77.
118. Takeuchi, T., et al., *Mechanism of Restoration of Forelimb Motor Function after Cervical Spinal Cord Hemisection in Rats: Electrophysiological Verification*. *Behav Neurol*, 2017. **2017**: p. 7514681.
119. Azari, M.F., et al., *Leukemia inhibitory factor arrests oligodendrocyte death and demyelination in spinal cord injury*. *J Neuropathol Exp Neurol*, 2006. **65**(9): p. 914-29.
120. Arvanian, V.L., et al., *Chronic spinal hemisection in rats induces a progressive decline in transmission in uninjured fibers to motoneurons*. *Exp Neurol*, 2009. **216**(2): p. 471-80.
121. De Laporte, L., et al., *Plasmid releasing multiple channel bridges for transgene expression after spinal cord injury*. *Mol Ther*, 2009. **17**(2): p. 318-26.
122. Smith, D.R., et al., *Polycistronic Delivery of IL-10 and NT-3 Promotes Oligodendrocyte Myelination and Functional Recovery in a Mouse Spinal Cord Injury Model*. *Tissue Eng Part A*, 2020. **26**(11-12): p. 672-682.
123. Hollis, E.R., 2nd, et al., *Induction of corticospinal regeneration by lentiviral *trkB*-induced Erk activation*. *Proc Natl Acad Sci U S A*, 2009. **106**(17): p. 7215-20.
124. Xia, Z., et al., *Macrophage-mediated biodegradation of poly(DL-lactide-co-glycolide) in vitro*. *J Biomed Mater Res A*, 2006. **79**(3): p. 582-90.
125. Zhou, X., X. He, and Y. Ren, *Function of microglia and macrophages in secondary damage after spinal cord injury*. *Neural Regen Res*, 2014. **9**(20): p. 1787-95.
126. Gensel, J.C. and B. Zhang, *Macrophage activation and its role in repair and pathology after spinal cord injury*. *Brain Res*, 2015. **1619**: p. 1-11.

127. Shamash, S., F. Reichert, and S. Rotshenker, *The cytokine network of Wallerian degeneration: tumor necrosis factor-alpha, interleukin-1alpha, and interleukin-1beta*. J Neurosci, 2002. **22**(8): p. 3052-60.
128. Giulian, D. and C. Robertson, *Inhibition of mononuclear phagocytes reduces ischemic injury in the spinal cord*. Ann Neurol, 1990. **27**(1): p. 33-42.
129. Chao, C.C., et al., *Activated microglia mediate neuronal cell injury via a nitric oxide mechanism*. J Immunol, 1992. **149**(8): p. 2736-41.
130. Bellver-Landete, V., et al., *Microglia are an essential component of the neuroprotective scar that forms after spinal cord injury*. Nat Commun, 2019. **10**(1): p. 518.
131. Xu, L., et al., *Current Knowledge of Microglia in Traumatic Spinal Cord Injury*. Front Neurol, 2021. **12**: p. 796704.
132. Miron, V.E. and R.J. Franklin, *Macrophages and CNS remyelination*. J Neurochem, 2014. **130**(2): p. 165-71.
133. Erwig, L.P., et al., *Initial cytokine exposure determines function of macrophages and renders them unresponsive to other cytokines*. J Immunol, 1998. **161**(4): p. 1983-8.
134. Fiorentino, D.F., et al., *Pillars Article: IL-10 Inhibits Cytokine Production by Activated Macrophages*. J Immunol. 1991. **147**: 3815-3822. J Immunol, 2016. **197**(5): p. 1539-46.
135. Nguyen, H.X. and J.G. Tidball, *Null mutation of gp91phox reduces muscle membrane lysis during muscle inflammation in mice*. J Physiol, 2003. **553**(Pt 3): p. 833-41.
136. Schlenker, E.H., *Integration in the PVN: another piece of the puzzle*. Am J Physiol Regul Integr Comp Physiol, 2005. **289**(3): p. R653-5.
137. Bratincsak, A. and M. Palkovits, *Activation of brain areas in rat following warm and cold ambient exposure*. Neuroscience, 2004. **127**(2): p. 385-97.
138. Sakamoto, F., S. Yamada, and Y. Ueta, *Centrally administered orexin-A activates corticotropin-releasing factor-containing neurons in the hypothalamic paraventricular nucleus and central amygdaloid nucleus of rats: possible involvement of central orexins on stress-activated central CRF neurons*. Regul Pept, 2004. **118**(3): p. 183-91.
139. Pyner, S. and J.H. Coote, *Identification of branching paraventricular neurons of the hypothalamus that project to the rostroventrolateral medulla and spinal cord*. Neuroscience, 2000. **100**(3): p. 549-56.
140. Kumagai, H., et al., *Importance of rostral ventrolateral medulla neurons in determining efferent sympathetic nerve activity and blood pressure*. Hypertens Res, 2012. **35**(2): p. 132-41.
141. Toth, Z.E., et al., *Decussations of the descending paraventricular pathways to the brainstem and spinal cord autonomic centers*. J Comp Neurol, 1999. **414**(2): p. 255-66.
142. Mantovani, A., et al., *Macrophage plasticity and polarization in tissue repair and remodelling*. J Pathol, 2013. **229**(2): p. 176-85.
143. Gordon, S., *Alternative activation of macrophages*. Nat Rev Immunol, 2003. **3**(1): p. 23-35.
144. Hanada, T. and A. Yoshimura, *Regulation of cytokine signaling and inflammation*. Cytokine Growth Factor Rev, 2002. **13**(4-5): p. 413-21.
145. Yoshimura, A., et al., *Negative regulation of cytokine signaling influences inflammation*. Curr Opin Immunol, 2003. **15**(6): p. 704-8.
146. Cai, D., et al., *Arginase I and polyamines act downstream from cyclic AMP in overcoming inhibition of axonal growth MAG and myelin in vitro*. Neuron, 2002. **35**(4): p. 711-9.
147. Kigerl, K.A., et al., *Identification of two distinct macrophage subsets with divergent effects causing either neurotoxicity or regeneration in the injured mouse spinal cord*. J Neurosci, 2009. **29**(43): p. 13435-44.
148. Ellman, D.G., et al., *Conditional Ablation of Myeloid TNF Improves Functional Outcome and Decreases Lesion Size after Spinal Cord Injury in Mice*. Cells, 2020. **9**(11).

149. Probert, L., *TNF and its receptors in the CNS: The essential, the desirable and the deleterious effects*. Neuroscience, 2015. **302**: p. 2-22.
150. Ousman, S.S. and S. David, *MIP-1alpha, MCP-1, GM-CSF, and TNF-alpha control the immune cell response that mediates rapid phagocytosis of myelin from the adult mouse spinal cord*. J Neurosci, 2001. **21**(13): p. 4649-56.
151. Parameswaran, N. and S. Patial, *Tumor necrosis factor-alpha signaling in macrophages*. Crit Rev Eukaryot Gene Expr, 2010. **20**(2): p. 87-103.
152. Chi, L.Y., et al., *The dual role of tumor necrosis factor-alpha in the pathophysiology of spinal cord injury*. Neurosci Lett, 2008. **438**(2): p. 174-9.
153. Yasuda, A., et al., *Significance of remyelination by neural stem/progenitor cells transplanted into the injured spinal cord*. Stem Cells, 2011. **29**(12): p. 1983-94.